2016

A Nanoparticle/enzyme System For The Simultaneous Detection And Decontamination Of Organophosphates

Brendon Mark Miller
University of Vermont

A NANOPARTICLE/ENZYME SYSTEM FOR THE SIMULTANEOUS DETECTION AND DECONTAMINATION OF ORGANOPHOSPHATES

A Dissertation Presented

by

Brendon Mark Miller

to

The Faculty of the Graduate College

of

The University of Vermont

In Partial Fulfillment of the Requirements
for the Degree of Doctor of Philosophy
Specializing in Chemistry

May, 2016

Defense Date: March 17, 2016
Dissertation Examination Committee:

Christopher C. Landry, Ph.D., Advisor
Christopher S. Francklyn, Ph.D., Chairperson
Rory Waterman, Ph.D.
Jose S. Madalengoitia, Ph.D.
Cynthia J. Forehand, Ph.D., Dean of the Graduate College

ABSTRACT

The need for a direct visual response system for the detection of organophosphorus compounds stems from the continued threat and use of these toxic agents in military and terrorist conflicts. The development of an enzyme-inhibitor triggered release system allows for direct visual detection with high specificity. Mesoporous silica nanoparticles (MSNs) have physical features that make them attractive as scaffolds for the construction of these systems, such as pore diameters (20-500 Å) that can be synthetically controlled, large surface areas (300-1500 m^2g^{-1}), large pore volumes, chemical inertness, stability at elevated temperatures, and surfaces that can be easily functionalized. In our studies, the dye Congo Red was loaded into the pores of MSNs, which were then capped by tethering an enzyme (organophosphorus hydrolase (OPH) or acetylcholinesterase (AChE)) to the external surfaces of MSNs through a competitive inhibitor (diethyl 4-aminobenzyl phosphonate (DEABP) or tacrine, respectively). OPH has been extensively studied for its ability to hydrolyze a wide range of organophosphorus compounds, rendering them non-toxic. AChE has been commonly used for organophosphate detection resulting from its sensitivity to phosphorylation. Upon addition of organophosphorus compounds to suspensions of the modified MSNs, the enzymes detached from the MSN surface, releasing the dye and providing a visual confirmation of organophosphate presence. Enzyme kinetics were studied using ^{31}P NMR or UV-Visible spectroscopy; Congo Red release was also monitored by UV-Visible spectroscopy. The system was sensitive and specific for organophosphorus compounds both in phosphate-buffered saline and in human serum. The rate of dye release directly correlated with the rate of organophosphorus conversion for OPH and the rate of phosphorylation for AChE.

ACKNOWLEDGEMENTS

I would like to thank the Chemistry program and the Graduate College for allowing me the opportunity to complete the program.

To my dissertation committee, Dr. Christopher Francklyn, Dr. Rory Waterman, Dr. Jose Madalengoitia, and Dr. Christopher Landry, thank you for your guidance and support throughout this process.

To all of the members of the Landry lab, thank you for all of your support throughout my time here.

To my parents, thank you for all of your support and encouragement throughout this process. You have always been there for me and my success is a direct reflection of both of you.

A special thanks to my wife, Melissa, who was always there and pushed me to my full potential. Words cannot describe how your support and love carried me to the end of this journey. To you and my parents, I dedicate this dissertation.

TABLE OF CONTENTS

Page

LIST OF TABLES

Table Page

LIST OF FIGURES

Figure Page

CHAPTER 1: BACKGROUND ON TRIGGERED-RESPONSE SYSTEMS AND MESOPOROUS SILICA NANOPARTICLES

1.1. Triggered-Response Systems

The unique ability of an organism or biological system to respond to an external stimulus has driven research to understand these complex systems.[1] Exploration of stimuli responsive processes has in turn driven the development of new materials and systems to mimic these complex response systems. The specific stimuli that results in a "triggered-response" of the system can be built into the material through synthetic or post-synthetic functionalization.[2-12] This requires the use of a material that can be readily tailored, to meet the specific requirements ("trigger-specificity") needed for the system to respond. This has made the use of polymer-based materials particularly attractive, because they can be produced in large amounts and chemical functionality can be incorporated during the synthesis or post-synthetically with a variety of molecular architectures.[1]

The use of polymer-based materials as trigger-responsive systems has contributed to the tremendous growth within this area over the past two decades. The breadth of combinations of polymeric architectures and functionality has allowed for manipulation of the material to effectively respond to a variety of small changes within their external environment. One of the earliest examples of thermosensitive polymers, poly(N-isopropylacrylamide), which formed transitions from linear to globular across its lower critical solution temperature (LCST = 32°C) in aqueous solution **(Figure 1.1**).[1] Similarly, the use of poly(acrylamide) crosslinking leads to the formation of polymeric gels that can

retain stability across the LCST during solvation/desolvation, resulting from changes in temperature, or pH (**Figure 1.1**).[1] Advancements in polymer-based materials have led to materials that response to a variety of additional environmental and chemical changes such as pH,[13-17] temperature,[18-22] magnetic fields,[23-27] light[28-29] or biological-based processes such as enzyme signaling.[30-34] The design of the material and response system controls directly the ability of the system to react when exposed to one of these external stimuli.[1, 25, 35-36]

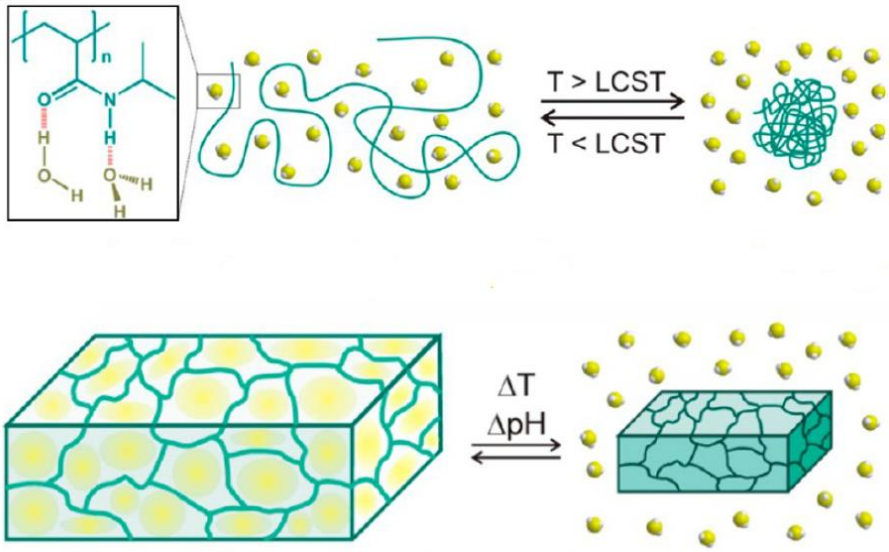

Figure 1.1: Coil-to-globular transition of poly(n-isoproplyacrylamide) dependent on temperature (top) and gel solvation/desolvation of poly(acrylamide) dependent on temperature, or pH.[1]

1.2. Design of a Triggered-Response System

Development of a triggered-response system based on a polymeric material requires several key aspects to be adequately addressed. These include: the selection of the

base scaffold (polymeric material), the trigger (change in external environment) and the response (chemical and/or physical). While each aspect can be individually considered as the primary controlling design factor, the cooperation of all three components is required in a complete triggered-response system.[37] In triggered-release systems for detection applications, an analyte molecule is the trigger releasing mechanism, activating a secondary signal such as a colorimetric[38-39] or fluorimetric[39-40] response to indicate the presence of the analyte such as the utilization of photo-induced electron transfer (PET) processes for fluorescent chemosensors to indicate the presence of organophosphorus substrates. These rely on an alcohol in close proximity to a tertiary amine with an appended fluorophore, quenched by the PET. The introduction of an organophosphorus compound converts the hydroxyl group to a phosphate ester followed by an ammonium salt, increasing the fluorescence (**Figure 1.2**).[41]

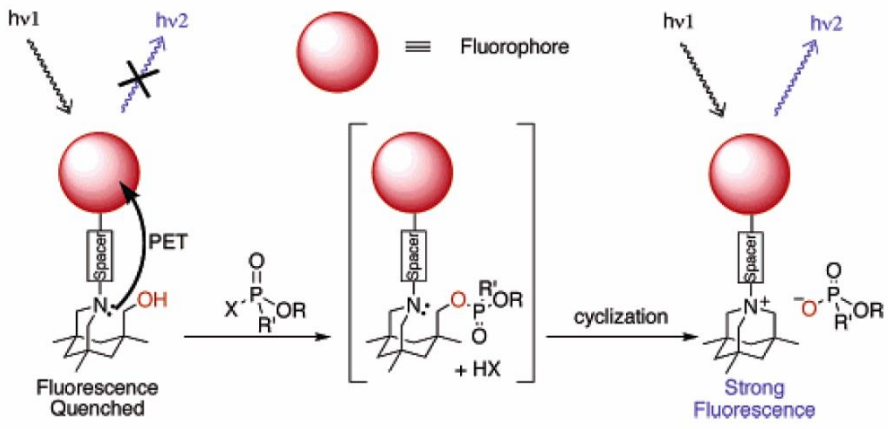

Figure 1.2: Detection of organophosphorus compound using a PET sensor.[41]

Increasing the "response" of the signal requires the immobilization of the

triggered-response system. Localization of the response increases the overall signal and stabilizes system. The utilization of MSNs, specifically, allow for the localization of not only the triggered-response system but offers stability, and rigidity to extend the life of the system through control of the physical characteristics and post-synthetic functionalization.[42]

1.3. Mesoporous Silica Nanoparticles (MSNs)

The use of a porous material offers several advantages over other polymeric architectures in triggered-release systems, primarily a large internal pore volume that can be used to load and retain large amounts of molecular cargo. Transporting the cargo within the scaffold can offer protection from the external environment until the desired location or stimulus is encountered. Controlling the loading and release of the cargo from the interior volume through the porous structure can be directly manipulated by the selection of pore diameter of the material. Silica-based materials are categorized based on their pore size. Microporous, mesoporous, and macroporous materials have pore diameters of less than 2 nm, 2-50 nm, and greater than 50 nm, respectively. Depending on the type of molecules that need to be loaded, carried and delivered, selection of the proper pore diameter and corresponding material can be determined.

Mesoporous silica nanoparticles (MSNs) offer several advantages over previous mesoporous silica microspheres. They have a tunable particle size (50 – 300 nm) that has shown to be endocytosed by living animals and plant cells without any significant cytotoxicity. The spherical structure has shown to be rigid and stable to changes in heat,

pH and mechanical stress compared to other polymeric forms. In combination with these attributes, MSNs have pore diameters corresponding to the sizes of many biomolecules.[37] This was seen with the MSN-based system that facilitated the intercellular delivery of cyclic adenosine monophosphate (cAMP), loaded in the interior pore volume. Manipulation of the MSN surface resulted in the immobilization of a gluconic acid-derivatized insulin that capped the material and was released in the presence of excess blood glucose (**Figure 1.3**).[43] This has propelled the use of MSNs in a variety of applications such as drug delivery,[42, 44-45] bioimaging,[46-47] biosensing,[43, 48] and biocatalysis.[49-51]

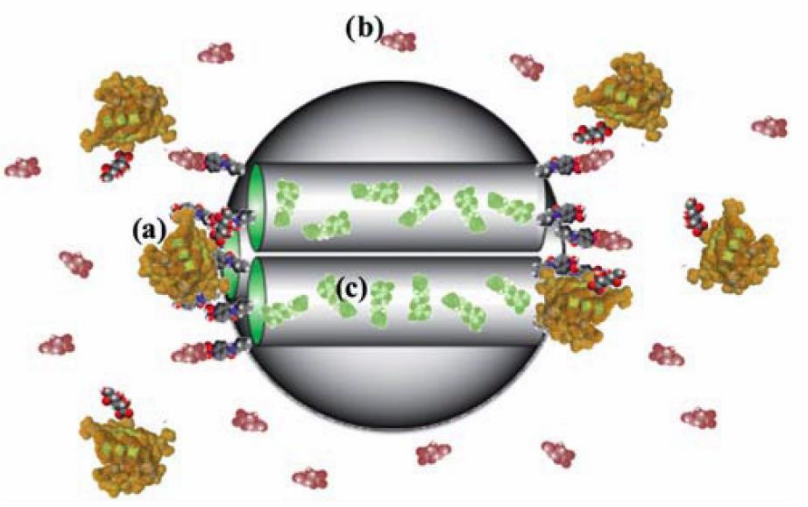

Figure 1.3: Insulin-capped MSN. The removal of cap (a) is triggered by blood glucose (b) to release cAMP (c).[43]

1.3.1. Synthesis of MSNs

The development of MSNs has progressed over the last two decades from their

application in several areas such as adsorption, chromatography, sensors, and drug delivery.[45, 52] This stemmed from their original development as a new class of molecular sieves by the Mobil oil company. Typical microporous molecular sieves (zeolites), used for separations, were limited by their small pore diameters and the molecular range in which they would be useful for separations. The development of MCM-41 in 1992, the first mesoporous material, began a surge of new materials that retained the large surface areas of zeolites but had pore diameters greater than 2 nm. The most prominent representatives of this emerging material were the class of MCM-type materials. The use of ionic structure directing surfactants during the condensation of a silica precursor under basic conditions allowed for the development of several different pore structures (**Figure 1.4**). This included the 2-dimensional, hexagonally arranged pores of MCM-41, MCM-48 with a 3-dimensional, cubic arrangement and MCM-50 that had a laminar structure.[52-54] Alternatively, other synthetic methods were employed using variations in structure directing agents, and under acidic conditions those led to the development of SBA-type materials, such as SBA-15, using triblock copolymer templates. [45]

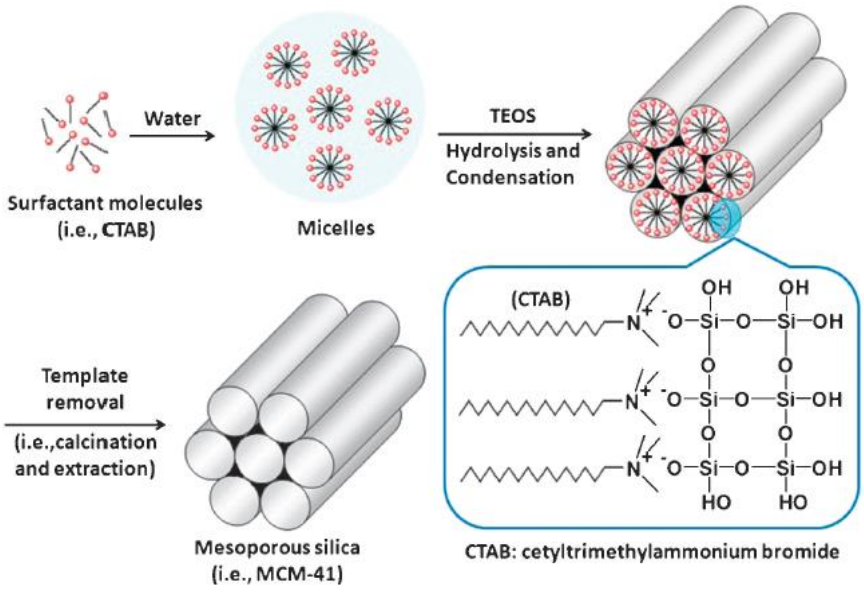

Figure 1.4: Scheme of the formation mechanism of MCM-41.TEOS: tetraethoxysilane.[45]

Since this initial development, a broad range of synthetic procedures have been developed. Manipulation of reaction conditions (pH), the silica monomers, and structure-directing surfactants chosen can all be used to control the synthesis of the desired material. These factors influence the type of interaction (electrostatic or hydrogen bonding) between the surfactant (S) and silica (I) (**Figure 1.5**). Electrostatic interactions can be manipulated by the pH of the reaction mixture and the type of surfactant. Under basic conditions, a cationic surfactant has a direct interaction with the silica giving a S^+ - S^- interaction. Alternatively, acidic conditions below the isoelectric point of the Si-OH (less than pH = 2) require the use of a counter-ion (X^-) to mediate the S^+ - I^+ interaction. The use of an anionic surfactant has similar interactions depending on the pH of the reaction conditions. Under acidic conditions the interaction is S^- - I^+, while basic conditions require the addition of a

mediator (M^+) for the S^- - I^- electrostatic interaction. When uncharged silica is used, a non-ionic surfactant (I^0) can form hydrogen bonds to have a S^0 – I^0 interaction. Hydrogen bonding can also occur in acidic conditions with the interaction of a charged silica surface and ion to form an ion pair $(IX)^0$ to have a S^0 – $(IX)^0$ interaction. With numerous combinations of surfactant, silica and pH, further manipulation of the concentrations, temperature and reaction time allows additional control over particle diameter, morphology and pore structure of the MSN.[52, 55-56]

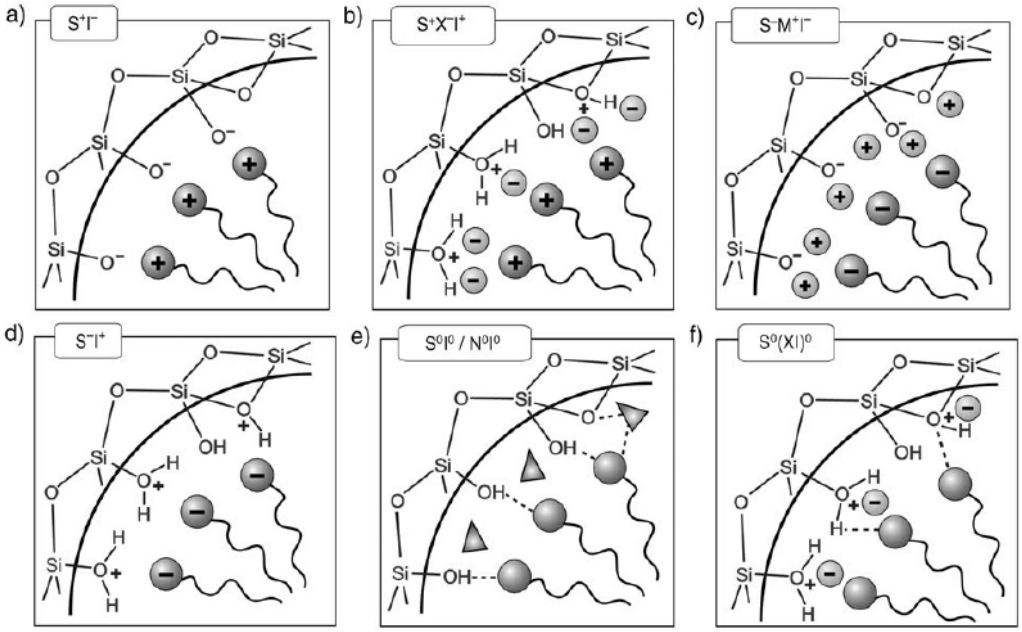

Figure 1.5: Interactions between the inorganic species and the head group of the surfactant with consideration of the possible synthetic pathway in acidic, basic or neutral medial. a) S^+I^-, b) $S^+X^-I^+$, c) $S^-M^+I^-$, d) S^-I^+, e) S^0I^0/N^0I^0 and f) $S^0(XI)^0$.[52]

1.3.2. Physical Characteristics of MSNs

The primary physical characteristics that govern the ability of the scaffold to be an effective release system are pore diameter, pore structure, surface area, pore volume particle diameter, and particle morphology. Depending on the molecular cargo to be transported and delivered, adjustments to these characteristics can greatly affect loading and/or release. Previous research into the influence of each of these characteristics has given insight on how each one specifically controls the overall function of the system.[45]

In general, pore diameter can drastically change the ability of a material to not only load a desired cargo but affect the release rate. Dependent on the size of the cargo, changing the diameter of the pore can increase or decrease the total amount loaded. Examples of this include the loading SBA-15 with a large cargo, such as a bovine serum albumin (BSA), in which increasing the pore diameter from 8.2 to 11.4 nm can almost double the loading from 0.15 grams BSA per gram of SBA-15 to 0.27 g/g. amount. This can be attributed to the steric constraints of pore diameter, and ability for the BSA to adjust its confirmation to pack tightly once in the interior.[57] In another example, release studies using ibuprofen have shown pore diameter to drastically control delivery. Increasing the pore diameter by only 11 Å can increase the release rate fivefold.[58] When factoring in the desired cargo that will be transported and its relative size, the selection of the proper pore diameter can be made.

Similarly, the availability of several different pore structures based on pore connectivity and geometry have shown to contribute to the loading and release of cargo. A SBA-1 mesoporous material with 3D cubic interconnected resulted in faster release of

ibuprofen compared to SBA-3 mesoporous material with a hexagonal geometry with a similar surface area, and pore diameter but unconnected pores. This was attributed to the interconnections between pores offering easier diffusion throughout the material, resulting in faster mass transport and release.[45, 59-61]

A major benefit of using mesoporous materials are their high surface areas and large pore volumes. While a small amount of surface area is derived from the exterior surface of the particle, the vast majority (at least 95% depending on the particle diameter) is from the interior surface of the material. This influences the quantity of cargo that can be loaded, controlled by the interaction of the cargo with the interior pore wall. Cargo that interacts with the interior pore surface has a direct correlation of surface area to the loading capacity of the material. Comparisons of unmodified materials with different surface areas, MCM-41 (1157 $m^2 g^{-1}$) versus SBA-15 (719 $m^2 g^{-1}$), have shown almost a twofold increase in loaded alendronate due to the direct interaction with the surface hydroxyl groups with hydrophilic molecules.[60, 62] For hydrophobic molecular cargo, interior modification of the surface hydroxyl groups such as with 3-aminoproplytriethoxysilane, has shown to increase the loading of camptothecin.[63] Whether the interaction with the pore wall occurs or not, filling of the remaining interior can be greatly influenced by the pore volume. Materials that have larger pore volumes, SBA-15 (1.1 $cm^3 g^{-1}$) versus mesocellular silica foams (1.9 $cm^3 g^{-1}$) have shown to load almost double the amount of cargo. This can be attributed to the packing of the cargo within the pore, limited by only the dimensions of the cargo.[45, 57, 64]

1.3.3. Functionalization of MSNs

The most beneficial aspect of using MSNs is their ability to easily modified with specific organic functional groups. Incorporation of a broad range of possible functionalities allows for the tailoring of the material as a specific triggered-release system. The three main ways of incorporating these new functionalities are through post-synthetic functionalization (grafting), co-condensation, and by using bridged alkoxysilane precursors ($(R'O)_3Si\text{-}R\text{-}Si(OR')_3$) (**Figure 1.6**). Each of these techniques differs in their approach to which the organic functionality can be added. Periodic mesoporous organosilicas (PMOs), created from bridged silanes, were designed to incorporate the functionality directly into the 3D network of the silica structure. This can be accomplished through the use of a bridge organosilica precursor, allowing for functionalization within the pore walls of the material.[52, 65-66] Co-condensation relies on the addition of trialkoxyorganosilanes ($(R'O)_3SiR$) in a one-pot synthesis, containing the surfactant and silica precursor. This results in organic modification positioned on the walls of the material.[52]

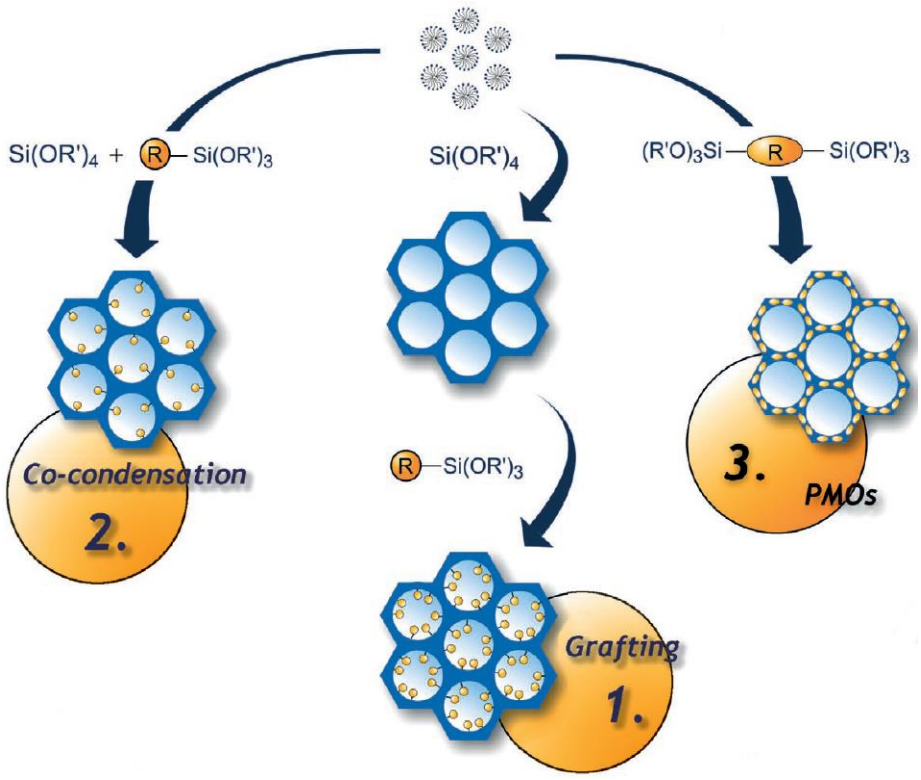

Figure 1.6: Silica-based mesoporous organic-inorganic hybrid materials.[52]

While each of these approaches result in the direct addition of organic moieties, both have several disadvantages for the use as a triggered release system. In general, PMOs often result in a disordered pore structure with a wide range of pore diameters, limiting the control of pore size. Similar effects have been seen with the co-condensation method, in which reductions in pore diameter, pore volume, and surface area can vary depending on the concentration of the trialkoxyorganosilane added. Uneven distribution, difficult access to the organic functionality, and the lack of compatible organic moieties to incorporate using these methods have all limited their use.[52]

1.3.3.1. Post-Synthetic Functionalization: Grafting

Grafting has become the primary method for adding organic functionality to MSNs when developing a triggered-release system. The complexity of building a system that can retain cargo and release it in the presence of a certain trigger requires specific functionality to be post-synthetically added to the scaffold. After synthesizing the desired scaffold, the exterior and/or interior can be functionalized with the condensation of organosilanes of the type $(R'O)_3SiR$ onto the MSN surface, allowing for a broad range of functionalities to be added, depending on the application.[52]

There are a variety of ways to post-synthetically control the location of the organosilane. If modification with the same organosilane is desired on both of the exterior and interior, removal of the interior surfactant template through calcination is performed. This allows the organosilane to modify the exterior surface and the now opened interior pore surface of the material. To modify the exterior surface and interior surface differentially, the surfactant can be retained, blocking the pores of the material and limiting the amount of organosilane entering the material. After grafting, the removal of surfactant can be accomplished through an extraction process, exchanging the surfactant with an appropriate solvent. With the opening of the pores of the material, a second grafting process can proceed adding a separate organic functionality to the interior pore surface.[42, 67]

Interior (pore) modification has several advantages for controlling the loading and release of cargo. Depending on the physical and electrostatic characteristics of the cargo, the degree of interaction can be easily manipulated. Some systems require a strong interaction (covalent bonding, electrostatic interaction versus weak interactions (hydrogen

bonding and/or physical adsorption) of the interior and cargo to control aspects of the delivery kinetics and rate of diffusion from the interior pore volume.[42, 68-70] Manipulating the interior separate from the exterior allows for tailoring of the material for the cargo that will be loaded and released from the system. The only limitations of interior modification are controlled by the ability of the silane to enter the interior pore system and the degree of modification. Depending on the size of the silane, pore diameter can limit the organosilane that can be introduced into the interior of the material. Additionally, organosilane modification has to be controlled to limit the propensity for pores to become blocked by extensive modification.[52]

Exterior modification of MSNs has been at the forefront of research on the tailoring of the material to interact with its external environment. Depending on the type of external trigger that is required to release the cargo, exterior modification plays an important role in helping to retain the loaded cargo. This has expanded the development of a "gating" systems in which access to the pores is restricted by blocking or modifying the pore to entrap the loaded cargo.

1.3.4. MSN Gating for Triggered Delivery of Cargo

Gating is a specific modification approach that restricts access to the pore of the MSN, acting as a "gate". Gating can be separated into three main categories based on the method of retaining the cargo. The first is based on the direct attachment of the cargo to the interior surface of the material through coordinate or covalent attachment. This allows retention and transport of the cargo until the presence of the trigger, which can be a reducing agent,[71-73] light,[74-78] a pH change,[75-76] or a temperature change,[79-81] such as with

the functionalization of a MSN with an azobenzene derivative that will undergo a cis-trans photoisomerization induced by light at 413 nm. The switch from cis to trans causes a propeller type motion, pushing the loaded molecular cargo out of the pores of the MSN (**Figure 1.7**).[77]

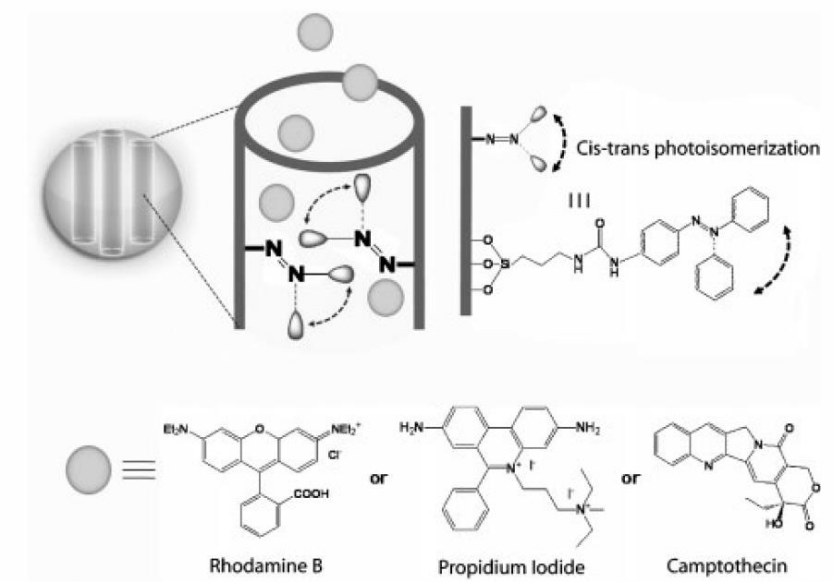

Figure 1.7: Release of cargo by cis-trans photoisomerization. [77]

Another approach to a gating system has been to fully coat the exterior surface to block the pores. Coating can be accomplished with a variety of materials such as polymers,[19, 82-85] polyelectrolyte mulitilayers[86-87] or biomolecules.[88-90] The release of the coatings from the surface of the MSNs allows for the loaded cargo to escape. The trigger can be based on changes in pH,[82, 85-87] temperature,[19, 82, 84-85] chemical environment[88] or on molecular recognition using enzymes[83] or competitive molecules.[89-90] This has been seen

by exterior surface functionalization with the long chain polymer, poly(N-isopropylacrylamide). At a temperature of 25°C, the chain is extended to allow for the loading of cargo. Increasing the temperature to 35°C, the chain is in a coiled confirmation, blocking the pores and retaining the loaded cargo until a decrease in temperature (**Figure 1.8**).[84]

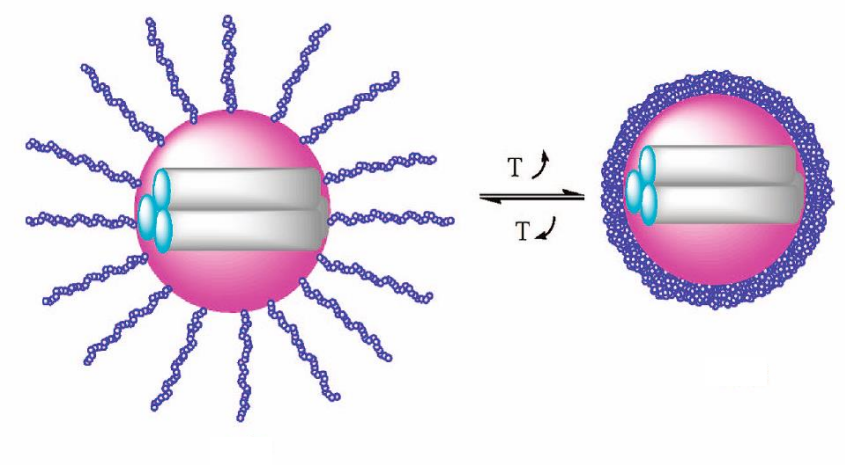

Figure 1.8: Coating approach to gating of MSN using a temperature sensitive poly(N-isopropylacrylamide).[84]

The third gating method involves the direct blocking of the pore with a bulky organic molecule (i.e. cyclodextrin[14, 28, 33, 91-95]), nanoparticle (i.e. Au,[29, 96] CdS,[97] Fe_3O_4[27, 98-99] or ZnO[100]) or long chain molecules (polyamine[101-102]). The introduction of an external stimulus such as light,[28-29, 96] pH,[14, 91-92, 94-96, 99-102] enzyme,[33, 93] magnetic field[98] or reducing agents[27, 97] results in the loss of the pore blockage and subsequent release of the cargo. This has been seen with blocking the pores with carboxylic acid-modified cadmium sulfide nanoparticles (CdS). Modification of the interior pore of the MSN with a long-chain amine,

containing a disulfide bond, allows for a peptide coupling between the CdS and MSN. This allows for entrapment of the loaded drug until the introduction of dithiothreitol (DTT) to cleave the disulfide bond, releasing the CdS, and opening the pores (**Figure 1.9**).[97]

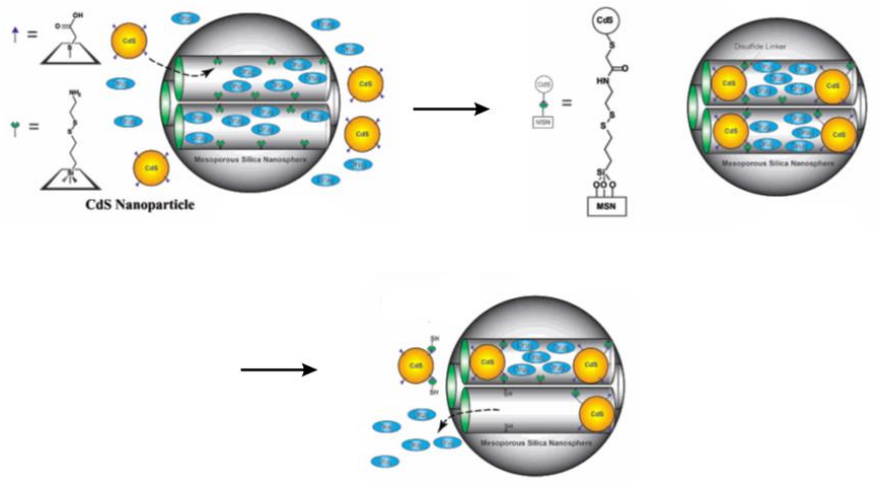

Figure 1.9: Direct blocking with a CdS nanoparticle with a reducing agent sensitive disulfide bond.[97]

Gating systems have an advantage over previous triggered-release systems that rely on simply changes in temperature, pH, or chemical environment. Gating allows for molecular recognition systems to control the release of molecular cargo from the MSN. This has been seen with the example of glucose oxidase tethered to an MSN surface through an enzyme-inhibitor interaction to retain the loaded Rhodamine B cargo. In the presence of the desired enzyme substrate (glucose), glucose oxidase is released from the surface to break down glucose, opening the pores of the material (**Figure 1.10**).[103] Narrowing down the release-trigger to a specific molecular recognition interaction reduces

the potential for premature release of the molecular cargo. This has led the use of these systems in areas in which specificity is essential, such as detection.[104-105]

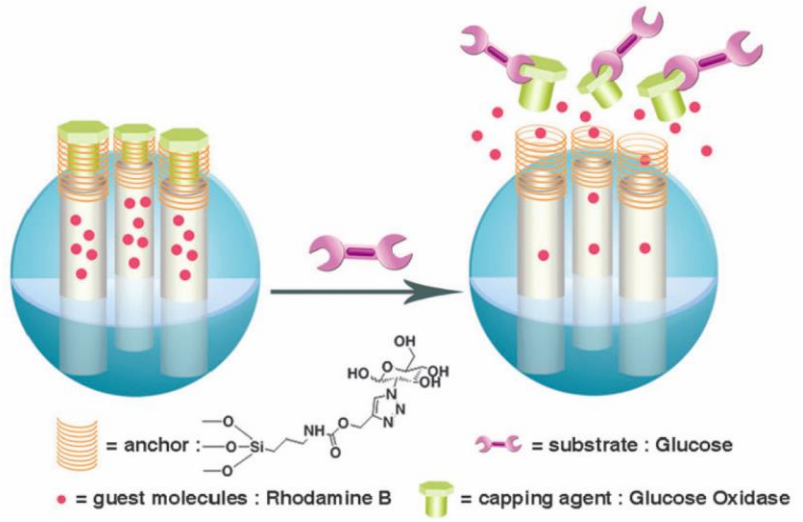

Figure 1.10: Molecular recognition controlled by recognition of substrate (glucose) by the degrading enzyme (glucose oxidase).[103]

1.4. Detection Through Gating Systems

An emerging category of the application of gating systems to the problems of molecular detection and sensing, specifically on the design of small-molecule based systems.[106-108] Free standing small molecule-based sensors have been widely used but several drawbacks have pushed for the integration of these systems within solid supports. A solid support allows for greater stability of the sensor and additional functionalization can be added to create a more effective detection system.[25] Integration into solid supports has been applied to the detection of a variety of analytes such as ions,[109] biomolecules,[107] explosives[108] and pesticides.[110]

1.4.1. Molecular Recognition

The goal of developing more complex detection systems is generally to enhance the sensitivity of the system. The use of molecular recognition systems, where the response is based on a specific molecular interaction, can lead to sensitive detection systems.[104-105] These are often based on biomolecules such as enzymes, amino acids, or nucleic acids. For example, the affinity of an enzyme for its substrate, can be built into a detection system, drastically increasing its sensitivity. In particular, this has been the trend in the development of biosensors for the detection of organophosphate pesticides.

1.4.2. Organophosphate Detection

Organophosphate detection and decontamination has continued to be an evolving field of research. Ranging from less toxic pesticides to extremely toxic nerve agents, organophosphorus compounds can have detrimental effects, in which the structural features will be discussed in Chapter 4. The neurotoxicity of these compounds arises from their inhibitory effect on acetylcholinesterase (AChE). AChE is responsible for the hydrolysis of acetylcholine (ACh), a neurotransmitter used in neuronal communication (**Figure 1.11**).[111-112] Exposure to an organophosphate results in the phosphorylation of a serine residue within the catalytic site of AChE. This inhibits the ability of AChE to hydrolyze ACh into choline and acetate, causing a buildup of ACh in nerve synapses and resulting in paralysis and death.[38-40, 110, 113-115]

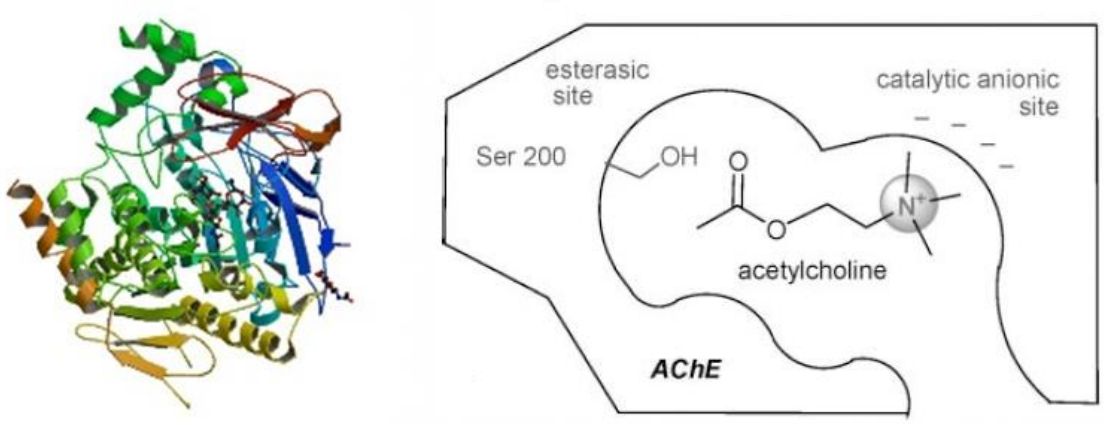

Figure 1.11: Acetylcholinesterase (AChE) and its active site in the presence of acetylcholine (ACh).[111-112]

Past methods for the detection of organophosphates have consisted of instrumental techniques such as gas chromatography, mass spectrometry, and NMR spectroscopy. While these techniques offer low detection limits, problems with portability, real-time and complex use, and false positives remain. [115-125] To address some of these issues, research has shifted towards the development of colorimetric[38-39] and fluorimetric[39-40] response systems, deriving from previous extensive use in small molecule detection. [106, 126-128] Optical response systems offer a rapid, highly portable, and quantitative detection method, often using only the naked eye. This helps to address issues of real-time and ease of use of these systems by military personnel and civilians. [38-39, 129]

1.4.2.1. Optical Biosensors

The development and use of optical biosensors for organophosphate detection covers a broad range of detection strategies. These strategies can be categorized by the triggering response method, whether inhibition or catalysis. (Each mechanism activates a

secondary action, giving the optical response). In triggered systems, using catalysis, the use of a bacterial enzyme capable of hydrolyzing organophosphotriesters allows specificity to be controlled by a substrate-enzyme interaction. Two of these bacterial enzymes are organophosphorus acid anhydrolase (OPAA) and organophosphorus hydrolase (OPH). OPAA has a high specificity for hydrolysis of P-F and P-CN bonds, which are present in the nerve agents sarin and tabun but cannot hydrolyze P-O or P-S bonds that are present in pesticides such as parathion, malathion, and demeton-s.

OPH has the ability to hydrolyze a wide variety of organophosphorus compounds through the cleavage of the P-O, P-F, P-S or P-CN group, with the catalytic rate dependent on the bond.[130-131] After the hydrolysis reaction, the production of an acid (XH) and alcohol offer a variety of ways in which to optically activate the biosensor. The acid can trigger a response from pH-sensitive dye, whereas the alcohol is often chromophoric, and can be tracked through spectroscopic techniques such as UV-Visible spectroscopy (**Figure 1.12**).[132]

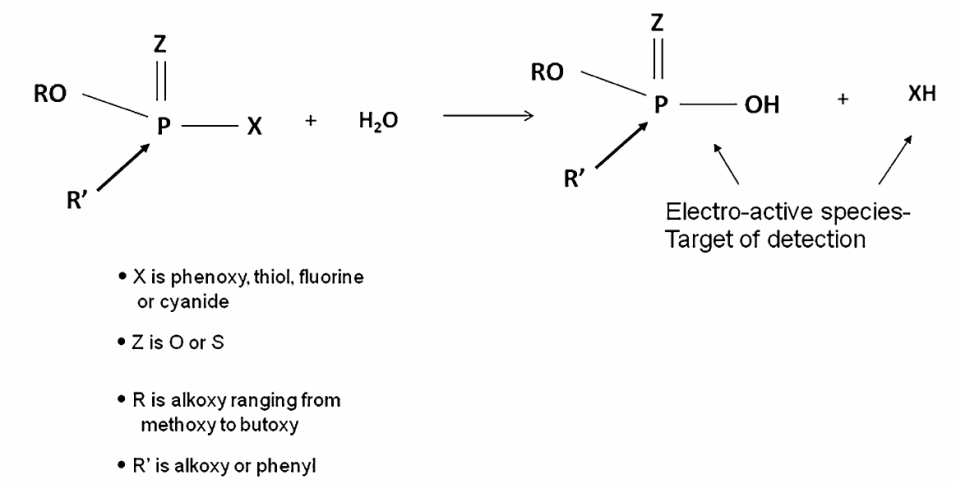

Figure 1.12: Reaction scheme for the OPH-catalyzed hydrolysis of organophosphates.[132]

Inhibition-based biosensors for organophosphates require the use of cholinesterases such as AChE. The activity of AChE hydrolyzing ACh is measured and compare to the activity of AChE after exposure to an organophosphate. The organophosphate will phosphorylate the active site of AChE, preventing hydrolysis of ACh, and slowing the hydrolysis rate. This allows the tracking of AChE activity and its inhibition by secondary process to give an optical signal.[129] The sensitivity of AChE to organophosphates has been routinely explored, most notably by the widely used colorimetric method for tracking the activity of AChE, the Ellman's method. The Ellman's method tracks the hydrolysis of acetylthiocholine (AtCh) to its product, thiocholine (tCh) that reacts with the Ellman's reagent, 5,5-dithio-bis-(2-nitrobenzoic acid), to give a color product (2-nitro-5-thiobenzoate) that can be tracked by UV-Visible spectroscopy.[133-134]

While each approach for the primary mechanism of the biosensors has shown

several benefits, they are still based on secondary signals. This limits the benefits of having an optical system that can effectively notify an individual of the presence of a toxic substance, where time is crucial. This flaw has pushed organophosphate detection in new directions that continue the use of an optical detection method but rely on a direct response to an organophosphate.

1.5. Rationale for This Study

The rationale for this study is that the use of a molecular recognition system for organophosphate detection will eliminate the problem of false positives seen with previous detection systems. To do this, the use of a MSN as the scaffold to contain the optical signal, the dye Congo Red, is capped with an enzyme to block the pores to retain the loaded dye. The mode of attachment of the enzyme (OPH or AChE) was through the use of a competitive inhibitor of the enzyme. Testing of the triggered-release mechanism with either substrate or organophosphates was thoroughly explored to test the stability of the tethering, and relate the dye release kinetics to the rate of AChE inhibition.

1.6. References

1. Lee, S.-M.; Nguyen, S. T. Smart nanoscale drug delivery platforms from stimuli-responsive polymers and liposomes. *Macromolecules* **2013**, *46*, 9169-9180.

2. Xu, J.; Liu, S. Polymeric nanocarriers possessing thermoresponsive coronas. *Soft Matter* **2008**, *4*, 1745-1749.

3. Kost, J.; Langer, R. Responsive polymeric delivery systems. *Adv. Drug Deliv. Rev.* **2001**, *46*, 125-148.

4. Jeong, B.; Gutowska, A. Lessons from nature: Stimuli-responsive polymers and their biomedical applications. *Trends Biotechnol.* **2002**, *20*, 305-311.

5. Ahn, S.-k.; Kasi, R. M.; Kim, S.-C.; Sharma, N.; Zhou, Y. Stimuli-responsive polymer gels. *Soft Matter* **2008**, *4*, 1151-1157.

6. Fleige, E.; Quadir, M. A.; Haag, R. Stimuli-responsive polymeric nanocarriers for the controlled transport of active compounds: Concepts and applications. *Adv. Drug Deliv. Rev.* **2012**, *64*, 866-884.

7. Ganta, S.; Devalapally, H.; Shahiwala, A.; Amiji, M. A review of stimuli-responsive nanocarriers for drug and gene delivery. *J. Control. Release* **2008**, *126*, 187-204.

8. Mura, S.; Nicolas, J.; Couvreur, P. Stimuli-responsive nanocarriers for drug delivery. *Nat. Mater.* **2013**, *12*, 991-1003.

9. Rapoport, N. Physical stimuli-responsive polymeric micelles for anti-cancer drug delivery. *Prog. Polym. Sci.* **2007**, *32*, 962-990.

10. Lu, Y.; Sun, W.; Gu, Z. Stimuli-responsive nanomaterials for therapeutic protein delivery. *J. Control. Release* **2014**, *194*, 1-19.

11. Peterson, G. I.; Larsen, M. B.; Boydston, A. J. Controlled depolymerization: Stimuli-responsive self-immolative polymers. *Macromolecules* **2012**, *45*, 7317-7328.

12. Randolph, L. M.; Chien, M. P.; Gianneschi, N. C. Biological stimuli and biomolecules in the assembly and manipulation of nanoscale polymeric particles. *Chem. Sci.* **2012**, *3*, 1363-1380.

13. Michalak, M.; Marek, A. A.; Zawadiak, J.; Kawalec, M.; Kurcok, P. Synthesis of phb-based carrier for drug delivery systems with ph-controlled release. *Euro. Polym. J.* **2013**, *49*, 4149-4156.

14. Du, L.; Liao, S.; Khatib, H. A.; Stoddart, J. F.; Zink, J. I. Controlled-access hollow mechanized silica nanocontainers. *J. Am. Chem. Soc.* **2009**, *131*, 15136-15142.

15. Lee, C. H.; Cheng, S. H.; Huang, I. P.; Souris, J. S.; Yang, C. S.; Mou, C. Y.; Lo, L. W. Intracellular ph-responsive mesoporous silica nanoparticles for the controlled release of anticancer chemotherapeutics. *Angew. Chem. Int. Ed. Engl.* **2010**, *49*, 8214-8219.

16. Zhou, K.; Wang, Y.; Huang, X.; Luby-Phelps, K.; Sumer, B. D.; Gao, J. Tunable, ultrasensitive ph-responsive nanoparticles targeting specific endocytic organelles in living cells. *Angew. Chem. Int. Ed. Engl.* **2011**, *50*, 6109-6114.

17. Gao, W.; Chan, J. M.; Farokhzad, O. C. Ph-responsive nanoparticles for drug delivery. *Mol. Pharm.* **2010**, *7*, 1913-1920.

18. Jiao, Y.; Sun, Y.; Chang, B.; Lu, D.; Yang, W. Redox- and temperature-controlled drug release from hollow mesoporous silica nanoparticles. *Chem. Eur. J.* **2013**, *19*, 15410-15420.

19. Chung, P.-W.; Kumar, R.; Pruski, M.; Lin, V. S. Y. Temperature responsive solution partition of organic-inorganic hybrid poly(n-isopropylacrylamide)-coated mesoporous silica nanospheres. *Adv. Funct. Mater.* **2008**, *18*, 1390-1398.

20. Liu, C.; Guo, J.; Yang, W.; Hu, J.; Wang, C.; Fu, S. Magnetic mesoporous silica microspheres with thermo-sensitive polymer shell for controlled drug release. *J. Mater. Chem.* **2009**, *19*, 4764-4770.

21. Chen, C.; Geng, J.; Pu, F.; Yang, X.; Ren, J.; Qu, X. Polyvalent nucleic acid/mesoporous silica nanoparticle conjugates: Dual stimuli-responsive vehicles for intracellular drug delivery. *Angew. Chem. Int. Ed. Engl.* **2011**, *50*, 882-886.

22. Aznar, E.; Mondragón, L.; Ros-Lis, J. V.; Sancenón, F.; Marcos, M. D.; Martínez-Máñez, R.; Soto, J.; Pérez-Payá, E.; Amorós, P. Finely tuned temperature-controlled cargo release using paraffin-capped mesoporous silica nanoparticles. *Angew. Chem.* **2011**, *123*, 11368-11371.

23. Thevenot, J.; Oliveira, H.; Sandre, O.; Lecommandoux, S. Magnetic responsive polymer composite materials. *Chem. Soc. Rev.* **2013**, *42*, 7099-7116.

24. Theato, P.; Sumerlin, B. S.; O'Reilly, R. K.; Epps, T. H., 3rd Stimuli responsive materials. *Chem. Soc. Rev.* **2013**, *42*, 7055-7056.

25. Hu, J.; Liu, S. Responsive polymers for detection and sensing applications: Current status and future developments. *Macromolecules* **2010**, *43*, 8315-8330.

26. Bonini, M.; Berti, D.; Baglioni, P. Nanostructures for magnetically triggered release of drugs and biomolecules. *Curr. Opin. Colloid In.* **2013**, *18*, 459-467.

27. Giri, S.; Trewyn, B. G.; Stellmaker, M. P.; Lin, V. S. Stimuli-responsive controlled-release delivery system based on mesoporous silica nanorods capped with magnetic nanoparticles. *Angew. Chem. Int. Ed. Engl.* **2005**, *44*, 5038-5044.

28. Ferris, D. P.; Zhao, Y. L.; Khashab, N. M.; Khatib, H. A.; Stoddart, J. F.; Zink, J. I. Light-operated mechanized nanoparticles. *J. Am. Chem. Soc.* **2009**, *131*, 1686-1688.

29. Vivero-Escoto, J. L.; Slowing, II; Wu, C. W.; Lin, V. S. Photoinduced intracellular controlled release drug delivery in human cells by gold-capped mesoporous silica nanosphere. *J. Am. Chem. Soc.* **2009**, *131*, 3462-3463.

30. Bocharova, V.; Zavalov, O.; MacVittie, K.; Arugula, M. A.; Guz, N. V.; Dokukin, M. E.; Halámek, J.; Sokolov, I.; Privman, V.; Katz, E. A biochemical logic approach to biomarker-activated drug release. *J. Mater. Chem.* **2012**, *22*, 19709-19717.

31. Mailloux, S.; Zavalov, O.; Guz, N.; Katz, E.; Bocharova, V. Enzymatic filter for improved separation of output signals in enzyme logic systems towards 'sense and treat' medicine. *Biomater. Sci.* **2014**, *2*, 184-191.

32. Munkhjargal, M.; Matsuura, Y.; Hatayama, K.; Miyajima, K.; Arakawa, T.; Kudo, H.; Mitsubayashi, K. Glucose-sensing and glucose-driven "organic engine" with co-immobilized enzyme membrane toward autonomous drug release systems for diabetes. *Sensor. Actuat. B-Chem.* **2013**, *188*, 831-836.

33. Patel, K.; Angelos, S.; Dichtel, W. R.; Coskun, A.; Yang, Y. W.; Zink, J. I.; Stoddart, J. F. Enzyme-responsive snap-top covered silica nanocontainers. *J. Am. Chem. Soc.* **2008**, *130*, 2382-2383.

34. Park, C.; Lee, K.; Kim, C. Photoresponsive cyclodextrin-covered nanocontainers and their sol-gel transition induced by molecular recognition. *Angew. Chem. Int. Ed. Engl.* **2009**, *48*, 1275-1278.

35. Schneider, H. J.; Strongin, R. M. Supramolecular interactions in chemomechanical polymers. *Acc. Chem. Res.* **2009**, *42*, 1489-1500.

36. Spruell, J. M.; Hawker, C. J. Triggered structural and property changes in polymeric nanomaterials. *Chem. Sci.* **2011**, *2*, 18-26.

37. Slowing, I. I.; Trewyn, B. G.; Giri, S.; Lin, V. S. Y. Mesoporous silica nanoparticles for drug delivery and biosensing applications. *Advanced Functional Materials* **2007**, *17*, 1225-1236.

38. Climent, E.; Marti, A.; Royo, S.; Martinez-Manez, R.; Marcos, M. D.; Sancenon, F.; Soto, J.; Costero, A. M.; Gil, S.; Parra, M. Chromogenic detection of nerve agent mimics by mass transport control at the surface of bifunctionalized silica nanoparticles. *Angew. Chem. Int. Ed. Engl.* **2010**, *49*, 5945-5948.

39. Royo, S.; Martinez-Manez, R.; Sancenon, F.; Costero, A. M.; Parra, M.; Gil, S. Chromogenic and fluorogenic reagents for chemical warfare nerve agents' detection. *Chem. Commun.* **2007**, 4839-4847.

40. Diaz de Grenu, B.; Moreno, D.; Torroba, T.; Berg, A.; Gunnars, J.; Nilsson, T.; Nyman, R.; Persson, M.; Pettersson, J.; Eklind, I.; Wasterby, P. Fluorescent discrimination between traces of chemical warfare agents and their mimics. *J. Am. Chem. Soc.* **2014**, *136*, 4125-4128.

41. Dale, T. J.; Rebek, J. Fluorescent sensors for organophosphorus nerve agent mimics. *J Am Chem Soc* **2006**, *128*, 4500-4501.

42. Argyo, C.; Weiss, V.; Bräuchle, C.; Bein, T. Multifunctional mesoporous silica nanoparticles as a universal platform for drug delivery. *Chem. Mater.* **2014**, *26*, 435-451.

43. Slowing, I. I.; Vivero-Escoto, J. L.; Trewyn, B. G.; Lin, V. S. Y. Mesoporous silica nanoparticles: Structural design and applications. *J. Mater. Chem.* **2010**, *20*, 7924-7937.

44. Li, Z.; Barnes, J. C.; Bosoy, A.; Stoddart, J. F.; Zink, J. I. Mesoporous silica nanoparticles in biomedical applications. *Chem. Soc. Rev.* **2012**, *41*, 2590-2605.

45. Yang, P.; Gai, S.; Lin, J. Functionalized mesoporous silica materials for controlled drug delivery. *Chem. Soc. Rev.* **2012**, *41*, 3679-3698.

46. Liong, M.; Lu, J.; Kovochich, M.; Xia, T.; Ruehm, S. G.; Nel, A. E.; Tamanoi, F.; Zink, J. I. Multifunctional inorganic nanoparticles for imaging, targeting, and drug delivery. *Nano* **2008**, *2*, 889-896.

47. Lee, J. E.; Lee, N.; Kim, T.; Kim, J.; Hyeon, T. Multifunctional mesoporous silica nanocomposite nanoparticles for theranostic applications. *Acc. Chem. Res.* **2011**, *44*, 893-902.

48. Liu, J.; Li, C.; Li, F. Fluorescence turn-on chemodosimeter-functionalized mesoporous silica nanoparticles and their application in cell imaging. *J. Mater. Chem.* **2011**, *21*, 7175-7181.

49. Johnson, B. F. G. Nanoparticles in catalysis. *Top. Catal.* **2003**, *24*, 147-159.

50. Popat, A.; Hartono, S. B.; Stahr, F.; Liu, J.; Qiao, S. Z.; Qing Max Lu, G. Mesoporous silica nanoparticles for bioadsorption, enzyme immobilisation, and delivery carriers. *Nanoscale* **2011**, *3*, 2801-2818.

51. Ariga, K.; Ji, Q.; Mori, T.; Naito, M.; Yamauchi, Y.; Abe, H.; Hill, J. P. Enzyme nanoarchitectonics: Organization and device application. *Chem. Soc. Rev.* **2013**, *42*, 6322-6345.

52. Hoffmann, F.; Cornelius, M.; Morell, J.; Froba, M. Silica-based mesoporous organic-inorganic hybrid materials. *Angew. Chem. Int. Ed. Engl.* **2006**, *45*, 3216-3251.

53. Kresge, C. T.; Leonowicz, M. E.; Roth, W. J.; Vartuli, J. C.; Beck, J. S. Ordered mesoporous molecular sieves synthesized by a liquid-crystal template mechanism. *Nature* **1992**, *359*, 710-712.

54. Beck, J. S.; Vartuli, J. C.; Roth, W. J.; Leonowicz, M. E.; Kresge, C. T.; Schmitt, K. D.; Chu, C. T. W.; Olson, D. H.; Sheppard, E. W. A new family of mesoporous molecular sieves prepared with liquid crystal templates. *J. Am. Chem. Soc.* **1992**, *114*, 10834-10843.

55. Huo, Q.; Margolese, D. I.; Ciesla, U.; Demuth, D. G.; Feng, P.; Gier, T. E.; Sieger, P.; Firouzi, A.; Chmelka, B. F. Organization of organic molecules with inorganic molecular species into nanocomposite biphase arrays. *Chem. Mater.* **1994**, *6*, 1176-1191.

56. Huo, Q.; Margolese, D. I.; Ciesla, U.; Feng, P.; Gier, T. E.; Sieger, P.; Leon, R.; Petroff, P. M.; Schüth, F.; Stucky, G. D. Generalized synthesis of periodic surfactant/inorganic composite materials. *Nature* **1994**, *368*, 317-321.

57. Vallet-Regí, M.; Balas, F.; Colilla, M.; Manzano, M. Bone-regenerative bioceramic implants with drug and protein controlled delivery capability. *Prog. Solid State Ch.* **2008**, *36*, 163-191.

58. Horcajada, P.; Rámila, A.; Pérez-Pariente, J.; Vallet-Regí, M. Influence of pore size of mcm-41 matrices on drug delivery rate. *Micropor. Mesopor. Mat.* **2004**, *68*, 105-109.

59. Andersson, J.; Rosenholm, J.; Areva, S.; Lindén, M. Influences of material characteristics on ibuprofen drug loading and release profiles from ordered micro- and mesoporous silica matrices. *Chem. Mater.* **2004**, *16*, 4160-4167.

60. Izquierdo-Barba, I.; Sousa, E.; Doadrio, J. C.; Doadrio, A. L.; Pariente, J. P.; Martínez, A.; Babonneau, F.; Vallet-Regí, M. Influence of mesoporous structure type on the controlled delivery of drugs: Release of ibuprofen from mcm-48, sba-15 and functionalized sba-15. *J. Sol-Gel Sci. Techn.* **2009**, *50*, 421-429.

61. Sakamoto, Y.; Kim, T. W.; Ryoo, R.; Terasaki, O. Three-dimensional structure of large-pore mesoporous cubic ia3d silica with complementary pores and its carbon replica by electron crystallography. *Angew. Chem. Int. Ed. Engl.* **2004**, *43*, 5231-5234.

62. Balas, F.; Manzano, M.; Horcajada, P.; Vallet-Regi, M. Confinement and controlled release of bisphosphonates on ordered mesoporous silica-based materials. *J. Am. Chem. Soc.* **2006**, *128*, 8116-8117.

63. Lu, J.; Liong, M.; Zink, J. I.; Tamanoi, F. Mesoporous silica nanoparticles as a delivery system for hydrophobic anticancer drugs. *Small* **2007**.

64. Schmidt-Winkel, P.; Lukens, W. W.; Zhao, D.; Yang, P.; Chmelka, B. F.; Stucky, G. D. Mesocellular siliceous foams with uniformly sized cells and windows. *J. Am. Chem. Soc.* **1999**, *121*, 254-255.

65. Loy, D. A.; Shea, K. J. Bridged polysilsesquioxanes. Highly porous hybrid organic-inorganic materials. *Chem. Rev.* **1995**, *95*, 1431-1442.

66. Shea, K. J.; Loy, D. A. Bridged polysilsesquioxanes. Molecular-engineered hybrid organic−inorganic materials. *Chem. Mater.* **2001**, *13*, 3306-3319.

67. Lin, Y. S.; Hurley, K. R.; Haynes, C. L. Critical considerations in the biomedical use of mesoporous silica nanoparticles. *J. Phys. Chem. Lett.* **2012**, *3*, 364-374.

68. Yang, Q.; Wang, S.; Fan, P.; Wang, L.; Di, Y.; Lin, K.; Xiao, F.-S. Ph-responsive carrier system based on carboxylic acid modified mesoporous silica and polyelectrolyte for drug delivery. *Chem. Mater.* **2005**, *17*, 5999-6003.

69. Rosenholm, J. M.; Linden, M. Towards establishing structure-activity relationships for mesoporous silica in drug delivery applications. *J. Control. Release* **2008**, *128*, 157-164.

70. Manzano, M.; Aina, V.; Areán, C. O.; Balas, F.; Cauda, V.; Colilla, M.; Delgado, M. R.; Vallet-Regí, M. Studies on mcm-41 mesoporous silica for drug delivery: Effect of particle morphology and amine functionalization. *Chem. Eng. J.* **2008**, *137*, 30-37.

71. Mendez, J.; Monteagudo, A.; Griebenow, K. Stimulus-responsive controlled release system by covalent immobilization of an enzyme into mesoporous silica nanoparticles. *Bioconjug. Chem.* **2012**, *23*, 698-704.

72. Mortera, R.; Vivero-Escoto, J.; Slowing, II; Garrone, E.; Onida, B.; Lin, V. S. Cell-induced intracellular controlled release of membrane impermeable cysteine from a mesoporous silica nanoparticle-based drug delivery system. *Chem. Commun.* **2009**, 3219-3221.

73. Sauer, A. M.; Schlossbauer, A.; Ruthardt, N.; Cauda, V.; Bein, T.; Brauchle, C. Role of endosomal escape for disulfide-based drug delivery from colloidal mesoporous silica evaluated by live-cell imaging. *Nano Lett.* **2010**, *10*, 3684-3691.

74. Knezevic, N. Z.; Trewyn, B. G.; Lin, V. S. Functionalized mesoporous silica nanoparticle-based visible light responsive controlled release delivery system. *Chem. Commun.* **2011**, *47*, 2817-2819.

75. Fang, W.; Yang, J.; Gong, J.; Zheng, N. Photo- and ph-triggered release of anticancer drugs from mesoporous silica-coated pd@ag nanoparticles. *Adv. Funct. Mater.* **2012**, *22*, 842-848.

76. Knezevic, N. Z.; Trewyn, B. G.; Lin, V. S. Light- and ph-responsive release of doxorubicin from a mesoporous silica-based nanocarrier. *Chem. Eur. J.* **2011**, *17*, 3338-3342.

77. Lu, J.; Choi, E.; Tamanoi, F.; Zink, J. I. Light-activated nanoimpeller-controlled drug release in cancer cells. *Small* **2008**, *4*, 421-426.

78. Angelos, S.; Yang, Y. W.; Khashab, N. M.; Stoddart, J. F.; Zink, J. I. Dual-controlled nanoparticles exhibiting and logic. *J. Am. Chem. Soc.* **2009**, *131*, 11344-11346.

79. Zhu, S.; Zhou, Z.; Zhang, D.; Jin, C.; Li, Z. Design and synthesis of delivery system based on sba-15 with magnetic particles formed in situ and thermo-sensitive pnipa as controlled switch. *Micropor. Mesopor. Mat.* **2007**, *106*, 56-61.

80. Zhu, S.; Zhou, Z.; Zhang, D. Control of drug release through the in situ assembly of stimuli-responsive ordered mesoporous silica with magnetic particles. *ChemPhysChem* **2007**, *8*, 2478-2483.

81. Tian, B.-S.; Yang, C. Temperature-responsive nanocomposites based on mesoporous sba-15 silica and pnipaam: Synthesis and characterization. *J. Phys. Chem. C* **2009**, *113*, 4925-4931.

82. Hu, X.; Hao, X.; Wu, Y.; Zhang, J.; Zhang, X.; Wang, P. C.; Zou, G.; Liang, X. J. Multifunctional hybrid silica nanoparticles for controlled doxorubicin loading and release with thermal and ph dually response. *J. Mater. Chem. B* **2013**, *1*, 1109-1118.

83. Zhu, Y.; Meng, W.; Gao, H.; Hanagata, N. Hollow mesoporous silica/poly(l-lysine) particles for codelivery of drug and gene with enzyme-triggered release property. *J. Phys. Chem. C* **2011**, *115*, 13630-13636.

84. Hong, C.-Y.; Li, X.; Pan, C.-Y. Smart core−shell nanostructure with a mesoporous core and a stimuli-responsive nanoshell synthesized via surface reversible addition−fragmentation chain transfer polymerization. *J. Phys. Chem. C* **2008**, *112*, 15320-15324.

85. Chang, B.; Sha, X.; Guo, J.; Jiao, Y.; Wang, C.; Yang, W. Thermo and ph dual responsive, polymer shell coated, magnetic mesoporous silica nanoparticles for controlled drug release. *J. Mater. Chem.* **2011**, *21*, 9239-9247.

86. Zhu, Y.; Shi, J.; Shen, W.; Dong, X.; Feng, J.; Ruan, M.; Li, Y. Stimuli-responsive controlled drug release from a hollow mesoporous silica sphere/polyelectrolyte multilayer core-shell structure. *Angew. Chem. Int. Ed. Engl.* **2005**, *44*, 5083-5087.

87. Zhu, Y.; Shi, J. A mesoporous core-shell structure for ph-controlled storage and release of water-soluble drug. *Micropor. Mesopor. Mat.* **2007**, *103*, 243-249.

88. Climent, E.; Bernardos, A.; Martinez-Manez, R.; Maquieira, A.; Marcos, M. D.; Pastor-Navarro, N.; Puchades, R.; Sancenon, F.; Soto, J.; Amoros, P. Controlled delivery systems using antibody-capped mesoporous nanocontainers. *J. Am. Chem. Soc.* **2009**, *131*, 14075-14080.

89. Climent, E.; Martinez-Manez, R.; Sancenon, F.; Marcos, M. D.; Soto, J.; Maquieira, A.; Amoros, P. Controlled delivery using oligonucleotide-capped mesoporous silica nanoparticles. *Angew. Chem. Int. Ed. Engl.* **2010**, *49*, 7281-7283.

90. Zhao, W.; Zhang, H.; He, Q.; Li, Y.; Gu, J.; Li, L.; Li, H.; Shi, J. A glucose-responsive controlled release of insulin system based on enzyme multilayers-coated mesoporous silica particles. *Chem. Commun.* **2011**, *47*, 9459-9461.

91. Meng, H.; Xue, M.; Xia, T.; Zhao, Y. L.; Tamanoi, F.; Stoddart, J. F.; Zink, J. I.; Nel, A. E. Autonomous in vitro anticancer drug release from mesoporous silica nanoparticles by ph-sensitive nanovalves. *J. Am. Chem. Soc.* **2010**, *132*, 12690-12697.

92. Park, C.; Oh, K.; Lee, S. C.; Kim, C. Controlled release of guest molecules from mesoporous silica particles based on a ph-responsive polypseudorotaxane motif. *Angew. Chem. Int. Ed. Engl.* **2007**, *46*, 1455-1457.

93. Park, C.; Kim, H.; Kim, S.; Kim, C. Enzyme responsive nanocontainers with cyclodextrin gatekeepers and synergistic effects in release of guests. *J. Am. Chem. Soc.* **2009**, *131*, 16614-16615.

94. Guo, W.; Wang, J.; Lee, S. J.; Dong, F.; Park, S. S.; Ha, C. S. A general ph-responsive supramolecular nanovalve based on mesoporous organosilica hollow nanospheres. *Chem. Eur. J.* **2010**, *16*, 8641-8646.

95. Zhao, Y. L.; Li, Z.; Kabehie, S.; Botros, Y. Y.; Stoddart, J. F.; Zink, J. I. Ph-operated nanopistons on the surfaces of mesoporous silica nanoparticles. *J. Am. Chem. Soc.* **2010**, *132*, 13016-13025.

96. Aznar, E.; Marcos, M. D.; Martinez-Manez, R.; Sancenon, F.; Soto, J.; Amoros, P.; Guillem, C. Ph- and photo-switched release of guest molecules from mesoporous silica supports. *J. Am. Chem. Soc.* **2009**, *131*, 6833-6843.

97. Lai, C. Y.; Trewyn, B. G.; Jeftinija, D. M.; Jeftinija, K.; Xu, S.; Jeftinija, S.; Lin, V. S. A mesoporous silica nanosphere-based carrier system with chemically removable cds nanoparticle caps for stimuli-responsive controlled release of neurotransmitters and drug molecules. *J. Am. Chem. Soc.* **2003**, *125*, 4451-4459.

98. Chen, P.-J.; Hu, S.-H.; Hsiao, C.-S.; Chen, Y.-Y.; Liu, D.-M.; Chen, S.-Y. Multifunctional magnetically removable nanogated lids of fe3o4–capped mesoporous silica nanoparticles for intracellular controlled release and mr imaging. *J. Mater. Chem.* **2011**, *21*, 2535.

99. Gan, Q.; Lu, X.; Yuan, Y.; Qian, J.; Zhou, H.; Lu, X.; Shi, J.; Liu, C. A magnetic, reversible ph-responsive nanogated ensemble based on fe3o4 nanoparticles-capped mesoporous silica. *Biomaterials* **2011**, *32*, 1932-1942.

100. Muhammad, F.; Guo, M.; Qi, W.; Sun, F.; Wang, A.; Guo, Y.; Zhu, G. Ph-triggered controlled drug release from mesoporous silica nanoparticles via intracelluar dissolution of zno nanolids. *J. Am. Chem. Soc.* **2011**, *133*, 8778-8781.

101. Casasus, R.; Climent, E.; Marcos, M. D.; Martinez-Manez, R.; Sancenon, F.; Soto, J.; Amoros, P.; Cano, J.; Ruiz, E. Dual aperture control on ph- and anion-driven supramolecular nanoscopic hybrid gate-like ensembles. *J. Am. Chem. Soc.* **2008**, *130*, 1903-1917.

102. Bernardos, A.; Aznar, E.; Coll, C.; Martinez-Manez, R.; Barat, J. M.; Marcos, M. D.; Sancenon, F.; Benito, A.; Soto, J. Controlled release of vitamin b2 using mesoporous materials functionalized with amine-bearing gate-like scaffoldings. *J. Control. Release* **2008**, *131*, 181-189.

103. Chen, M.; Huang, C.; He, C.; Zhu, W.; Xu, Y.; Lu, Y. A glucose-responsive controlled release system using glucose oxidase-gated mesoporous silica nanocontainers. *Chem. Commun.* **2012**, *48*, 9522-9524.

104. Famulok, M.; Mayer, G. Aptamer modules as sensors and detectors. *Acc. Chem. Res.* **2011**, *44*, 1349-1358.

105. Oliveira, O. N., Jr.; Iost, R. M.; Siqueira, J. R., Jr.; Crespilho, F. N.; Caseli, L. Nanomaterials for diagnosis: Challenges and applications in smart devices based on molecular recognition. *ACS Appl. Mater. Interfaces* **2014**, *6*, 14745-14766.

106. Cho, D. G.; Sessler, J. L. Modern reaction-based indicator systems. *Chem. Soc. Rev.* **2009**, *38*, 1647-1662.

107. Basabe-Desmonts, L.; Reinhoudt, D. N.; Crego-Calama, M. Design of fluorescent materials for chemical sensing. *Chem. Soc. Rev.* **2007**, *36*, 993-1017.

108. Germain, M. E.; Knapp, M. J. Optical explosives detection: From color changes to fluorescence turn-on. *Chem. Soc. Rev.* **2009**, *38*, 2543-2555.

109. Nolan, E. M.; Lippard, S. J. Tools and tactics for the optical detection of mercuric ion. *Chem. Rev.* **2008**, *108*, 3443-3480.

110. Kim, K.; Tsay, O. G.; Atwood, D. A.; Churchill, D. G. Destruction and detection of chemical warfare agents. *Chem. Rev.* **2011**, *111*, 5345-5403.

111. Reeves, T. E.; Wales, M. E.; Grimsley, J. K.; Li, P.; Cerasoli, D. M.; Wild, J. R. Balancing the stability and the catalytic specificities of op hydrolases with enhanced v-agent activities. *Protein Eng. Des. Sel.* **2008**, *21*, 405-412.

112. Bohn, P.; Le Fur, N.; Hagues, G.; Costentin, J.; Torquet, N.; Papamicael, C.; Marsais, F.; Levacher, V. Rational design of central selective acetylcholinesterase inhibitors by means of a "bio-oxidisable prodrug" strategy. *Org Biomol Chem* **2009**, *7*, 2612-2618.

113. Yang, Y. C.; Baker, J. A.; Ward, J. R. Decontamination of chemical warfare agents. *Chem. Rev.* **1992**, *92*, 1729-1743.

114. El-Boubbou, K.; Schofield, D. A.; Landry, C. C. Enhanced enzymatic activity of oph in ammonium-functionalized mesoporous silica: Surface modification and pore effects. *J. Phys. Chem. C* **2012**, *116*, 17501-17506.

115. Yu, D.; Volponi, J.; Chhabra, S.; Brinker, C. J.; Mulchandani, A.; Singh, A. K. Aqueous sol-gel encapsulation of genetically engineered moraxella spp. Cells for the detection of organophosphates. *Biosens. Bioelectron.* **2005**, *20*, 1433-1437.

116. Nieuwenhuizen, M. S.; Harteveld, J. L. N. Studies on a surface acoustic wave (saw) dosimeter sensor for organophosphorous nerve agents. *Sens. Actuators B* **1997**, *40*, 167-173.

117. Ngeh-Ngwainbi, J.; Foley, P. H.; Kaun, S. S.; Guilbault, G. G. Parathion antibodies on piezoelectric crystals. *J. Am. Chem. Soc.* **1986**, *108*, 5444-5447.

118. Yang, Y. M.; Ji, H.-F.; Thundat, T. Nerve agents detection using a cu2+/l-cysteine bilayer-coated microcantilever. *J. Am. Chem. Soc.* **2003**, *125*, 1124-1125.

119. Hartmann-Thompson, C.; Hin, J.; Kaganove, S. N.; Keinath, S. E.; Keeley, D. L.; Dvornic, P. R. Hydrogen-bond acidic hyperbranched polymers for surface acoustic wave (saw) sensors. *Chem. Mater.* **2004**, *16*, 5357-5364.

120. Yuehe, L.; Fang, L.; Joseph, W. Disposable carbon nanotube modified screen-printed biosensor for amperometric detection of organophosphorus pesticides and nerve agents. *Electroanalysis* **2004**, *16*, 145-149.

121. Zhou, Y.; Yu, B.; Shiu, E.; Levon, K. Potentiometric sensing of chemical warfare agents: Surface imprinted polymer integrated with an indium tin oxide electrode. *Anal. Chem.* **2004**, *76*, 2689-2693.

122. Anitha, K.; Mohan, S. V.; Reddy, S. J. Development of acetylcholinesterase silica sol-gel immobilized biosensor - an application towards oxydemeton methyl detection. *Biosens. Bioelectron.* **2004**, *20*, 848-856.

123. Simonian, A. L.; Grimsley, J. K.; Flounders, A. W.; Schoeniger, J. S.; Cheng, T. C.; DeFrank, J. J.; Wild, J. R. Enzyme-based biosensor for the direct detection of fluorine-containing organophosphates. *Anal. Chem. Acta* **2001**, *442*, 15-23.

124. Wang, J. Microchip devices for detecting terrorist weapons. *Anal. Chem. Acta* **2004**, *507*, 3-10.

125. Steiner, W. E.; Klopsch, S. J.; English, W. A.; Clowers, B. H.; Hill, H. H. Detection of a chemical warfare agent simulant in various aerosol matrixes by ion mobility time-of-flight mass spectrometry. *Anal. Chem.* **2005**, *77*, 4792-4799.

126. Mancin, F.; Rampazzo, E.; Tecilla, P.; Tonellato, U. Self-assembled fluorescent chemosensors. *Chem. Eur. J.* **2006**, *12*, 1844-1854.

127. de Silva, A. P.; Uchiyama, S.; Vance, T. P.; Wannalerse, B. A supramolecular chemistry basis for molecular logic and computation. *Coordin. Chem. Rev.* **2007**, *251*, 1623-1632.

128. Yildiz, I.; Deniz, E.; Raymo, F. M. Fluorescence modulation with photochromic switches in nanostructured constructs. *Chem. Soc. Rev.* **2009**, *38*, 1859-1867.

129. Mulchandani, A.; Rajesh Microbial biosensors for organophosphate pesticides. *Appl. Biochem. Biotechnol.* **2011**, *165*, 687-699.

130. Dumas, D. P.; Caldwell, S. R.; Wild, J. R.; Raushel, F. M. Purification and properties of the phosphotriesterase from pseudomonas diminuta. *J. Biol. Chem.* **1989**, *264*, 19659-19665.

131. Efremenko, E. N.; Sergeeva, V. S. Organophosphate hydrolase an enzyme catalyzing degradation of phosphorus-containing toxins and pesticides. *Russ. Chem. B+* **2001**, *50*, 1826-1832.

132. Mulchandani, P.; Chen, W.; Mulchandani, A. Microbial biosensor for direct determination of nitrophenyl-substituted organophosphate nerve agents using genetically engineered moraxella sp. *Anal Chim Acta* **2006**, *568*, 217-221.

133. Eyer, P.; Worek, F.; Kiderlen, D.; Sinko, G.; Stuglin, A.; Simeon-Rudolf, V.; Reiner, E. Molar absorption coefficients for the reduced ellman reagent: Reassessment. *Anal. Biochem.* **2003**, *312*, 224-227.

134. Ellman, G. L.; Courtney, K. D.; Andres, V., Jr.; Feather-Stone, R. M. A new and rapid colorimetric determination of acetylcholinesterase activity. *Biochem. Pharmacol.* **1961**, *7*, 88-95.

CHAPTER 2: SIMULTANEOUS DETECTION AND DECONTAMINATION OF ORGANOPHOSPHORUS COMPOUNDS USING A TRIGGERED ENZYME RELEASE SYSTEM

2.1. Introduction

Organophosphorus compounds have an expansive toxicity range from pesticides to chemical warfare agents (CWAs), specifically nerve agents. Neurotoxicity arises from the inhibitory effect on acetylcholine esterase that causes buildup of acetylcholine in nerve synapses resulting in paralysis and death.[1-7] The extreme toxicity and extent of destruction nerve agents can and do have caused resulted in part the development of the Chemical Weapons Convention. This was an agreement to stop the production and eliminate stockpiles of all CWAs but the continued exploitation during conflicts has persisted.[8-9] The recurrent threat of exposure to military organizations and the general public within conflict zones has continued the effort towards the design of more effective detection and degradation systems.

Detection of nerve agents has been at the forefront of detection and degradation systems. The ease of exposure and the severity of toxicity have driven this area to include a wide range of detection methods. The major drawback of these systems has been problems with portability, real-time and complex use, and false positives.[7, 10-19] To address some of these issues, a shift towards the use of colorimetric[3-4] and fluorimetric[4-5] response systems has been seen. Optical response systems offered a rapid detection method, often

using only the naked eye as the detector. Though these systems have complications with false positives even now. [3-4]

While detection of toxic organophosphorus compounds has seen progress, degradation of these species is equally as important. There are several different methods that have been developed to destroy or degrade CWAs including incineration, hydrolysis or oxidation.[19-20] Often though, these degradation methods result in problems such as the transportation of the CWA's to only a few incineration plants and the use of toxic or corrosive chemicals such as bleach that further hinder decontamination.[2, 19, 21] A way to circumvent these problems is through the use of enzymes to degrade certain CWAs.[2] Enzymatic degradation of organophosphorus pesticides and nerve agents (**Figure 2.1**)[20] has been performed with organophosphorus hydrolase enzymes (OPH).[2, 6, 22-26] The general scheme for deactivating organophosphorus compounds is through the hydrolysis of P-S, P-O, P-F, and P-CN bonds.[22, 27]

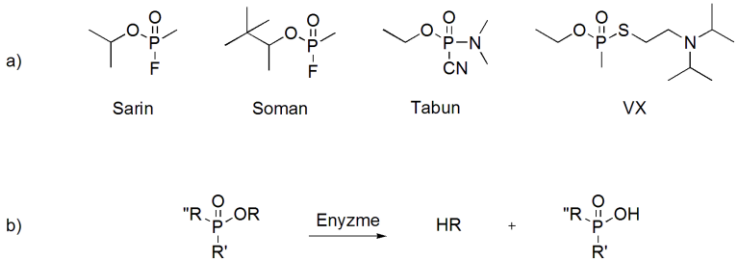

Figure 2.1: a) Structures of organophosphorus pesticides and nerve agents. b) General enzymatic hydrolysis.

While there has been great advancement in the areas of detection and decontamination separately, ideally, an all in one detection and decontamination system is desired. When considering the use of these systems in real-world applications, it is much more efficient to have a dual system. There are several aspects to consider when designing a dual system such as who is using this system, how effective is it and how much does this system cost. The goal of the current system addresses these issues by having a visual detection system that is easily discernable by an individual without specialized training, costs kept low by using a scaffold that can be produced in large quantities and utilizing a dual detection and decontamination system for increased efficiency.

The use of OPH as an efficient decontamination method has shown promise. Using an enzyme to accomplish the degradation of organophosphorus compounds has many advantages over the other common methods of degradation. The use of OPH allows for fast and efficient catalytic hydrolysis without leaving further toxic byproducts. This makes the system environmentally friendly and allows the system to be easily transported to areas that have been contaminated. The only complications with using an enzyme are their tendency to denature, however this can be avoided through immobilization.[28]

For the detection method for this system, visual indication will be used to keep the system easy to use. By only having to use the naked eye as a detector, portability is possible without the use of a physical detection system. There are a wide range of dyes

that can be used to give a quick response that the decontamination process is occurring.

To combine the detection and decontamination aspects, porous silica can be used as a scaffold to integrate these two systems. Using a porous silica support, specifically mesoporous silica, has several advantages. Immobilization will help prevent denaturation of OPH to extend the lifetime and has even been shown to increase the activity of OPH.[23, 28] The large range of pore diameters (2-50 nm), large surface areas (300-1500 m^2g^{-1}) and surfaces that can be easily functionalized, allows the mesoporous silica to be tailored.[28-30]

Utilization of the mesoporous silica scaffold will begin by first loading dye into the interior pore volume of the mesoporous silica to which OPH can be immobilized onto the silica surface. This serves a dual functionality of blocking the pores to keep the dye in, as well as decontaminating organophosphorus compounds upon its triggered release. To temporarily hold OPH to the surface, a competitive inhibitor of OPH can be used and will release OPH when in the presence of an organophosphorus compound (**Figure 2.2**). This system would offer an effective detection and decontamination method that is easily synthesized and simple to use by showing a visual change caused by a triggered release of the decontaminate.

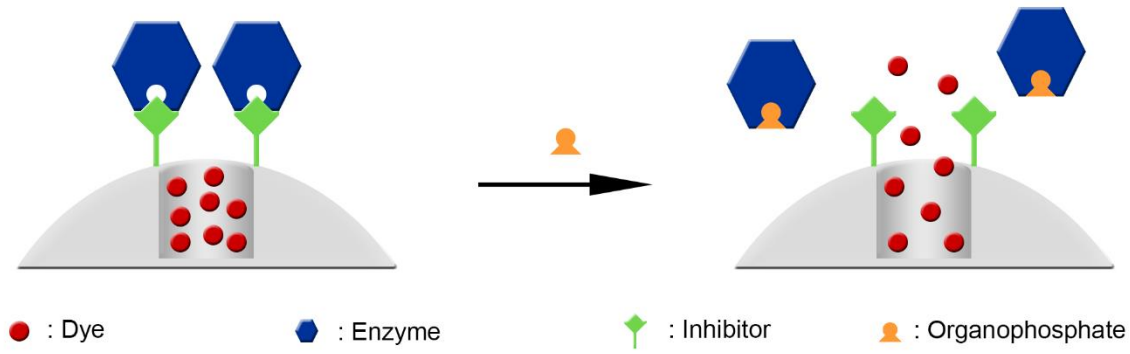

Figure 2.2: A model of simultaneous detection and decontamination of organophosphorus compounds.

2.2. Experimental Section

2.2.1. Materials and Instrumentation

All materials were purchased from Sigma-Aldrich, VWR and Life Technologies, unless otherwise noted. Nuclear Magnetic Resonance (NMR) spectra were recorded on a Bruker AVANCE III 500 MHz high-field NMR spectrophotometer with a multi nuclear observation capability. UV/Vis spectra were measured using a Perkin-Elmer Lambda 35 spectrophotometer system. Thermogravimetric analysis (TGA) was performed on a PerkinElmer Pyris 1 DSC-TGA. Scans were performed under a mixed flow of nitrogen (85%) and oxygen (15%) between 25 °C and 800 °C at 20 °C/min with a thermal hold at 100°C for 15 minutes to get rid of water. N_2 adsorption and desorption isotherms were obtained on a Micromeritics TriStar instrument. Surface areas were measured using the Brunauer-Emmett-Teller (BET) method and pore size distributions were calculated from a modified Kruk, Jaronic and Sayari (KJS) method using the adsorption branch.

2.2.2. Synthesis, Functionalization and Characterization of APMS

2.2.2.1. Synthesis of Acid-Prepared Mesoporous Silica (APMS)

APMS was synthesized as previously described. [31-32]

2.2.2.2. Synthesis of APMS-(s)-NH_2

Pore-blocked APMS (1.8 g) was suspended in hexanes (400 mL) to which 3-aminoproplytriethoxysilane (APTES) (1.8 mL) was added. The solution was refluxed for 3.5 hours under an inert atmosphere (N_2) to form the product APMS-(s)-NH_2. To remove surfactant from the pores, APMS-(s)-NH_2 was extracted by refluxing with acidified ethanol (0.1 M HCl in ethanol) for 24 hours (3X), filtering and letting dry between each cycle. The degree of modification was characterized by thermogravimetric analysis (2.02 mmol modification/g APMS) and the physical properties characterized by nitrogen physisorption. The resulting APMS was then placed under vacuum to keep dry until further modification.

2.2.2.3. Synthesis of APMS-(s)-NH-COOH

Extracted APMS-(s)-NH_2 (1.5 g) was suspended in acetonitrile (dry) under an inert atmosphere (N_2) to which triethylamine (950 µL) and succinic anhydride (355 mg) was added. The solution was stirred at 60°C for 21.5 hours then collected by vacuum filtration. Several washings with trifluoroacetic acid (0.1% in water) and acetonitrile were followed by drying overnight. The degree of modification was characterized by thermogravimetric analysis (0.606 mmol modification/g APMS) and the physical properties characterized by nitrogen physisorption. The resulting APMS-(s)-NH-COOH was then placed under vacuum to keep dry until further modification.

2.2.2.4. Synthesis of APMS-(s)-DEABP

To 200 mg APMS-(s)-NH-COOH suspended in 40 mL MES buffer (50 mM, pH

= 6.0), N-hydroxysuccinimide (10, 28 or 50 mg) was added and stirred at room temperature for 20 minutes. To this solution *N*-(3-Dimethylaminopropyl)-*N′*-ethylcarbodiimide hydrochloride (22, 55 or 90 mg) was added and stirred an additional 2.25 hours. A solution of diethyl 4-aminobenzyl phosphonate (DEABP) (20, 53 or 78 mg) in acetonitrile (dry, 1 mL) was then added slowly and stirred for 21 hours. The particles were collected by vacuum filtration and washed with deionized H_2O and acetonitrile and left to dry overnight. The degree of modification (0.151, 0.214, 0.414 mmol modification/g APMS, respectively) was determined by thermogravimetric analysis and the physical properties characterized by nitrogen physisorption. The resulting APMS-(s)-DEABP was then placed under vacuum to keep dry until further modification.

2.2.2.5. Synthesis of APMS-(s)-DEABP-OPH

To 5 mg APMS-(s)-DEABP suspended in 425 µL CHES buffer (20 mM, pH = 9.0), 175 µL OPH (453 µg/mL) was added and placed on a rotating platform for 21.75 hours. The sample was centrifuged, supernatant removed and immobilized OPH determined. The particles were washed with CHES buffer (3X) and re-suspended in the appropriate amount of CHES buffer for kinetics testing. Free OPH concentrations and amounts of OPH immobilized onto APMS-(s)-DEABP were calculated using the Bradford method (reference in main text) from a standard bovine serum albumin (BSA) calibration curve. Triplicate samples measured for standard curve.

2.2.3. Measurement of Enzymatic Activity.

2.2.3.1. ^{31}P NMR Assay

Samples were spun at 20 rps at 25 °C and ^{31}P shift was referenced to external

H_3PO_4 shift standard at 0 ppm. A 90° phosphorous pulse prior to acquisition was used to give maximum signal response for shorter acquisition time. An aliquot of deuterium oxide (50 µL) was added to each sample after the reaction was terminated but before transfer to the NMR tube for a field lock. A 100 ppm sweep width was used with approximately 20-200 scans depending on the conversion rate of the reaction.

2.2.3.2. Degradation of Paraoxon by Free OPH

To CHES buffer (20 mM, pH= 9.0, 440 µL), $CoCl_2$ (1.25 mM, 20 µL) and OPH (2.5 µg/mL, 20 µL) were added. A paraoxon stock (301 mM in methanol) was prepared and an aliquot added to give varying concentrations of paraoxon (2.45- 6.14 mM) in the solution and the time recorded. The sample was shaken for two minutes at which time OPH was denatured using sodium dodecyl sulfate (0.3 M, 50 µL). Each sample was run in triplicate and the enzymatic activity determined using ^{31}P NMR with a phosphoric external standard.

2.2.3.3. Inhibition of Free OPH by DEABP

To CHES buffer (20 mM, pH= 9.0, 440 µL), $CoCl_2$ (1.25 mM, 20 µL) and OPH (0.05 µg) were added. A stock solution of DEABP (100.5 mM) was prepared to which an aliquot was added to give varying concentrations of DEABP (16.4, 24.6 and 30.8 mM) in the reaction. The sample was shaken for five minute and then from a paraoxon stock (301 mM in methanol), an aliquot was added to give varying concentrations of paraoxon (2.45-6.14 mM) in the reaction and the time recorded. The sample was shaken for two minutes at which time OPH was denatured using sodium dodecyl sulfate (0.3 M, 50 µL). Each

sample was ran in triplicate and the enzymatic activity determined using ^{31}P NMR with a phosphoric external standard.

2.2.3.4. Degradation of Paraoxon Using APMS-(s)-DEABP-OPH

To CHES buffer (20 mM, pH= 9.0, 440 µL), $CoCl_2$ (1.25 mM, 20 µL) and APMS-(s)-DEABP-OPH (0.05 µg OPH total) were added. From a paraoxon stock (301 mM in methanol), an aliquot was added to give varying concentrations of paraoxon (2.45- 6.14 mM) in the reaction and the time recorded. The sample was shaken for 2 minutes at which the entire reaction mixture was filtered using a 0.2µm nylon membrane (25 mm) syringe filter. Each sample was run in triplicate and the enzymatic activity determined using ^{31}P NMR with a phosphoric external standard.

2.2.4. Congo Red Loading and Release Using OPH-Tethered Particles

2.2.4.1. Loading of Congo Red (APMS-CR-(s)-DEABP)

Congo Red (CR) (51.9 mg) was added to a citrate buffer (10 mL, 0.1 M, pH 2.3) to make a CR stock. In a typical loading procedure, APMS-(s)-DEABP (11.5 mg) was shaken (20 hr) with the CR stock (5 mL, 7.45 mM). The sample was centrifuged and the supernatant measured by UV-vis to determine the amount of CR loaded. The material was washed once with CHES buffer (20 mM, pH= 9.0) to prepare for loading with OPH.

2.2.4.2. Loading OPH (APMS-CR-(s)-DEABP-OPH)

To 11.5 mg APMS-CR-(s)-DEABP suspended in 400 µL CHES buffer (20 mM, pH = 9.0), 200 µL OPH (818 µg/mL) was added and placed on a rotating platform for

21.75 hours. The sample was centrifuged, supernatant removed and immobilized OPH determined. The particles were washed with CHES buffer until all non-encapsulated CR was removed. The particles were then re-suspended in the appropriate amount of CHES buffer for kinetics testing.

2.2.4.3. Release of Congo Red from APMS-CR-(s)-DEABP-OPH

In a typical reaction, to CHES buffer (20 mM, pH= 9.0, 1185 µL), $CoCl_2$ (1.25 mM, 60 µL) and APMS-(s)-OPH-DEABP (25.5 µg OPH total) were added. Testing using cell culture media was a 10% Fetal bovine serum (FBS) in Dulbecco's Modified Eagle Medium (DMEM) (no phenol red, glutamine or glucose, pH 7.4). A typical reaction sample, unless noted otherwise, was shaken for 15 minutes, centrifuged and supernatant measure to show no CR releasing. An aliquot of paraoxon was then added

resulting in final concentrations of paraoxon (1.66 – 8.28 mM). The sample was shaken for five minutes, centrifuged, supernatant measured and particles re-suspended. This process was repeated every five minutes for a total of 35 minutes unless otherwise noted. The amount of CR released was determined by UV-vis based on a calibration curve.

2.3. Results

2.3.1. ^{31}P NMR Assay of OPH Activity

Since ^{31}P NMR can be applied to a broad spectrum of organophosphorus compounds, it is a useful technique in comparing the activity of OPH with respect to various substrates. Although UV-Visible spectroscopy (UV-Vis) is somewhat simpler, it

requires the substrate to contain a chromophore, therefore it is only applicable to a subset of compounds. Similarly, gas chromatography techniques can be a problem for low volatility substrates. In contrast, ^{31}P NMR can be used for a wide variety of compounds, and the chemical shifts of the substrates and their hydrolyzed products are typically well-separated. As has been shown in our previous experiments, the integrated areas of the paraoxon peak at -6.45 ppm and diethyl phosphate peak at 0.80 ppm can be referenced to an internal standard (phosphoric acid, d = 0.00 ppm, inserted into the NMR sample in a sealed capillary), and ratios of the peak areas can then be used to give the percent conversion of the substrate. Removal of aliquots from the enzyme-substrate reaction solution at various points during the conversion process followed with a Lineweaver-Burk double-reciprocal plot, which in turn is used to extract information about the activity of OPH. In this manner, ^{31}P NMR was used to measure OPH activity in all of our experiments.

2.3.2. Inhibition of OPH Using DEABP

To determine the type of inhibition exhibited by DEABP, free OPH (i.e. not attached to a particle surface) was exposed to DEABP at several concentrations (16.4, 24.6 and 30.8 mM) in CHES buffer for five minutes, and then the activity of OPH toward paraoxon was determined by ^{31}P NMR (**Figure 2.3**). This was compared to the activity of OPH in the absence of DEABP with all samples (with or without inhibitor) containing the same amount of OPH (0.05 µg total) per sample.

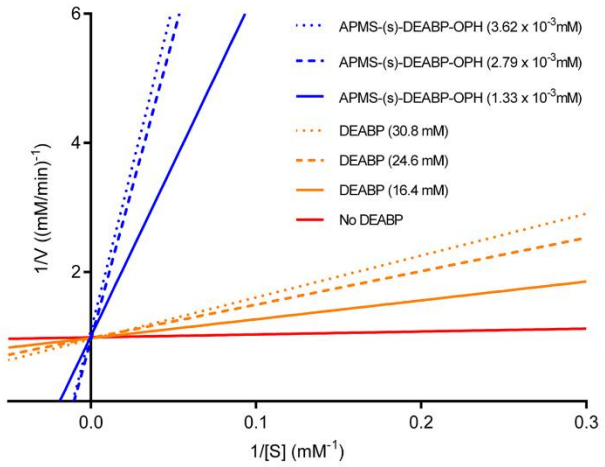

Figure 2.3: Lineweaver-Burk plots comparing competitive inhibition by tethered and free DEABP.

2.3.3. Preparation and Characterization of APMS-(s)-DEABP

Construction of the inhibitor-tethered substrate was accomplished as shown in **Figure 2.4**. First, as-prepared APMS (i.e., with surfactant remaining in the pores) was reacted with 3-aminopropyltriethyoxysilane (APTES). The surfactant was then extracted in HCl/EtOH to open the pores of the substrate, and the primary amine was reacted with succinic anhydride to produce a carboxylate-terminated surface. Standard peptide coupling methodology was then used to tether DEABP to the particle surface at three different concentrations. The resulting materials are designated APMS-(s)-DEABP (low), -DEABP (med), and -DEABP (high).

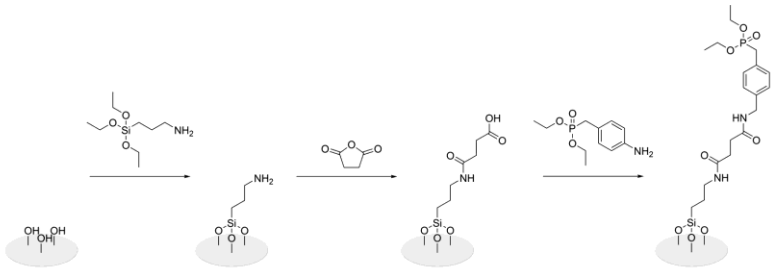

Figure 2.4: Synthesis of APMS-(s)-DEABP.

Thermogravimetric analysis (TGA) and N_2 physisorption (**Table 2.1**) were used to characterize the physical properties of the materials at each stage of modification. To provide a basis for the calculation of the amount of organic modification of each material, a portion of the initial batch of APMS was calcined to completely remove the surfactant. This represented the maximum possible porosity of the material. The surface area of the base material was modest (385 m^2/g), although it was consistent with a pore diameter of 11 nm.

Table 2.1: Physical properties of APMS and modified APMS.

Sample	SA_{BET} (m^2/g)	V_{pore} (cm^3/g)	d_{pore} (nm)	modification (mmol/g)
APMS (calcined)	385	0.89	11	--
APMS-(s)-NH_2 (extracted)	270	0.62	11	2.02
APMS-(s)-NH-COOH	233	0.54	9.1	0.61
APMS-(s)-DEABP-(low)	238	0.53	9.1	0.15
APMS-(s)-DEABP-(med)	192	0.43	8.5	0.21
APMS-(s)-DEABP-(high)	178	0.40	8.6	0.41

2.3.4. Inhibition Testing of APMS-(s)-DEABP-OPH

OPH was stirred with APMS-(s)-DEABP (low, med, and high) for 21.75 h, and the particles were washed with CHES buffer. The amount of OPH remaining was determined in each case by the Bradford Assay on the loading solution supernatant after centrifugation. The amount of OPH loaded was determined from the initial Bradford Assay on the loading solution. Each APMS-(s)-DEABP-OPH material loaded different amounts of OPH, so adjustments were made so that each reaction contained the same amount of OPH (0.05 μg OPH total). Inhibition tests were then performed on the basis of the amount of immobilized DEABP, using the ^{31}P NMR assay described above (**Figure 2.3**).

2.3.5. Dye Release from APMS-CR-(s)-DEABP-OPH (Single Addition)

The loading of CR within APMS-(s)-DEABP (high) varied depending on the

material, but a typical loading was 0.168 mM dye/mg particles that resulted in a deep red coloring (**Figure 2.5**). A control experiment was conducted to determine the amount of CR that would release without OPH capping the pores. After loading, APMS-CR-(s)-DEABP was washed extensively CHES buffer, centrifuging and re-suspending in fresh CHES each time. It was then shaken for one hr and supernatant measured by UV-Vis for any CR in solution. This was repeated for a total of five cycles until no further CR could be detected by UV-Vis. The particles were now faint pink in color and were dried under vacuum and TGA performed. There was approximately 15% of CR left in the particles that could not be removed.

OPH was then added as described previously, to form APMS-CR-(s)-DEABP-OPH. Before paraoxon was used to test the complete detection and decontamination system, the particles were shaken for 15 minutes and the supernatant measured to ensure no CR was releasing. A 2.5 µL aliquot of paraoxon was added, resulting in a paraoxon concentration of 8.28 mM in the system. The concentration of dye in the supernatant was measured every five minutes to track the release of CR after triggered release of OPH using UV-Vis (**Figure 2.5**).

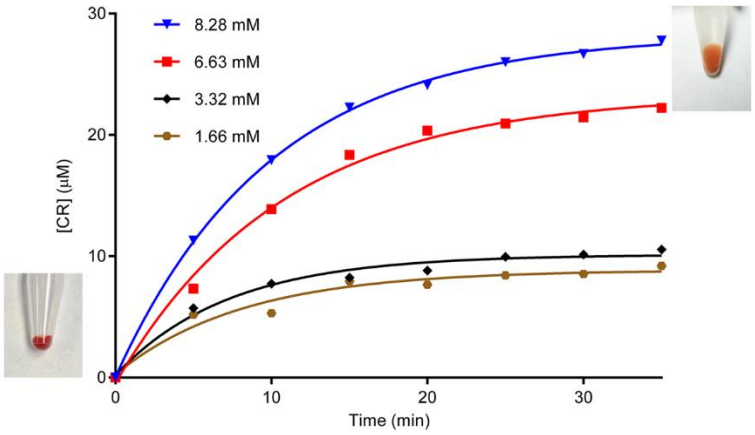

Figure 2.5: Congo Red release at several concentrations of paraoxon.

This was repeated with three additional concentrations of paraoxon 6.63, 3.32 and 1.66 mM. The release profiles were plotted and fit as pseudo-first order association kinetics to determine the initial release rates and maximum (plateau) amount of dye released (**Table 2.2**). A change of particle color from a deep red to a dark pink could be seen by the naked eye (**Figure 2.5**).

Table 2.2: Congo Red release rates from APMS-CR-(s)-DEABP-OPH vs. [Paraoxon].

[Paraoxon] (mM)	Initial Rate (μM/min)	Maximum Release (μM)
8.28	2.26	28.3
6.63	1.46	23.4
3.32	1.14	10.1
1.66	1.04	8.9

2.3.6. Dye Release from APMS-CR-(s)-DEABP-OPH (Multiple Additions)

APMS-CR-(s)-DEABP-OPH (high) was prepared as previously described. Compared to previous testing, more OPH (0.071 µg) was used compared to the previous experiments. To ensure that CR was not leaching from the particles, the supernatant was measured every four min before the first addition of paraoxon (6.63 mM in solution) after the 12 min measurement (**Figure 2.6**). Subsequent measurement of the supernatant by UV-Vis tracked the release of CR. After the plateau (~20 min) and additional aliquot of paraoxon (6.63 mM in solution) was added after the 28 min measurement. The supernatant continued to be measured until the second plateau was reached (~48 min).

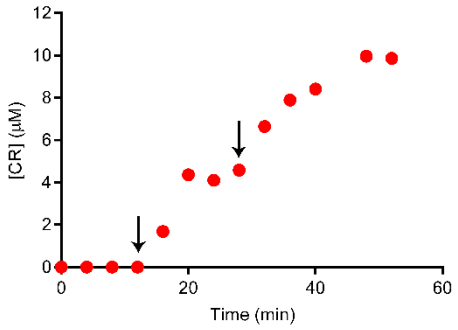

Figure 2.6: Congo Red release with multiple additions of paraoxon (indicated by arrow).

2.3.7. Dye Release from APMS-CR-(s)-DEABP-OPH (Recycling)

To show the recycling ability of APMS-CR-(s)-DEABP-OPH, the material was sequentially exposed to paraoxon, 4.97 mM total in the system, with several washes with CHES buffer between exposures. This was to insure that the only measured dye would be released from the particles and not physisorbed (**Figure 2.7**). The amount of dye released

in the second test was approximately 60% of the original amount (3.3 vs. 5.5 µM).

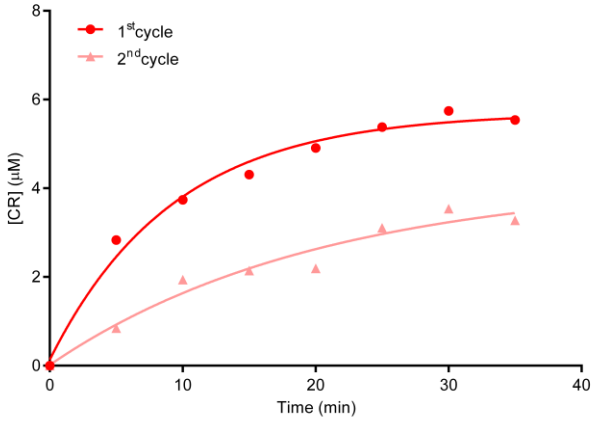

Figure 2.7: Sequential release of dye from APMS-CR-(s)-DEABP-OPH.

2.3.8. Dye Release from APMS-CR-(s)-DEABP-OPH (10% FBS)

APMS-CR-(s)-DEABP-OPH was prepared as previously described. After the final wash with CHES buffer, the buffer was exchanged by washing three times with 10% FBS. The particles were shaken and centrifuged every five minutes and the supernatant measured by UV-Vis for 35 min to track any release of CR (less than 8 % of the total released). A 2.5 µL aliquot of paraoxon was added after the 35 min reading, resulting in a paraoxon concentration of 8.28 mM in the system. The concentration of dye in the supernatant was measured every five minutes to track the release of CR after triggered release of OPH using UV-Vis (**Figure 2.8**). With the addition of paraoxon, a large release of CR was seen with a rate of 0.41 µM/min with a maximum release (plateau) of 9.5 µM.

In comparison to previous experiments with a similar concentration of paraoxon (8.28 mM), the amount of CR red released was about one-third that of the maximum release (28.3 µM). The final supernatant was diluted 100-fold to measure the absorbance of the product peak (4-nitrophenol, 405 nm) to ensure that the hydrolysis of paraoxon occurred.

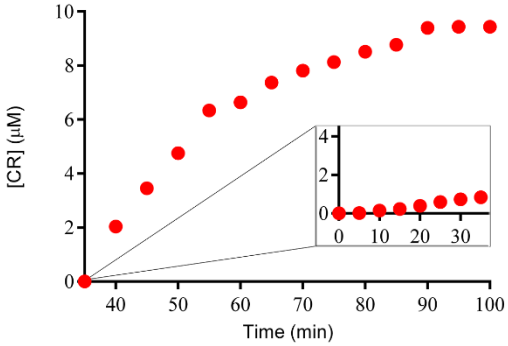

Figure 2.8: Dye release in 10% FBS, pH 7.4.

2.3.9. Dye Release from APMS-CR-(s)-DEABP-OPH (10% FBS) (Recycling)

After the previous release in FBS was completed, the material was washed several times with fresh FBS to remove any remaining paraoxon, CR or OPH (previously released). A second aliquot of paraoxon was added to give a total concentration of 0.3 mM of paraoxon. The hydrolysis of paraoxon was tracked by UV-Vis, measuring the absorbance of the hydrolysis product, 4-nitrophenol at 405 nm. This was done every five minutes for 30 minutes. This was then compared to a background hydrolysis of paraoxon in FBS over the course of 90 minutes (**Figure 2.9**). Using a calibration curve of 4-nitrophenol, the concentration of product in solution could be attained. The tracking of the hydrolysis was

confirmed by recycling the material, as previously done, however using a lower concentration of paraoxon to easily track the hydrolysis product (**Figure 2.9**). This was compared to a background hydrolysis of paraoxon to ensure that conversion of the substrate was due to OPH and not by the other proteins within the culture media. The background conversion was minimal and appeared immediately after addition of the aliquot of paraoxon and held constant throughout the remaining measurements.

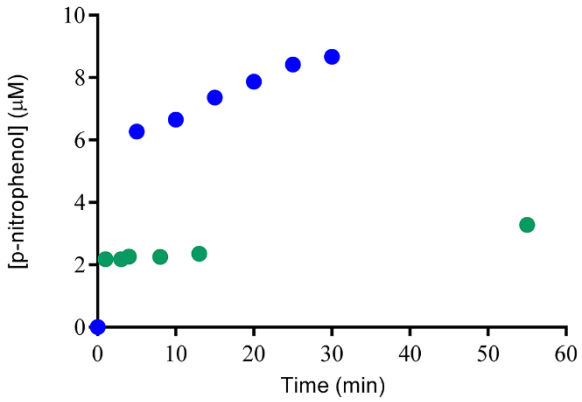

Figure 2.9: Hydrolysis of paraoxon in 10% FBS, pH 7.4. APMS-CR-(s)-DEABP-OPH (blue); Paraoxon only (green).

2.4. Discussion

2.4.1. Selection of Scaffold

The duality of a detection and decontamination system for organophoshates relies on the cooperation of several elements simulataniously within a self-contained system. The system presented has several parts that are controlled by the initial response to an organophosphate. This triggered response controls both parts of the detetection and

decontamination system by releasing OPH to decontaminate and the visual change to occur. The sensitiviy and speed of the system relies on the mechanism which releases OPH from the scaffold. This required a scaffold that could retain the activity of OPH and allow for the addtion of a visual indicator.

The use of APMS as the solid support for the self-contained system had several advantages. We[23] and others[33-35] have previously shown that the activity and thermal stability of OPH can be altered upon immobilization within the pores of mesoporous silica. Manipultion of the physical characteristics such as surface area and pore diameter allowed for the tailoring of the material for surface functionalization and dye loading and release. Larger pores (8-9 nm) permitted CR to easily enter and exit the interior volume of APMS and the exterior surface functionalized to readily accept OPH to trap CR inside. Preparation of the surface of APMS to temporarly hold OPH was the most important but challenging aspect of the system. OPH had to function as the decontaminat, as well as hold back the release of CR from the interior pore volume. The desired trigger for the release of OPH had to be more specific than a chemical or physical change in the reaction conditions to be a self-contained system. The temporary hold of OPH eluded to the possibility of using an inhibitor of OPH that could be displaced by the substrate, paraoxon.

2.4.2. Selection of Inhibitor

In these studies, our goal was not to permanently immobilize OPH, but to tether it to the surface of a porous silica nanoparticles with an inhibitor that could be displaced upon recognition of a different organophosphorus substrate. There were several factors to consider when selecting the inhibitor, the most important of these was the type of inibition

it had on OPH. As the trigger, the inibitor had to be competitive to ensure that OPH would release and in the shortest amount of time. Noncompetitive and uncompetitive inhibitors would result in slow or no release of OPH and could decrease the rate of hydrolysis. Using an inhibitor that was similar in structure to paraoxon and had previously been found to be a competitive inhibitor[36] was the starting point for probing its use as an immobilized inhibitor.

We chose diethyl-4-nitrophenyl phosphate (paraoxon) and diethyl-4-aminobenzyl phosphonate (DEABP) as the substrate and inhibitor for these experiments (**Figure 2.10**). OPH rapidly reacts with paraoxon, making it easy to determine enzyme activity. DEABP has a similar structure to paraoxon, but the *p*-nitrophenyl group is connected to the phosphorus atom through a carbon atom instead of an oxygen atom. This ensures that the hydrolytic cleavage of the *p*-nitrophenyl group cannot occur, although the molecule's size is similar to paraoxon. In addition, the terminal amine allows DEABP to covalently attached to the particle's surface with standard peptide coupling methodology. This would allow for the temporary holding of OPH to the surface of APMS in the absence of a compadiable substrate and then release in the prensence of paraoxon or other organophosphate.

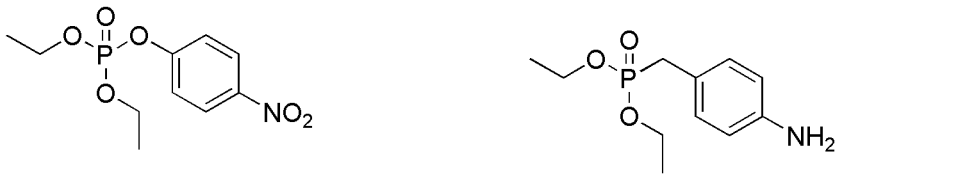

Figure 2.10: Structures of the substrate and inhibitor used in these experiments.

2.4.3. Type of Inhibition

To confirm the type of inhibition DEABP has with OPH, activity of OPH hydrolyzing paraoxon with and without DEABP were measured and plotted as Lineweaver-Burk plot. A Lineweaver-Burk plot is a useful tool to study enzymatic inhibition, because the effects of competitive and non-competitive inhibition produce graphically distinct results that are easily observed. In competitive inhibition, the y intercept ($1/V_{max}$) remains the same in the presence of the inhibitor although the x intercept ($-1/K_M$) decreases because the observed binding constant of the substrate changes in the presence of a competitive inhibitor, although at sufficiently high concentrations of substrate the maximum velocity of the reaction remains the same. The new x intercept, $-1/(1+[I]K_I$, where [I] = the concentration of inhibitor and K_I is the dissociation constant of the inhibitor with respect to the enzyme, is sensitive to the concentration of inhibitor.[3738] (The results are shown in **Figure 2.3)** The y-intercept of all plots was identical, and the x intercepts of each plot decreased as the concentration of DEABP increased. This shows that DEABP is a competitive inhibitor of OPH, reversibly binding at the active site and being released at higher concentrations of paraoxon.

2.4.4. Synthesis of APMS-(s)-DEABP

The characterization of APMS-(s)-APMS was important to ensure that the design of the scaffold not only was correct but retained the desired structural characteristics. Characterization of the as-prepared APMS (calcined) confirmed an appropriate starting material for the final desired APMS-(s)-DEABP. A larger pore diameter was desired to compensate for the tightening of the pore diameter resulting from the organic functionalization. This allowed for the final pore diameter to be large enough for the dye to enter but more importantly allow for a faster release of dye from the interior pore volume without restriction. The pore volume (0.89 cm^3/g) of a material with this surface area and pore diameter suggested a porous material with highly interconnected pore structure, consistent with previous publications on APMS. This allowed for adequate volume for the dye to be held after addition of OPH to cap the pores.

The desired surface functionalization of APMS can be seen in **Figure 2.11 (Ideal)**. Each synthetic step factored into the number of potential inhibition sites because the degree of each modification is dependent on the previous. The goal of the amine addition was to thoroughly populate the surface of APMS to keep OPH on the surface of the particle, although some diffusion of APTES within the surfactant micelles is expected.[38] Surface functionalization not only increases the potential of OPH to block the pores of the material but increases the potential for a faster triggered release. If functionalization occurred deeper within the mesoporous structure, the more problematic the diffusion of substrate would be to active site of OPH (**Figure 2.11 A**). Functionalization of the interior could also increase the surface charge to more positive due to the protonation

of the amine groups. Retention of the interior volume was also necessary for maximum dye loading needed to increase the potential amount and rate of dye released after loss of OPH.

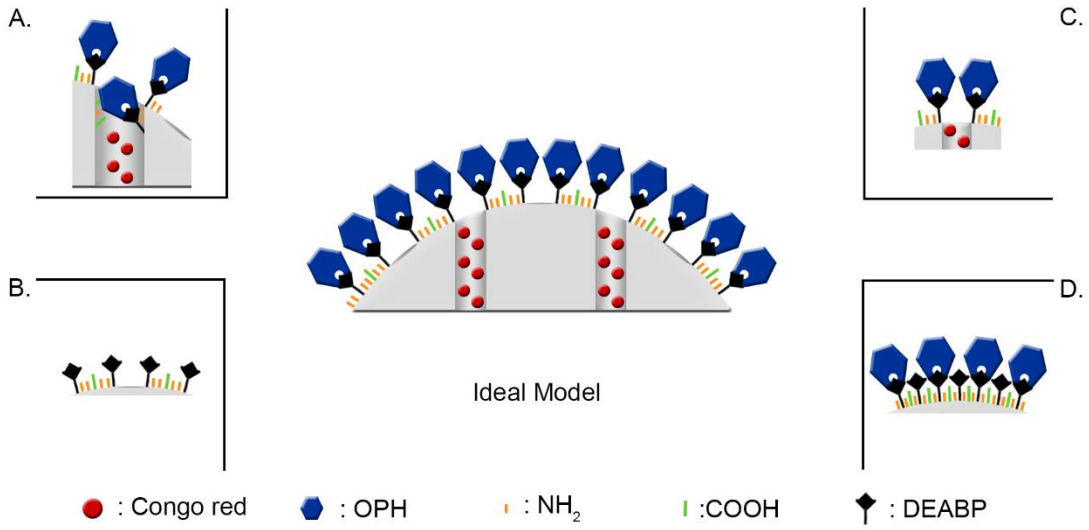

Figure 2.11: Conceptual influences on surface functionalization and OPH loading and CR releasing.

TGA data used to show the extent of modification indicated that the external surface was easily modified with APTES, though because the amount of modification with succinic anhydride was less than the total amount of amines available (0.61 mmol/g versus 2.02 mmol/g), not all of the amine groups reacted with succinic anhydride. However, coupling to DEABP appeared to be successful and controllable, with the amount of DEABP on the surface directly related to the amount used in the synthesis (**Table 2.1**). The capping of unreacted amine and succinic anhydride groups was found to not be necessary because it did not influence the inhibition of OPH or its release, shown later in activity

testing (**Figure 2.11 B**). The porosity of the material decreased after each modification, as indicated by the decreasing SA_{BET}, V_{pore}, and d_{pore} in each step. This indicated that there was likely some modification not only of the external particle surface, but of the pore entrances as well. However, the amount of pore modification was not significant enough to completely close the pores, so that they could still be loaded with dye in a later step.

2.4.5. Immobilization of OPH

The immobilization of OPH onto the surface of APMS-(s)-DEABP was controlled by many factors. An ideal material would have the maximum amount of OPH directly proportional to the amount of DEABP on the surface because of the single catalytic site of OPH (**Figure 2.11 (Ideal)**).[36] Nevertheless, this does not account for other variables that influence the amount OPH that could be immobilized. The main restriction was the amount of OPH that could physically fit on the surface of APMS. A single OPH molecule is approximately 6.1 nm x 8.6 nm x 5.1 nm.[39] If two inhibitor molecules were at a distance less than the smallest dimension (51Å), only one OPH would attach. This can be extended to the other dimensions of OPH, as well as the density of inhibitor on the surface.

The packing on the surface of APMS was also influenced by the size of the pores (8.6-9.1 nm) that were desired for the fast loading and release of dye. To ensure that the pores would be effectively capped, two or more OPH molecules had to be in close enough proximity (**Figure 2.11 C**). Without the close packing on the surface, the dye would leach from the interior pore volume. As previously discussed, steps were taken to control the number of inhibitor molecules available but always exceeded the amount of OPH that attached **(Table 2.3**). This was to ensure that there was adequate surface coverage of OPH

on the surface (**Figure 2.11 D**).

Table 2.3: Ratio of each linker on APMS surface to OPH loaded.

	Linker/Sample/OPH		
Sample	*[NH_2]* (mM/µg OPH)	*[COOH]* (mM/µg OPH)	*[DEABP]* (mM/µg OPH)
APMS-(s)-DEABP-(low)	2.49E-01	8.02E-02	2.66E-02
APMS-(s)-DEABP-(med)	3.68E-01	1.02E-01	5.57E-02
APMS-(s)-DEABP-(high)	2.47E-01	3.35E-02	7.25E-02

2.4.6. Inhibition Testing of APMS-(s)-DEABP-OPH

With DEABP successfully tethered to the particle surfaces, we next confirmed that DEABP still acted as a competitive inhibitor of paraoxon after the tethering process. The Lineweaver-Burk plot (**Figure 2.3**) for tethered OPH shows that DEABP continued to act as a competitive inhibitor, because the y-intercept for the samples did not change when the amount of DEABP changed. What is quite interesting about this plot was that although the amount of tethered DEABP was much lower than that in tests using free DEABP (µM here versus mM in **Figure 2.3**), the slopes of the lines here are significantly larger. As described above, smaller concentrations of a competitive inhibitor are expected to show smaller slopes. This is likely due to a concentration effect produced by immobilizing the DEABP. When it is free, OPH must diffuse through solution between encounters with

DEABP. However, when the DEABP is tethered to a surface, its local concentration is much higher (**Table 2.3**), so the diffusion length between DEABP-OPH encounters is much shorter, and the effective inhibition of OPH is larger. Thus, it appears that when it is tethered to a surface, less inhibitor is required to achieve a significant inhibitory effect than if the inhibitor were dissolved in solution.[40] This is evident in the calculation of the K_I values for the free inhibitor (2.55 mM) versus immobilized (1.37×10^{-5} mM**).** The drastic decrease in K_I for immobilized was attributed to the immobilization of the inhibitor the surface, locking it into a set orientation. Once OPH was in the correct orientation to bind the inhibitor within its active site, it was held tightly. Comparing this to the free inhibitor and free enzyme, the inhibitor was free to move about the solution allowing it to bind weakly within the active site. This results with the free inhibitor have a much larger K_I. In terms of a triggered release system, the large slope indicates that the system is effective at very low concentrations of substrate and is sensitive to small chan,es in substrate concentrations.

2.4.7. Dye Selection

We tested several dyes for use in this detection system, and found that optimizing hydrophobic and electrostatic interactions with the silica surface were critical factors. Some dyes bound to the silica particles tightly but would not be released in sufficient quantities once the pores were opened; others bound so loosely that not enough dye was loaded into the particles in the first place. After multiple experiments, Congo Red (CR) (pK_a = 4.1, **Figure 2.12**) was selected as the detection dye because it could be loaded in significant amounts at pH = 2.3, where it was protonated and had a neutral charge, binding

weakly to the anionic surface of APMS.

Under the conditions used to allow the interaction of OPH with the surface-bound inhibitor (pH ≈ 9), the surface of APMS had a negative ζ potential due to the deprotonation of surface silanols.[23] CR deprotonated at this pH and was now repelled from the pore surfaces, but the OPH-inhibitor interaction occurred faster than the release of the dye, so the majority of the dye remained trapped within the pores. Control experiments showed the potential release of almost all of the CR with only about 15% remaining within the particles. This was attributed to the structural characteristics of the modified material. The interconnected pore system allows for loading deep within the pore system and pockets of differing surface charge. This retained a small amount CR permanently but the majority freely releasing. The particles were then washed several times to insure that any physisorbed dye was removed. It was now ready for rapid release once OPH encountered its substrate.

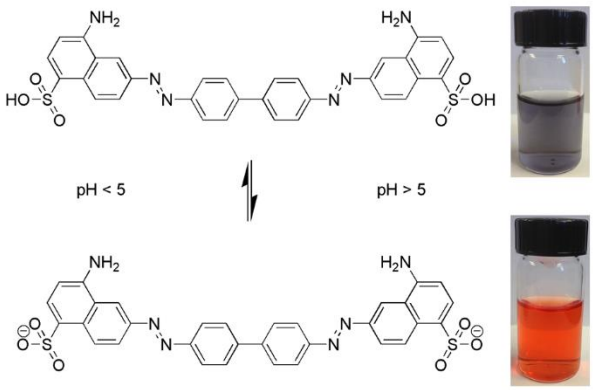

Figure 2.12: Structure and color of protonated and deprotonated forms of Congo Red.

2.4.8. Response of APMS-CR-(s)-DEABP-OPH to Paraoxon

Several experiments were first performed to test the response of the system with the ideal substrate, paraoxon. The release of OPH with a single, set concentration of paraoxon showed several key benefits of the system (**Figure 2.5**). One of the major goals of the system design was to visually indicate the presence of an organophosphate for ease of use in real-world applications. A change in color by the naked eye could be easily detected before and after exposure to paraoxon. The initial color of the material was deep red and the release of CR after exposure to paraoxon, resulted in a material that was noticeably lighter in color (dark pink) in a short amount of time. This allows for facile determination of the presence of an organophosphate without instrumentation and specialized training. The use of UV-Vis to quantify the CR release but helps to confirm not only the response time of this visual indication, but also lends to information about the response of the system in the presence of paraoxon.

Of the four concentrations tested (1.66, 3.32, 6.63, and 8.28 mM) a measurable signal could already be detected after only five minutes and the maximum signal (plateau) reached within 15-25 minutes, depending on the paraoxon concentration. This fast response resulted from the effective combination of having a competitive inhibitor as the trigger mechanism and the fast release of CR from the interior pore volume. This release profile also gives insight on the mechanism of the triggered release.

At lower concentrations (1.66 to 3.32 mM), doubling the paraoxon concentration only increases the amount of CR released from 8.9 to 10.1 μM (**Table 2.1**). Comparing this to doubling the paraoxon concentration from 3.32 to 6.63 mM, the amount of CR more

than doubles, resulting from a large burst release. Once OPH is released from the surface, it is free to begin hydrolyzing any substrate molecules within its reach. With lower concentrations of paraoxon, there is less substrate to initially release OPH and what does release, quickly hydrolyzes the substrate so no further OPH is needed. With only a small amount of OPH releasing, the potential amount of CR released was limited by the pores that were now uncapped. With higher concentrations, there was a large amount of substrate initially that caused a larger amount of OPH to release from the surface. This resulted in a greater number of pores to be uncapped and resulted in a higher potential amount of CR releasing from the particles. The amount of CR released lead to the faster plateau of the lower paraoxon concentrations (~10 min), compared to the large initial burst but longer time until plateau (~20-25 min) due to the CR still releasing from the larger number of uncapped pores.

The idea that the quick release of CR at low concentrations resulted from a small number of OPH enzymes leaving, would result with the potential to continue to release OPH and recycle the particles. In similar fashion to testing with a single aliquot of paraoxon, APMS-CR-(s)-DEABP-OPH was subjected to two aliquots of paraoxon while allowing the material to reach a plateau before the addition of the second aliquot (**Figure 2.6**). The concentration of paraoxon (6.63 mM) added was adjusted to compensate for the larger amount of OPH used for the experiment. A larger ratio of OPH to paraoxon of the first aliquot allowed the equilibrium to be reached quickly (less than eight min) and the second aliquot of the same concentration added. This took a longer time to reach plateau (20 min) but the total amount of CR released with similar kinetics to that of the first plateau

of about 5 μM. The slower time to reach the plateau was attributed to the smaller number of OPH molecules on the surface of APMS-CR-(s)-DEABP-OPH after the first release, as well as competition with released OPH. Released OPH was still viable for hydrolyzing any further paraoxon entering the system. With the addition of more paraoxon, a temporary increase in the total concentration paraoxon prompted additional OPH to be released. This resulted in the increase of CR similar to that seen with previous experiments with larger concentrations of paraoxon with a large initial burst and slower plateau. The temporary increase in paraoxon concentration was a result of the experiment itself in which the addition of paraoxon resulted from the plateau of CR, not the complete degradation of paraoxon.

The recycling of APMS-CR-(s)-DEABP-OPH was such that after exposure to an aliquot of paraoxon, the particles were washed, isolated and experiment performed again with an additional aliquot of paraoxon (**Figure 2.7**). The isolation and thorough washing of the particles ensured that the CR released would be from the second aliquot of paraoxon and not residual CR still releasing from the pores. It also ensured that any released OPH was fully removed from the solution and that OPH released would be only from the paraoxon used in the second cycle. Using the low (1.66 mM) and high (8.28 mM) concentrations of paraoxon as the boundaries, a mid-range concentration (4.97 mM) was used to probe the recyclability and determine the type of release at this range. The initial loading of CR in APMS-(s)-DEABP was lower than in previous samples which resulted in a lower plateau as compared to previous samples but the design of the system was still the same. This resulted in the expected release profile in which there was steady release of CR

that took longer than the lower concentrations of paraoxon but did not have the burst release as with the higher concentrations of paraoxon. This mid-range concentration also helped to ensure that there would be OPH still left on the surface for a second use. The second exposure to paraoxon showed a similar but slightly slower release profile. When the plateau was reached, the second cycle still released approximately 60% of the CR that the first cycle produced. This shows that there were still enough OPH-capped pores left after a single cycle the material could still produce a measurable signal within a short amount of time.

2.4.9. Selectivity of Trigger

The final set of experiments was to test the selectivity of the system in the presence of cell culture media. Generally, FBS contributes to the cell growth and division by providing necessary of growth factors and other proteins in culture media.[41] The use of this solution was to see if the designed triggered release system could differentiate between the variety of other proteins in solution and the desired substrate, paraoxon. To ensure that CR was released only by paraoxon, the APMS-CR-(s)-DEABP-OPH was first shaken and the supernatant measured to track any release of CR from the material, which was negligible in comparison to the release of CR after paraoxon addition (**Figure 2.8**).

Comparison of the ideal conditions to the cell culture media resulted in a maximum release concentration that was about 66% lower than under ideal conditions The ideal conditions were in CHES buffer at a more basic pH of 9.0, in which OPH is most active for the hydrolysis of paraoxon.[42] Using FBS drops the pH to physiological conditions of pH 7.4, which lowers the rate of hydrolysis of paraoxon by OPH. This would

lead to a change in the release pattern of OPH from the surface of APMS-CR-(s)-DEABP-OPH. The other contributing influence would be the other proteins that are present within the media. Interaction of paraoxon and APMS-CR-(s)-DEABP-OPH with these proteins (attraction and/or repulsion) will alter the rate at which OPH is displaced and the resulting release of CR.

Despite the lower release maximum of CR in culture media, the actual amount of CR released was more than sufficient to be easily detected and quantified. The ability for the system to differentiate between the desired substrate mixed within a system of a variety of biological proteins was attributed the design of the triggered release system. Using a competitive inhibitor based trigger allows for substrate specificity that is controlled solely by the enzyme, drastically improving the overall efficiency of the detection and decontamination system.

With confirmation that CR was releasing from APMS-CR-(s)-DEABP-OPH, the last step was to confirm that the OPH that was released continued with the hydrolysis of paraoxon. This could be easily obtained by measuring the UV-active hydrolysis product, 4-nitrophenol. The concentration of 4-nitrophenol (**Figure 2.9**) for the background reaction that contained only paraoxon and FBS remained constant after an initial spike after addition of the paraoxon. This differentiated from the sample that contained APMS-CR-(s)-DEABP-OPH, in which the hydrolysis reaction was evident by the increasing concentration of 4-nitrophenol over time. The increase in 4-nitrophenol proves that the OPH is still actively hydrolyzing paraoxon after the triggered release from the competitive inhibitor. This ensures that the release system does not deactivate OPH once released from

the surface in the presence of CR and that the other proteins within the cell media do not hinder the hydrolysis of paraoxon by OPH.

The use of this detection and decontamination system within physiological conditions adds in multiple factors that could have negatively affected the system from release of OPH without the substrate or prevention of CR release. The triggered release of active OPH from the competitive inhibitor proves the high substrate specificity of the system and the ease of the detection system by CR release shows the versatility of the dual system, outside of ideal conditions.

2.5. Conclusions

The detection and degradation of organophosphorus compounds is an important chemical and biochem research focus, because many of these compounds are neurotoxins that have been used as insecticides and stockpiled as chemical warfare agents. The ideal systems for this purpose would be triggered by the presence of the organophosphorus compound, decontaminate it, and give a visual response of this process. The use of APMS as the scaffold has several physical characteristics that can be tailored to support the decontaminate (OPH) and contain the detection element (CR) as a dual functioning system.

In the system described here, the interior pore volume of APMS was loaded with CR, and the exterior of particle was capped with an inhibited OPH that was released in the presence of a target organophosphorus compound. Specifically, the exterior of mesoporous silica nanoparticles was functionalized with diethyl 4-aminobenzyl phosphonate (DEABP). The competitive inhibition of OPH, both free in solution and immobilized DEABP, was confirmed through enzyme kinetics testing using ^{31}P NMR. The competitive

inhibition was used as the trigger for the release of OPH, uncapping the pores and releasing of CR. Color change of the particles was used as visual indication, along with quantification by UV-Vis. This system worked with not only the ideal conditions, but within cell culture media containing a variety proteins and growth factors,

maintain the activity of OPH and detection of CR.

The use of a dual detection and decontamination system is beneficial not only in the realm of organophosphate disposal and protection but the mechanism in which the system is triggered. The concept of using the desired substrate as the trigger is ideal but often difficult to obtain. Utilization of a competitive enzyme-inhibitor pair allows substrate specificity to be built in to the trigger mechanism for a system that requires no additional influence, chemical or physical, to give a visual response. Extension of the use of this type of trigger can be realized in other applications in which substrate specificity is highly desired.

2.6. References

1. Kim, K.; Tsay, O. G.; Atwood, D. A.; Churchill, D. G. Destruction and detection of chemical warfare agents. *Chem. Rev.* **2011**, *111*, 5345-5403.

2. Yang, Y. C.; Baker, J. A.; Ward, J. R. Decontamination of chemical warfare agents. *Chem. Rev.* **1992**, *92*, 1729-1743.

3. Climent, E.; Marti, A.; Royo, S.; Martinez-Manez, R.; Marcos, M. D.; Sancenon, F.; Soto, J.; Costero, A. M.; Gil, S.; Parra, M. Chromogenic detection of nerve agent mimics by mass transport control at the surface of bifunctionalized silica nanoparticles. *Angew. Chem. Int. Ed. Engl.* **2010**, *49*, 5945-5948.

4. Royo, S.; Martinez-Manez, R.; Sancenon, F.; Costero, A. M.; Parra, M.; Gil, S. Chromogenic and fluorogenic reagents for chemical warfare nerve agents' detection. *Chem. Commun.* **2007**, 4839-4847.

5. Diaz de Grenu, B.; Moreno, D.; Torroba, T.; Berg, A.; Gunnars, J.; Nilsson, T.; Nyman, R.; Persson, M.; Pettersson, J.; Eklind, I.; Wasterby, P. Fluorescent discrimination between traces of chemical warfare agents and their mimics. *J. Am. Chem. Soc.* **2014**, *136*, 4125-4128.

6. El-Boubbou, K.; Schofield, D. A.; Landry, C. C. Enhanced enzymatic activity of oph in ammonium-functionalized mesoporous silica: Surface modification and pore effects. *J. Phys. Chem. C* **2012**, *116*, 17501-17506.

7. Yu, D.; Volponi, J.; Chhabra, S.; Brinker, C. J.; Mulchandani, A.; Singh, A. K. Aqueous sol-gel encapsulation of genetically engineered moraxella spp. Cells for the detection of organophosphates. *Biosens. Bioelectron.* **2005**, *20*, 1433-1437.

8. Chauhan, S.; Chauhan, S.; D'Cruz, R.; Faruqi, S.; Singh, K. K.; Varma, S.; Singh, M.; Karthik, V. Chemical warfare agents. *Environ. Toxicol. Pharmacol.* **2008**, *26*, 113-122.

9. Syria and the organisation for the prohibition of chemical weapons. http://www.opcw.org/special-sections/syria-and-the-opcw/ (accessed April 18, 2014).

10. Nieuwenhuizen, M. S.; Harteveld, J. L. N. Studies on a surface acoustic wave (saw) dosimeter sensor for organophosphorous nerve agents. *Sens. Actuators B* **1997**, *40*, 167-173.

11. Ngeh-Ngwainbi, J.; Foley, P. H.; Kaun, S. S.; Guilbault, G. G. Parathion antibodies on piezoelectric crystals. *J. Am. Chem. Soc.* **1986**, *108*, 5444-5447.

12. Yang, Y. M.; Ji, H.-F.; Thundat, T. Nerve agents detection using a cu2+/l-cysteine bilayer-coated microcantilever. *J. Am. Chem. Soc.* **2003**, *125*, 1124-1125.

13. Hartmann-Thompson, C.; Hin, J.; Kaganove, S. N.; Keinath, S. E.; Keeley, D. L.; Dvornic, P. R. Hydrogen-bond acidic hyperbranched polymers for surface acoustic wave (saw) sensors. *Chem. Mater.* **2004**, *16*, 5357-5364.

14. Yuehe, L.; Fang, L.; Joseph, W. Disposable carbon nanotube modified screen-printed biosensor for amperometric detection of organophosphorus pesticides and nerve agents. *Electroanalysis* **2004**, *16*, 145-149.

15. Zhou, Y.; Yu, B.; Shiu, E.; Levon, K. Potentiometric sensing of chemical warfare agents: Surface imprinted polymer integrated with an indium tin oxide electrode. *Anal. Chem.* **2004**, *76*, 2689-2693.

16. Anitha, K.; Mohan, S. V.; Reddy, S. J. Development of acetylcholinesterase silica sol-gel immobilized biosensor - an application towards oxydemeton methyl detection. *Biosens. Bioelectron.* **2004**, *20*, 848-856.

17. Simonian, A. L.; Grimsley, J. K.; Flounders, A. W.; Schoeniger, J. S.; Cheng, T. C.; DeFrank, J. J.; Wild, J. R. Enzyme-based biosensor for the direct detection of fluorine-containing organophosphates. *Anal. Chem. Acta* **2001**, *442*, 15-23.

18. Wang, J. Microchip devices for detecting terrorist weapons. *Anal. Chem. Acta* **2004**, *507*, 3-10.

19. Steiner, W. E.; Klopsch, S. J.; English, W. A.; Clowers, B. H.; Hill, H. H. Detection of a chemical warfare agent simulant in various aerosol matrixes by ion mobility time-of-flight mass spectrometry. *Anal. Chem.* **2005**, *77*, 4792-4799.

20. Russell, A. J.; Berberich, J. A.; Drevon, G. F.; Koepsel, R. R. Biomaterials for mediation of chemical and biological warfare agents. *Annu Rev Biomed Eng* **2003**, *5*, 1-27.

21. Pearson, G. S.; Magee, R. S. Critical evaluation of proven chemical weapon destruction technologies (iupac technical report). *Pure Appl. Chem.* **2002**, *74*, 187-316.

22. Reeves, T. E.; Wales, M. E.; Grimsley, J. K.; Li, P.; Cerasoli, D. M.; Wild, J. R. Balancing the stability and the catalytic specificities of op hydrolases with enhanced v-agent activities. *Protein Eng. Des. Sel.* **2008**, *21*, 405-412.

23. El-Boubbou, K.; Schofield, D. A.; Landry, C. C. Enhanced enzymatic thermal stability and activity in functionalized mesoporous silica monitored by (31) p nmr. *Adv. Healthc. Mater.* **2012**, *1*, 183-188.

24. Aubert, S. D.; Li, Y.; Raushel, F. M. Mechanism for the hydrolysis of organophosphates by the bacterial phosphotriesterase. *Biochemistry* **2004**, *43*, 5707.

25. Grimsley, J. K.; Scholtz, J. M.; Pace, C. N.; Wild, J. R. Organophosphorus hydrolase is a remarkably stable enzyme that unfolds through a homodimeric intermediate. *Biochemistry* **1997**, *36*, 14366.

26. Tsai, P.-C.; Bigley, A.; Li, Y.; Ghanem, E.; Cadieux, C. L.; Kasten, S. A.; Reeves, T. E.; Cerasoli, D. M.; Raushel, F. M. Stereoselective hydrolysis of organophosphate nerve agents by the bacterial phosphotriesterase. *Biochemistry* **2010**, *49*, 7978.

27. Lewis, V. E.; Donarski, W. J.; Wild, J. R.; Raushel, F. M. Mechanism and stereochemical course at phosphorus of the reaction catalyzed by a bacterial phosphotriesterase. *Biochemistry* **1988**, *27*, 1591-1597.

28. Sheldon, R. A. Enzyme immobilization: The quest for optimum performance. *Adv. Synth. Catal.* **2007**, *349*, 1289-1307.

29. Cheng, K.; Landry, C. C. Diffusion-based deprotection in mesoporous materials: A strategy for differential functionalization of porous silica particles. *J. Am. Chem. Soc.* **2007**, *129*, 9674-9685.

30. Sing, K. S. W. Reporting physisorption data for gas/solid systems with special reference to the determination of surface area and porosity (recommendations 1984). *Pure Appl. Chem.* **1985**, *57*, 603-619.

31. Landry, C. C.; Nassivera, T. W. *US Patent Appl. 20090220791*.

32. Gallis, K. W.; Landry, C. C. *US Patent* **2002**, 6334988.

33. Lei, C.; Shin, Y.; Magnuson, J. K.; Fryxell, G.; Lasure, L. L.; Elliott, D. C.; Liu, J.; Ackerman, E. J. Characterization of functionalized nanoporous supports for protein confinement. *Nanotechnology* **2006**, *17*, 5531-5538.

34. Lei, C.; Soares, T. A.; Shin, Y.; Liu, J.; Ackerman, E. J. Enzyme specific activity in functionalized nanoporous supports. *Nanotechnology* **2008**, *19*, 125102.

35. Chen, B.; Lei, C.; Shin, Y.; Liu, J. Probing mechanisms for enzymatic activity enhancement of organophosphorus hydrolase in functionalized mesoporous silica. *Biochem. Biophys. Res. Commun.* **2009**, *390*, 1177-1181.

36. Grimsley, J. K.; Calamini, B.; Wild, J. R.; Mesecar, A. D. Structural and mutational studies of organophosphorus hydrolase reveal a cryptic and functional allosteric-binding site. *Arch. Biochem. Biophys.* **2005**, *442*, 169-179.

37. Garrett, R. H.; Grisham, C. M., *Biochemistry*. 4th ed.; Brooks/Cole: Boston, 2010.

38. Munoz, B.; Ramila, A.; Perez-Pariente, J.; Diaz, I.; Vallet-Regi, M. Mcm-41 organic modification as drug delivery rate regulator. *Chem. Mat.* **2003**, *15*, 500-503.

39. Benning, M. M.; Kuo, J. M.; Raushel, F. M.; Holden, H. M. Three-dimensional structure of phosphotriesterase: An enzyme capable of detoxifying organophosphate nerve agents. *Biochemistry* **1994**, *33*, 15001-15007.

40. Krajewska, B.; Zaborska, W. a.; Leszko, M. Inhibition of chitosan-immobilized urease by slow-binding inhibitors: Ni2+, f− and acetohydroxamic acid. *J. Mol. Catal. B-Enzym.* **2001**, *14*, 101-109.

41. Vetsch, J. R.; Paulsen, S. J.; Muller, R.; Hofmann, S. Effect of fetal bovine serum on mineralization in silk fibroin scaffolds. *Acta Biomater.* **2015**, *13*, 277-285.

42. Lavey, B. J.; Janda, K. D. Catalytic antibody mediated hydrolysis of paraoxon. *J. Org. Chem.* **1996**, *61*, 7633-7636.

CHAPTER 3: ORGANOPHOSPHORUS DETECTION SYSTEM USING ACETYLCHOLINESTERASE

3.1. Introduction

The detection of organophosphorus compounds has grown into a broad field, with a variety of different ways to combat human exposure. The range of toxicity of these compounds, and their use in a variety of applications from military conflicts to agriculture, contribute to a range of possible exposure routes.[1-8] The widespread impact of these compounds has pushed the need for organophosphorus detection methods to be faster, and easier for an untrained individual to use. Detection methods based on nanomaterials[9-13] have been increasingly useful in optical and electrochemical sensing systems, many based on assays measuring the activity of acetylcholinesterase (AChE).[10]

Organophosphorus compounds are toxic due to their irreversible inhibition of AChE by phosphorylation.[1-8] AChE is responsible for the hydrolysis of the neurotransmitter acetylcholine (ACh), found within neural tissues. Inhibition of AChE leads to the buildup of ACh in neuronal gaps, preventing the neurons from returning to their resting states. [1-8, 14-15] The rate at which inhibition occurs is dependent on the chemical nature of the specific organophosphorus compounds (**Figure 3.1**)[16] and is also dependent on the exposure time and concentration.

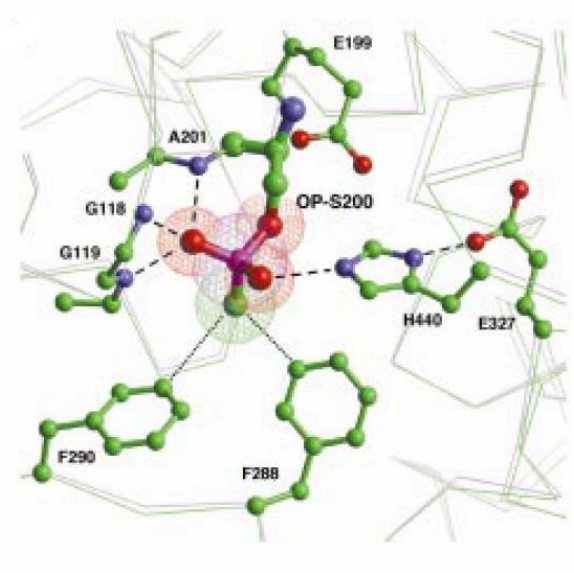

Figure 3.1: Binding of an organophosphorus compound (sarin) in the active site of AChE.[16]

The use of optical response systems, specifically those based on colorimetric responses,[3-4] have offered increased portability and ease of use with real-time detection.[7, 17-26] Many of these systems rely on the measurement of activity of AChE by tracking the hydrolysis of acetylthiocholine (AtCh) to its product, thiocholine (tCh).[10, 27] Typically, Ellman's method has been used to detect tCh due to the formation of a colored product, 2-nitro-5-thiobenzoate (yellow) with the addition of 5,5-dithio-bis-(2-nitrobenzoic acid) (**Figure 3.2**).[27-28] One of the major drawbacks to this method is the use of additional chemicals or materials to induce these colorimetric responses based on a secondary response to the hydrolysis product. Many compounds can react with Ellman's reagent, leading to false positives and reduced response signals.[3-4]

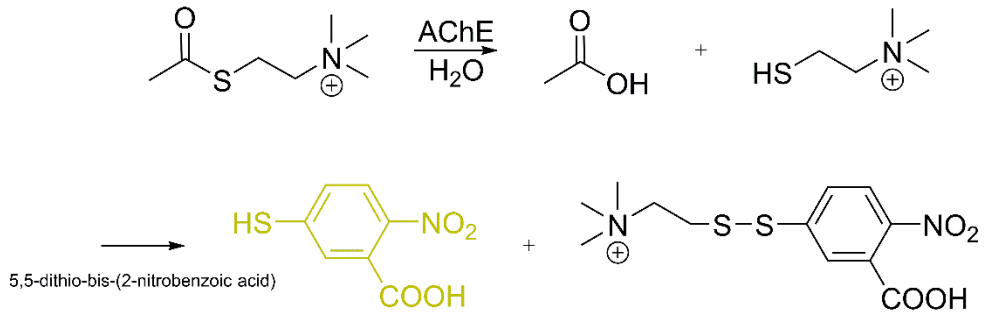

Figure 3.2: Hydrolysis of AtCh by AChE and detection by the Ellman's method to form a UV-Vis active product 2-nitro-5-thiobenzoate (yellow).[27-28]

Recent advances in the use of enzyme-modified nanomaterials in clinical diagnosis[29-30] have highlighted the use of molecular recognition as an efficient way to increase sensitivity towards a specific substrate.[30-31] Control of this recognition by the use of enzyme-specific inhibitors has been demonstrated, for example in the triggered release of an enzyme in response to substrate exposure.[32] A molecular recognition system using a substrate-triggered release system based on the reversible inhibition of AChE would decrease false positives, due to substrate specificity. Combining this specificity with a direct visual response would result in a system that is easy to use with high sensitivity.

Our design of a system that combines a direct visual response with high sensitivity began by selecting a nanoparticle scaffold. The use of a porous silica support, specifically mesoporous silica, has several advantages. One key feature is that silica is easily modified with organosilanes to allow for attachment of an inhibitor, tacrine, to the surface, in turn allowing AChE to be immobilized.[33-35] Tacrine has been commonly used as a competitive inhibitor of AChE and will hold AChE only temporarily, ensuring a fast release from the

surface of the particle. Tacrine also offers a primary amine that can be used to tether the inhibitor to the surface.[8, 36-42] Immobilization of AChE not only helps to prevent denaturation but places the enzyme in a set confirmation to be released by substrate or organophosphate.[33,43] Prior to introduction of substrate or organophosphate, immobilization of AChE on the surface will cap the pores of the mesoporous silica. Capping allows for the containment of a dye that can act as the optical response. After immobilization, inhibition of the AChE active site by an organophosphorus compound interferes with the AChE-tacrine interaction, triggering the release of AChE from the scaffold and resulting in the release of the dye (**Figure 3.3**). The proposed detection method offers a primary response system in which the signal of the system is in direct response to the substrate itself, giving high substrate specificity and limiting false positives.

While similar to the system described in Chapter 2 using OPH, AChE will not be active after the release from the surface of the particle. Using AChE as a sacrificial enzyme offers several advantages over the OPH based system. Sequential additions of paraoxon resulted in OPH actively hydrolyzing after releasing from the surface. After the first aliquot, any additional aliquots were primarily hydrolyzed by OPH free in solution. With phosphorylation of AChE, sequential additions of paraoxon will continue to release AChE from the surface. This resulted in testing the full concentration of each paraoxon aliquot and testing of system to trigger a false positive. Additionally, AChE was commercially available, and low cost, compared to OPH that requires lengthy production and purification.

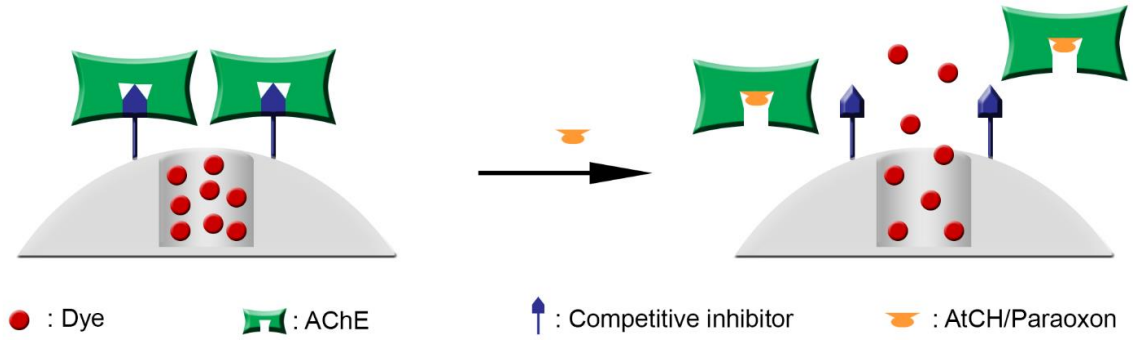

Figure 3.3: A model of molecular recognition using inhibitor-enzyme triggered release system.

3.2. Experimental Section

3.2.1. Materials and Instrumentation

All materials were purchased from Sigma-Aldrich, VWR and Life Technologies, unless otherwise noted. UV/Vis spectra were measured using a Perkin-Elmer Lambda 35 spectrophotometer system. Thermogravimetric analysis (TGA) was performed on a PerkinElmer Pyris 1 DSC-TGA. Scans were performed under a mixed flow of nitrogen (85%) and oxygen (15%) between 25 °C and 800 °C at 20 °C/min with a thermal hold at 100°C for 15 minutes to remove any residual water. Nitrogen adsorption and desorption isotherms were obtained on a Micromeritics TriStar instrument. Surface areas were measured using the Brunauer-Emmett-Teller (BET) method and pore size distributions were calculated from a modified Kruk, Jaronic and Sayari (KJS) method using the adsorption branch.

3.2.2. Synthesis, Functionalization and Characterization of APMS

3.2.2.1. Synthesis of Acid-Prepared Mesoporous Silica (APMS)

APMS was synthesized as previously described.[43-44]

3.2.2.2. Synthesis of APMS-(s)-NH_2

Pore-blocked APMS (1.8 g) was suspended in hexanes (400 mL) to which 3-aminoproplytriethoxysilane (APTES) (1.8 mL) was added. The solution was refluxed for 3.5 hours under an inert atmosphere (N_2) to form the product APMS-(s)-NH_2. To remove surfactant from the pores, APMS-(s)-NH_2 was extracted by refluxing with acidified ethanol (0.1 M HCl in ethanol) for 24 hours (3X), filtering and letting dry between each cycle. The degree of modification was characterized by TGA (2.02 mmol modification/g APMS) and the physical properties characterized by nitrogen physisorption. The resulting material was then placed under vacuum to keep dry until further modification.

3.2.2.3. Synthesis of APMS-(s)-NH-COOH

Extracted APMS-(s)-NH_2 (1.5 g) was suspended in acetonitrile (dry) under an inert atmosphere (N_2) to which triethylamine (950 µL) and succinic anhydride (355 mg) was added. The solution was stirred at 60°C for 21.5 hours then collected by vacuum filtration. Several washings with trifluoroacetic acid (0.1% in water) and acetonitrile were followed by drying overnight. The degree of modification was characterized by TGA (0.606 mmol modification/g APMS) and the physical properties characterized by nitrogen physisorption. The resulting APMS-(s)-NH-COOH was then placed under vacuum to keep dry until further modification.

3.2.2.4. Synthesis of APMS-(s)-Tac

To APMS-(s)-NH-COOH (128 mg or 57 mg) suspended in 15 or 8 mL

dimethylformamide (DMF), hydroxybenzotriazole (HOBt) (312, 82, or 42 mg), N, N'-diisopropylcarbodiimide (352, 90, or 48 mg) and 4-dimethylaminopyridine (DMAP) (16, 4, or 1 mg) were added and stirred for 1 hour. Tacrine hydrochloride (Tac) (66, 14 or 7 mg) was then added and stirred for 19 hours. The particles were collected by vacuum filtration and washed with DMF and MeOH and left to dry overnight. The degree of modification (0.228, 0.281, 0.323 mmol modification/g APMS, respectively) was determined by TGA and the physical properties characterized by nitrogen physisorption. The resulting APMS-(s)-Tac was then placed under vacuum to keep dry until further modification.

3.2.2.5. Determination of [AChE]

Free AChE concentrations and amounts of AChE immobilized onto APMS-(s)-Tac were calculated using a Pierce™ BCA protein assay kit using a standard bovine serum albumin (BSA) calibration curve (reference in text). Triplicate samples measured for the standard curve.

3.2.2.6. Synthesis of APMS-(s)-Tac-AChE

An acetylcholinesterase (AChE) stock (0.5 units/mL) in phosphate buffer (100 mM, pH = 7.3) was diluted (195 µL AChE stock in 155 µL phosphate buffer). 280 µL of this solution was added to 2.5 mg APMS-(s)-Tac and shaken for 24 hours. The sample was centrifuged, supernatant removed and immobilized AChE determined. The particles were washed with phosphate buffer (3X) and re-suspended in the appropriate amount of phosphate buffer for kinetics testing.

3.2.3. Measurement of Enzymatic Activity

3.2.3.1. Degradation of AtCh by Free AChE

To phosphate buffer (100 mM, pH = 7.3, 747.5 µL), Ellman's reagent (20 µL) (reference in main text) and AChE (24.7 µg/mL, 5 µL, 6.8 ng per sample) were added. An acetylthiocholine stock (AtCh) (2.5 µL, 75 mM in deionized water) was prepared and an aliquot added to give varying concentrations of AtCh (0.24 - 1.38 mM) in the solution and the time recorded. The sample was shaken for 4 minutes at which time AChE was denatured using sodium dodecyl sulfate (0.3 M, 50 µL). Each sample was ran in triplicate and the absorbance peak of 2-nitro-5-thiobenzoate at 412 nm and the extinction coefficient (14250 M^{-1} cm^{-1}) were used to determine kinetics.

3.2.3.2. Inhibition of Free AChE by Tac

To phosphate buffer (100 mM, pH = 7.3, 747.5 µL), AChE (18.9 µg/mL, 5 µL, 6.8 ng per sample) was added. A stock solution of Tac (9.34 µM) was prepared and an aliquot added to give varying concentrations of Tac (0.06, 0.12 and 0.30 mM) in the reaction. The sample was shaken for five minutes and then from an AtCh stock (75 mM in deionized water), an aliquot was added to give varying concentrations of AtCh (0.24 - 0.95 mM) in the reaction and the time recorded. The sample was shaken for 6-12 minutes at which time AChE was denatured using sodium dodecyl sulfate (0.3 M, 50 µL). Each sample was run in triplicate and were used to determine kinetics using the Ellman's method.[27]

3.2.3.3. Degradation of AtCh Using APMS-(s)-Tac-AChE

To phosphate buffer (100 mM, pH = 7.3, 1121 µL), APMS-(s)-Tac-AChE (6.8 ng AChE total) was added. From an AtCh stock (75 mM in deionized water), an aliquot was

added to give varying concentrations of AtCh (0.24 - 0.95 mM) in the reaction and the time recorded. The sample was shaken for 10 minutes and the entire reaction mixture was filtered using a 0.2 µm nylon membrane (25 mm) syringe filter. Each sample was ran in triplicate and were used to determine kinetics using the Ellman's method.

3.2.4. Congo Red Loading and Release Using AChE-Tethered Particles

3.2.4.1. Loading of Congo Red (APMS-CR-(s)-Tac)

Congo Red (CR) (31.4 mg) was dissolved in a citrate buffer (5 mL, 0.01 M, pH 3.98) to make a CR stock. In a typical loading procedure, APMS-(s)-Tac (4.2 mg) was suspended in a CR stock (3 mL, 9.01 mM) and shaken (20 hr). The sample was centrifuged and the supernatant measured by UV-Vis to determine the amount of CR loaded. The material was washed once with citrate buffer then with phosphate buffer (100 mM, pH = 7.3) to prepare for loading with AChE.

3.2.4.2. Loading AChE (APMS-CR-(s)-Tac-AChE)

A typical loading required 4.2 mg APMS-CR-(s)-Tac suspended in 950 µL phosphate buffer (100 mM, pH = 7.3), to which 250 µL AChE (499 µg/mL) was added and placed on a rotating platform for 24 hours. The sample was centrifuged, supernatant removed and immobilized AChE determined by the BCA assay. The particles were washed with phosphate buffer until all non-encapsulated CR was removed. The particles were then re-suspended in the appropriate amount of phosphate buffer for kinetics testing.

3.2.4.3. Release of Congo Red from APMS-CR-(s)-Tac-AChE

In a typical reaction, phosphate buffer (100 mM, pH = 7.3, 950 µL) and APMS-(s)-Tac-AChE (25.5 µg AChE total) were added. Testing using alternative solutions

included using cell culture media (10% Fetal bovine serum (FBS) in Dulbecco's Modified Eagle Medium (DMEM) (no phenol red, glutamine or glucose, pH 7.4)) and 100% Human serum (male, AB plasma). Exchange of the AChE loading buffer with either FBS or human serum was performed by centrifuging and re-suspending the particles 3X to ensure full exchange into the new solution. A typical reaction sample, unless noted otherwise, was shaken for 15 minutes, centrifuged and supernatant measure to ensure no CR was releasing. An aliquot of substrate (paraoxon or AtCh) was then added, adjusting this volume for the desired final concentration in solution. This was shaken for five minutes, centrifuged, supernatant measured and particles re-suspended. This process was repeated every five minutes for 60 minutes unless otherwise noted. The amount of CR released was determined by UV-Vis based on a calibration curve.

3.3. Results

3.3.1. Ellman's Method: Assay of AChE Activity

Ellman's method has been widely used as a colorimetric method for the determination of AChE activity by quantifying the amount of tCh produced by the hydrolysis reaction of AtCh. The thiol containing product (tCh) reacts with the Ellman's reagent, 5,5'-dithio-bis-(2-nitrobenzoic acid) (DTNB), to produce 2-nitro-5-thiobenzoate (TNB) (**Figure 3.2**). This can be measured using UV-Visible spectroscopy (UV-Vis) at 412 nm with a known extinction coefficient of 14250 M^{-1} cm^{-1} in phosphate buffer (pH 7.4, 25 °C) (**Figure 3.4**).[27-28] Removal of aliquots from the enzyme-substrate reaction solution at specific time points during the conversion process allows for the data to be used

in a Lineweaver-Burk double-reciprocal plot, which in turn is used to extract information about the activity of AChE.

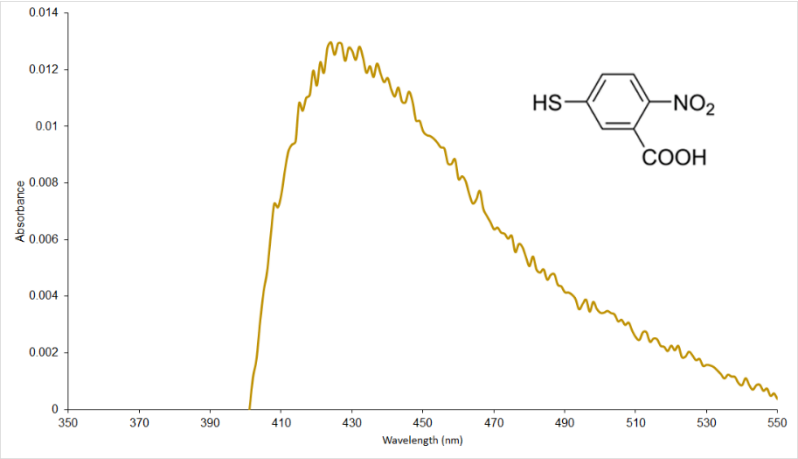

Figure 3.4: Absorption spectra of 2-nitro-5-thiobenzoate.

3.3.2. Inhibition of Free AChE Using Tac

To determine the type of inhibition exhibited by Tac, free AChE (i.e. not attached to a particle surface) was exposed to Tac at several concentrations in phosphate buffer. The activity of AChE with AtCh in the presence of Tac was determined by Lineweaver-Burk plots from UV-Vis (**Figure 3.5**). The activity of AChE in the absence of Tac was then determined in a similar manner; the same amount of AChE (6.8 ng) was used in all experiments.

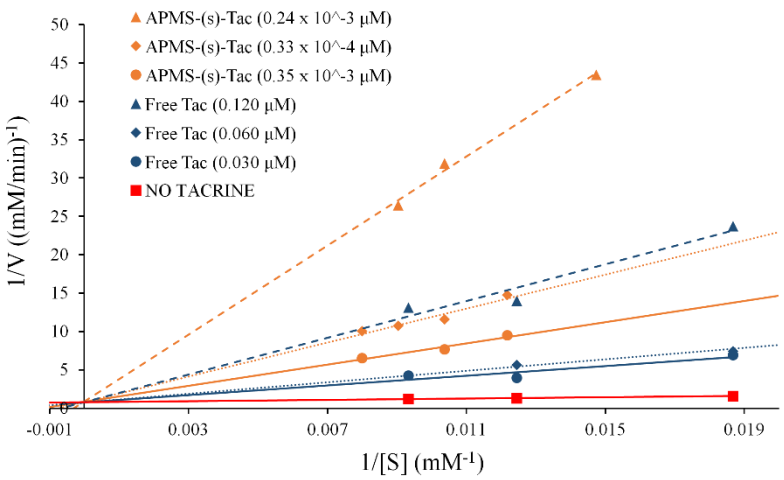

Figure 3.5: Lineweaver-Burk plots comparing inhibition of free vs. immobilized Tac.

3.3.3. Preparation and Characterization of APMS-(s)-Tac

Construction of the inhibitor-tethered scaffold was accomplished as shown in **Figure 3.6**. First, as-prepared APMS (i.e., with surfactant remaining in the pores) was reacted with 3-aminopropyltriethyoxysilane (APTES). The surfactant was then extracted in a solution of HCl/EtOH, to open the pores of the scaffold. The primary amine was reacted with succinic anhydride to produce a carboxylate-terminated surface. Activation of the carboxylic acid using N, N'-diisopropylcarbodiimide, followed by the addition of HOBt for generation of an active ester for efficient acylation of amino groups.[45] This was used to tether Tac to the particle surface at three different concentrations. The resulting materials are designated APMS-(s)-Tac (low), -Tac (med), and -Tac (high); having 0.23, 0.28, and 0.32 mmol tacrine per gram of APMS, respectively.

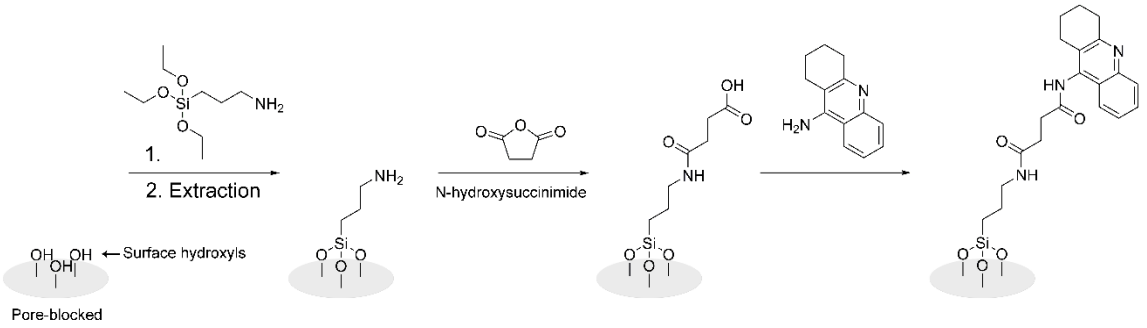

Figure 3.6: Synthesis of APMS-(s)-Tac.

Thermogravimetric analysis (TGA) and N_2 physisorption (**Table 3.1**) were used to characterize the physical properties of the materials at each stage of modification. To provide a basis for the calculation of the amount of organic modification of each material, a portion of the initial batch of APMS was calcined to completely remove the surfactant. This represented the maximum possible porosity of the material. The surface area of the base material was modest (385 m^2/g), although it was consistent with a pore diameter of 11 nm.

Table 3.1: Physical properties of APMS and modified APMS.

Sample	SA_{BET} (m^2/g)	V_{pore} (cm^3/g)	d_{pore} (nm)	modification (mmol/g)
APMS (calcined)	385	0.89	11	--
APMS-(s)-NH_2 (extracted)	270	0.62	11	2.02
APMS-(s)-NH-COOH	233	0.54	9.1	0.61
APMS-(s)-Tac-(low)	219	0.52	9.1	0.23
APMS-(s)-Tac-(med)	210	0.50	9.1	0.28
APMS-(s)-Tac-(high)	224	0.53	9.1	0.32

3.3.4. Inhibition Testing of APMS-(s)-Tac-AChE

AChE was stirred with APMS-(s)-Tac (low, med, and high), and the particles were washed to ensure removal of unbound AChE. The amount of AChE loaded was determined by BCA assay[46] that was performed before and after loading. Each APMS-(s)-Tac-AChE (low, med, high) material loaded different amounts of AChE (3.2, 1.2, 5.0 μg AChE/APMS (mg), respectively) so adjustments were made by re-suspending the APMS-(s)-Tac-AChE in phosphate buffer and adding an aliquot of this suspension to the reaction solution so that each reaction sample contained the same amount of AChE (6.8 ng AChE total). Inhibition tests were then performed using the Ellman's method assay described above.

3.3.5. Loading of Congo Red in APMS-(s)-Tac

The loading of Congo Red (CR) within APMS-(s)-Tac (high) varied depending on the sample, but a typical loading was 1.3 mM dye/mg particles, resulting in a deep red nanoparticle, APMS-CR-(s)-Tac (**Figure 3.7**). A control experiment was conducted to determine the maximum amount of CR that would release without AChE capping the pores. In this experiment, APMS-CR-(s)-Tac was washed six times with phosphate buffer, centrifuging and re-suspending in fresh phosphate buffer each time. It was then shaken for one hour in phosphate buffer and supernatant measured by UV-Vis to determine the amount of CR in solution. This was repeated for a total of five cycles until no further CR could be detected by UV-Vis. The particles were now faint pink in color and were dried under vacuum and TGA performed. Approximately 1% of CR could not be removed from the particles.

3.3.6. Dye Release from APMS-CR-(s)-Tac-AChE (Single Addition)

After this experiment, AChE was attached to fully CR-loaded nanoparticles through the tacrine inhibitor to form APMS-CR-(s)-Tac-AChE. Experiments were then performed to confirm that tacrine was inhibiting AChE through its active site. Prior to the addition of AtCh, the particles (4.1 mg APMS-CR-(s)-Tac-AChE in 659 μL phosphate buffer) were shaken for 15 minutes, and the supernatant measured to ensure no CR was releasing. An aliquot of AtCh was then added, resulting in an AtCh concentration of 1.70 mM. The concentration of dye in the supernatant was measured every five minutes to track the release of CR after detachment of AChE from the nanoparticle surface using UV-Vis (**Figure 3.7**).

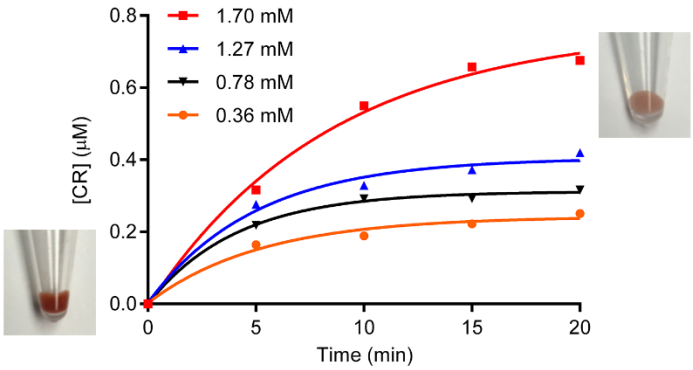

Figure 3.7: Congo Red release at several concentrations of AtCh.

This was repeated with three additional concentrations of AtCh (1.27, 0.78 and 0.36 mM). The release profiles were plotted and fit as pseudo-first order association kinetics (Rate = k'[A]) to determine the initial release rates and maximum (plateau) amount of dye (**Table 3.2**). Pseudo-first order (A + B → P) has a second order reaction (Rate = k[A][B]) where [B] is has a high enough concentration that when the reaction goes to completion, the [B] remains constant (independent of [A]), defining it as k' = k[B]. For these experiments, AtCh has to first displace AChE and then CR must leave the interior of the particle. Similar to the pseudo-first order, the initial release of AChE can be defined as [B], releasing a set amount of AChE, independent of the amount of CR in the particle. The release of CR can be defined as [A], giving a pseudo-first order rate equation. A change of particle color from a deep red to a pink color could be seen by the naked eye (**Figure 3.6**).

Table 3.2: Congo Red release rates from APMS-CR-(s)-Tac-AChE vs. [AtCh].

[AtCh] (mM)	Initial Rate (μM/min)	Maximum Release (μM)
1.70	0.063	0.68
1.27	0.055	0.42
0.78	0.044	0.32
0.36	0.033	0.25

3.3.7. Dye Release from APMS-CR-(s)-Tac-AChE (Multiple Additions)

APMS-CR-(s)-Tac-AChE (high) was prepared and washed as previously described. AtCh was then added (0.781 mM in solution) and the concentration of CR in the supernatant was measured every five minutes to track the release of CR (**Figure 3.8**). After a plateau was reached (~20 min), an additional aliquot of AtCh (0.781 mM in solution) was added. The supernatant continued to be measured until the second plateau was reached (~50 min). This process was repeated with a third aliquot of the same concentration of AtCh and the supernatant measured until a third plateau was reached (~75 min).

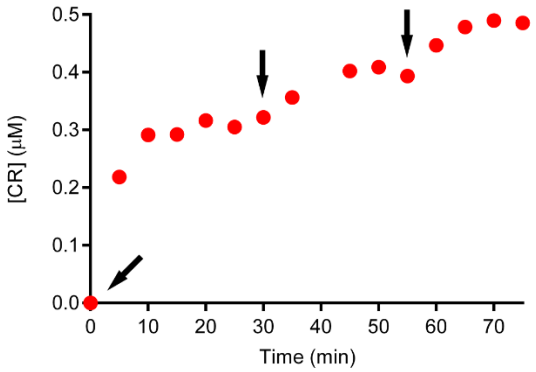

Figure 3.8: Congo Red release with multiple additions of AtCh (indicated by arrow).

3.3.8. Dye Release from APMS-CR-(s)-Tac-AChE (Recycling)

To show the recycling ability of APMS-CR-(s)-Tac-AChE, the material was sequentially exposed to AtCh, 0.36 mM total in solution, with several washes with phosphate buffer between cycles. This was to ensure that any release of CR or AChE was removed before the second cycle (**Figure 3.9**). The amount of dye released in the second test was approximately 56% of the original amount (0.14 vs. 0.25 µM).

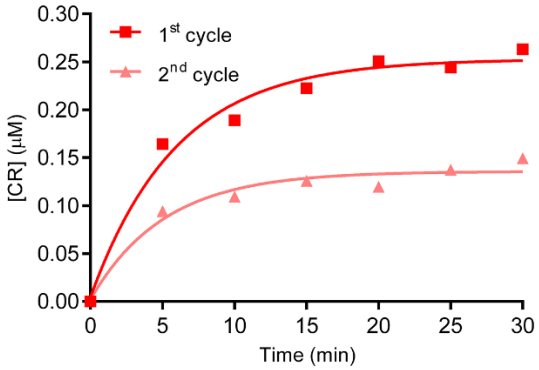

Figure 3.9: Sequential release of dye from APMS-CR-(s)-Tac-AChE.

3.3.9. Dye Release from APMS-CR-(s)-Tac-AChE (Solution Comparison (AtCh))

The triggered release system was also tested in protein-containing solutions. Attachment of AChE was accomplished using the procedure described above to form APMS-CR-(s)-Tac-AChE. Three separate experiments were conducted in phosphate buffer, 10 % fetal bovine serum (FBS), and human serum. The particles used in the human serum were allowed to reach an equilibrium with any proteins binding to the surface of APMS-CR-(s)-TAC-AChE by shaking the particles for 60 minutes in human serum. Prolonged shaking to reach equilibrium for the particles in FBS was reduced to 15 minutes to reach equilibrium, resulting from the smaller concentration of proteins in solution. A single aliquot of AtCh (8.2 mM total in solution) was added and the release of CR tracked by UV-Vis (**Figure 3.10**). The release of CR was measured every five minutes until a plateau was reached, and then the experiment was terminated. Addition of the Ellman's reagent to the final supernatant for the phosphate buffer sample and subsequent

measurement by UV-Vis ensured that the hydrolysis of AtCh had occurred. The initial release rates and maximum release amounts were: phosphate buffer (0.136 mM/min, 1.35 mM), FBS (0.105 mM/min, 0.96 mM) and human serum (0.074 mM/min, 0.87 mM).

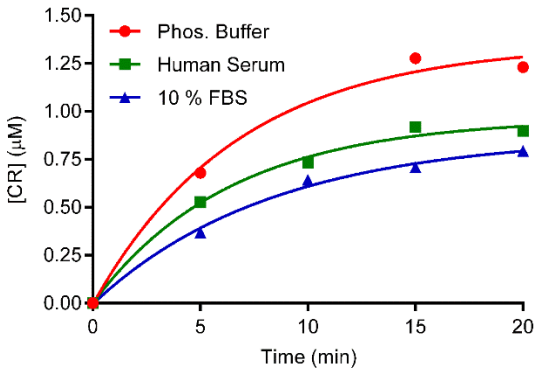

Figure 3.10: Dye release comparison in different solutions with set [AtCh].

3.10. Dye Release from APMS-CR-(s)-Tac-AChE (Solution Comparison (Paraoxon))

Testing the triggered release system in alternative solutions using paraoxon instead of AtCh was performed. Attachment of AChE was accomplished through the previously described procedure to form APMS-CR-(s)-Tac-AChE. The same experimental procedure as described in section 3.3.9 was followed with each alternative testing solution using a single aliquot of paraoxon (8.2 mM total in solution), and the release of CR was tracked by UV-Vis (**Figure 3.11**). The amount of CR released into the solution was measured every five minutes until a plateau was reached, and then the experiment was terminated. The initial release rates and maximum release amounts were: phosphate buffer

(0.455 mM/min, 2.90 mM), FBS (0.246 mM/min, 1.76 mM) and human serum (0.154 mM/min, 1.67 mM). The supernatant from the phosphate buffer solution was removed and AChE actitivty tested to confirm the inhibtion by paraoxon. The Ellman's method was perfromed with the addtion of AtCh (0.69 mM in solution) and DTNB and shaken for 30 minutes. This resulted with no measurable production of 2-nitro-5-thiobenzoate, confirming the inhibition of AChE. For FBS and human serum solutions, the Ellman's method resulted in false positives due to the DTNB reacting with thiol-containing proteins present in solution.

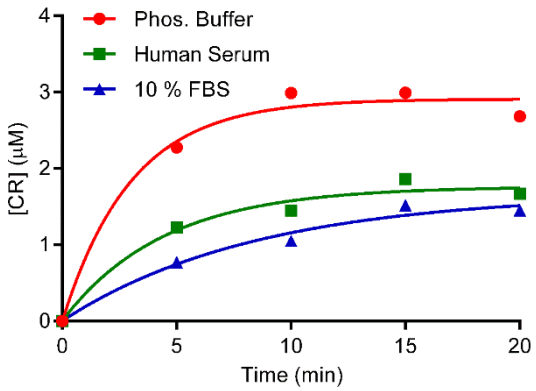

Figure 3.11: Dye release comparison in different solutions with set [Paraoxon].

3.4. Discussion

3.4.1. Selection of Scaffold

The detection system requires the cooperation of several components within close proximity of each other to act as a triggered release system. The use of porous silica allows the structural integrity of the detection device to be retained, allowing the scaffold to

withstand repeated washing cycles and re-cycling of the material without deteriorating. Mesoporous silica offers a way to control important structural characteristics such as surface area and pore diameter and allows for a large interior pore volume to retain a dye. The surface of mesoporous silica can be readily modified with various functional groups, tailoring the material to allow for attachment of the desired inhibitor.

3.4.2. Selection of Inhibitor

The selection of a proper inhibitor relies on several factors, which must be considered to allow for the system to function properly. These factors consist of the nature of inhibition, ability to immobilize the inhibitor on the scaffold, and nature of inhibition after immobilization. With these in mind, the starting point of the selection process was to find an inhibitor that was competitive to allow for only a temporary tether of the enzyme within the AChE active site. While paraoxon is not the substrate for AChE, paraoxon will phosphorylate the active site of AChE, disrupting the inhibitor-enzyme interaction.

Reversible inhibition of AChE has been used to treat neurodegenerative disorders such as Alzheimer's disease (AD), which is caused by a reduced number of cholinergic neurons and ACh.[8, 47] Reversible inhibitors can be separated into two categories dependent on their role in substrate conversion. Competitive inhibitors compete with the substrate for the active site of the enzyme, whereas non-competitive inhibitors can react with the substrate-enzyme complex, binding to a site separate from the active site, decreasing the conversion rate to product.[48] Examples of both types of inhibitors have been studied to find their interaction with the AChE active site and how this determines the nature of their inhibition.[8]

AChE has an elongated pocket in which the catalytic anionic site (CAS) is located at the base with an additional peripheral anionic site (PAS) located at the mouth of the pocket (**Figure 1.11**). Both of these sites have shown to play a crucial role in determining the type and degree of inhibition. For example, the AChE inhibitor donepezil binds to the PAS, resulting in non-competitive inhibition, while tacrine binds to the CAS, resulting in competitive inhibition at high concentrations.[8, 36-42] It is also possible to block both the PAS and CAS with a dual binding inhibitor using a bivalent ligand. The use of two tacrine molecules, bound by a polymethylene spacer, made contact with the CAS and PAS (**Figure 3.12**).[36]

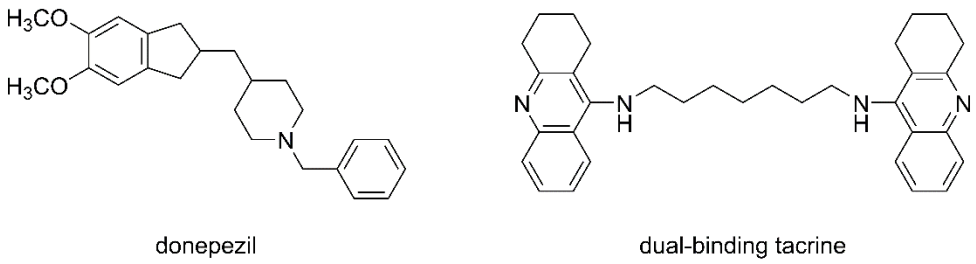

Figure 3.12: AChE inhibtiors.[8, 36-42]

For the nanoparticle-based triggered release system, binding of the inhibitor to the CAS must occur for competitive inhibition, resulting in the fast release of AChE from the surface of the silica. Tacrine has been commonly used as a competitive inhibitor of AChE and offers functional groups that can be used to tether the inhibitor to the surface. [8, 36-42] Immobilizing AChE allows the pores of the scaffold to be capped, retaining the loaded dye and acting as the triggered release system. The attachment of tacrine can be accomplished

through a peptide bond with the available primary amine on the center ring (**Figure 3.6**).

To ensure interaction with the CAS, the chain length from the silica surface to the end of the inhibitor must be at least 14 Å to reach within the deep pocket of the AChE active site.[36] Without this minimum chain length, interaction with the PAS could result, leading to non-competitive inhibition. In our case, after the peptide bond formation, the chain length could be estimated to be around 19 Å using average bond lengths for C-C (154 pm) and C-N (147 pm) bonds molecular modeling would be needed for maximum accuracy.[49]

3.4.3. Type of Inhibition

The last point to address was whether tacrine maintained its role as a competitive inhibitor after immobilization. Enzyme inhibition can be determined through a variety of methods by comparing the activity of the free enzyme with and without the inhibitor. A Lineweaver-Burk plot is a useful tool to study enzymatic inhibition, because the effects of competitive and non-competitive inhibition produce graphically distinct results that are easily observed. In competitive inhibition, the y intercept ($1/V_{max}$) remains the same in the presence of the inhibitor and the x intercept ($-1/K_M$) decreases. This is a result of the observed binding constant of the substrate changing in the presence of a competitive inhibitor, although at sufficiently high concentrations of substrate the maximum velocity of the reaction remains the same. The new x intercept, $-1/(1+[I]K_I)$, where [I] = the concentration of inhibitor and K_I is the dissociation constant of the inhibitor with respect to the enzyme, is sensitive to the concentration of inhibitor.[48] The comparison of AChE activity with and without tacrine are shown in **Figure 3.5**. The y intercept of all plots were

identical, and the x intercepts of each plot decreased as the concentration of tacrine increased. Lower concentrations of tacrine were tested but resulted in non-competitive inhibition, as previously found in literature.[41, 50-52] To ensure competitive inhibition, a higher ratio of inhibitor to AChE was maintained. Confirmation of competitive inhibition of tacrine free in solution under the set conditions allowed for a standard to which the immobilized inhibitor could be compared.

3.4.4. Synthesis of APMS-(s)-Tac

The design of the scaffold and its functionalization, as previously discussed, played an important role in trying to maintain the competitive inhibition of tacrine with AChE. Calcined APMS was first characterized to ensure that the starting material was adequate to not only allow for addition of the organic moieties but also to allow for loading of dye (**Table 3.1**). A large pore diameter (~1 nm) and large pore volume for the final functionalized material were both desired. This results in easier loading and release of dye from the interior pore volume. The large pore volume allowed the amount of dye that would release once AChE was displaced to be maximized. Analysis of the pore volume (0.89 cm^3/g) of a material with this surface area and pore diameter suggested a porous material with highly interconnected pore structure, consistent with previous publications on APMS.[6, 53] A pore volume of this size was suitable to continue with surface modification.

Next, the surface functionalization steps to add the inhibitor to APMS were performed (**Figure 3.6**). The first synthetic step was the attachment of the primary amine to the surface. Limiting the aminosilane functionalization primarily to the external particle surface was controlled by using as-prepared APMS, in which the surfactant was still intact,

preventing modification of the pore surfaces. AChE was required to be on the surface not only to block the pores, but also to allow the substrate easier access to the CAS. Removal of the surfactant following functionalization with the primary amine, confirming that modification hard primarily taken place on the external surface. A short functionalization time also helped to control the location of the amine, although some diffusion of APTES within the surfactant micelles is expected.[54]

Thorough population of the surface with the amine (2.02 mmol/g) allowed the carboxylic acid functionality to be added. The extent of modification with succinic anhydride was less than with the amine addition (0.61 mmol/g versus 2.02 mmol/g) resulting with some unreacted amine groups, which was expected. The last functionalization step was the controlled addition of tacrine to the surface at several concentrations by adjusting the amount of tacrine available during the peptide coupling (**Table 3.1**). The coupling procedure begins with the activation of the carboxylic acid with the introduction of the diisopropylcarbodiimide to form the highly reactive o-acyl-urea. To prevent racemization, HOBt reacts with the o-acyl-urea to form an active ester. Introduction of tacrine at set concentrations limits the amount that can be immobilized through the peptide bond formation.[45] The resulting mixed surface of unreacted amines, carboxylic acid groups, and tacrine did not appear to influence inhibition testing with AChE (**Figure 3.13**). Porosity was retained throughout the modification process, determined by analysis of the SA_{BET}, V_{pore}, and d_{pore} after each step (**Table 3.1**). A decrease in each of these physical parameters is typical of functionalization in which small amounts of silane may modify the mouths of the pore. Increasing the length of the linker to the

tacrine would decrease the porosity even further. Despite the decrease, the final porosity and pore volume was sufficient to retain the dye and allow for the capping by AChE.

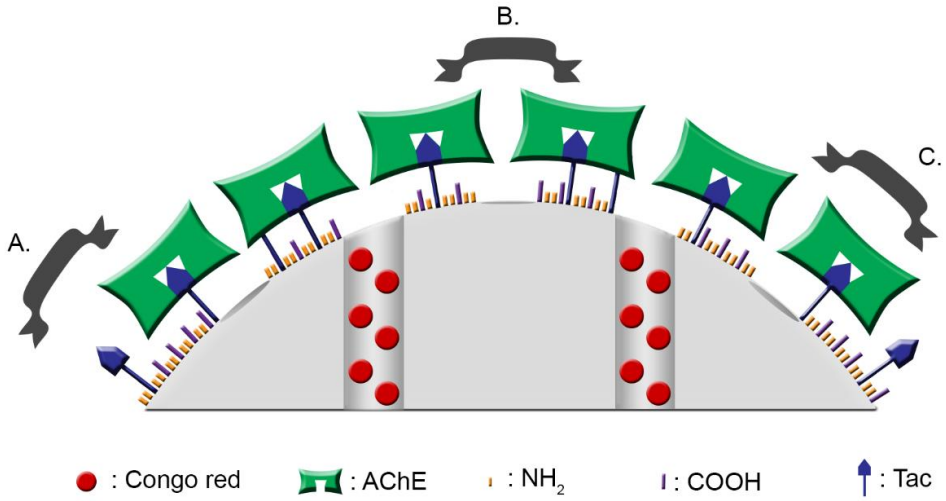

Figure 3.13: Conceptual influences on surface functionalization and AChE loading and CR releasing.

3.4.5. Immobilization of AChE

The immobilization of AChE onto the surface of APMS-(s)-Tac was controlled by many factors resulting from the physical characteristics of AChE in relation to the surface functionalization of APMS. For example, a comparison of the amount of AChE loaded to the amount of tacrine that was present on the surface showed that excess tacrine was always present. For example, even at the lowest immobilized tacrine concentration, APMS-(s)-Tac (low) had approximately 0.014 mM tacrine per mM AChE. Comparison of these concentrations showed that the packing of AChE on the surface was not limited by

the number of available tacrine molecules. This would result in a surface that had not only unreacted amine and carboxylic acid groups but free tacrine (**Figure 3.13 A**). The high ratio of tacrine to AChE could result from the relative size of AChE (9.3 nm x 8.1 nm x 9.7 nm).[55] If two or more inhibitor molecules were less than 81 Å apart, then AChE would bind to one of them and cover the others. The benefit of having an excess of available inhibitor was to increase the likelihood of tight packing on the surface, allowing the pores to be capped most effectively. The large size of AChE in comparison to the average pore diameter (~ 9.1 nm) also resulted in the possibility that only one AChE would be needed to cover a pore (**Figure 3.13 C**). Two or more AChE could also cover a pore (**Figure 3.13 B**); the difference between these two scenarios was controlled by the distance between pores and the density of AChE packing on the surface. The ability for a single or multiple AChE to cap a pore further increases the potential for retaining the dye.

3.4.6. Inhibition Testing of APMS-(s)-Tac-AChE

For the triggered release system to be functional, the immobilized tacrine had to continue to perform as a competitive inhibitor. As in the case of free tacrine and AChE, APMS-(s)-Tac-AChE kinetics were evaluated using a Lineweaver-Burk plot (**Figure 3.5**). Intersection of the three APMS-(s)-Tac-AChE samples at the same point on the y-axis found with and without tacrine confirms that tacrine is still a competitive inhibitor after immobilization. The concentration of immobilized tacrine was calculated based on the amount of AChE needed (6.8 ng per sample) for each of the sample. The concentrations of tacrine do not directly correspond to the slopes of the lines such that the higher the concentration of inhibitor, the steeper the slope. This resulted from the variation in AChE

Loaded, 3.2, 1.2, 5.0 μg AChE/APMS (mg) for each of the materials, APMS-(s)-Tac (low, med, high), respectively. However, the slope increase corresponded directly to the starting material concentration of immobilized inhibitor, from 0.23 to 0.32 mmol/g APMS. The larger slope using immobilized AChE compared to free AChE can be attributed to a higher localized concentration of tacrine on the surface compared to free in solution.[56] This helped to ensure the ratio of tacrine to AChE was large enough to force competitive inhibition over non-competitive inhibition. In terms of a triggered release system, the large slope indicates that the system is effective at very low concentrations of substrate and is sensitive to small changes in substrate concentrations.

3.4.7. Dye Selection

Congo Red (CR) (pK_a = 4.1, **Figure 3.14**) was selected as the dye in this system because it could be loaded in significant amounts at pH = 2.3, above the isoelectric point (IEP = ~ pH = 2) of SiO_2. The majority of the surface of silica nanoparticles at all pHs contains ≡Si-O-Si≡ and ≡Si-OH. At a pH below the IEP of silica, the surface has an overall positive charge, with the surface containing protonated silanols (≡Si-OH^{2+}) where it will remain mainly deprotonated. At a pH above the IEP of silica, the surface has an overall negative charge, with the surface containing deprotonated silanols (≡Si-O^-).[57] This allowed for weak interaction with the anionic surface of APMS. During the release experiments, the use of a basic buffer (phosphate buffer, pH = 7.3) results in a deprotonation of the surface silanols and the surface of APMS will have a negative ζ potential.[53] This change in buffer results in the deprotonation of CR, repelling it from the pore surface and releasing the dye. Although the pore capping step was performed above pH = 4.1, the interaction of

AChE with the surface bound tacrine occurred with sufficient speed that the majority of the dye remained within the pores. In control experiments, it was found that the only about 1% of the loaded CR remained within the particles. APMS has a highly inter-connected pore structure, which allows dye to be loaded deep within the nanoparticles. The native and modified material may have pockets of different surface charge that could also trap CR. Despite this, the majority of dye could be released to give direct visual indication of the AChE reaction.

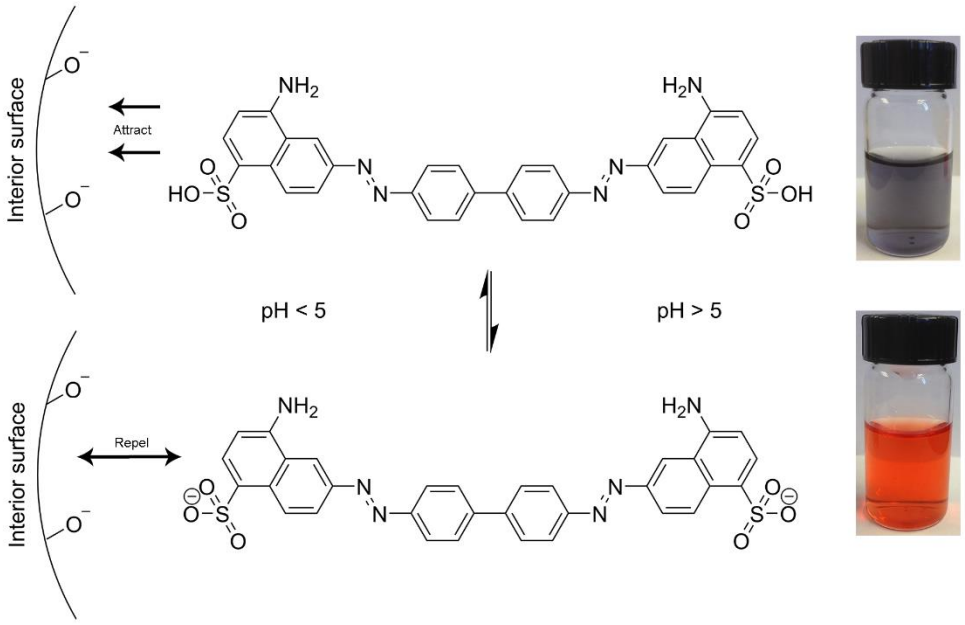

Figure 3.14: Structure and color of protonated and deprotonated forms of Congo Red

3.4.8. Release of CR from APMS-CR-(s)-Tac-AChE

The release of CR using a single aliquot of AtCh at several concentrations allowed a release profile to be constructed under ideal conditions. Quantification of CR release provided

confirmation of the visual change and also provided information about the kinetics of the system.

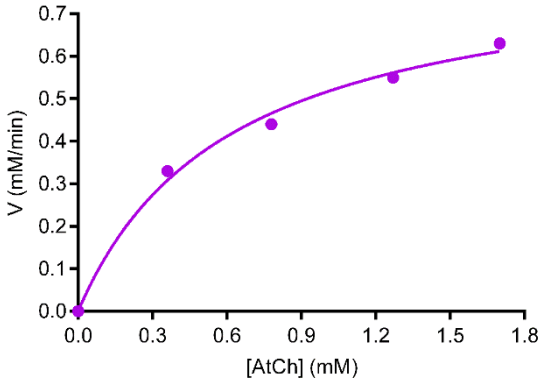

Figure 3.15: Michaelis-Menten kinetics of CR release.

If the rate of dye release is sufficiently rapid, it should reflect enzymatic kinetics, following a Michaelis-Menten model.[48] Indeed, plotting the rate of CR release versus substrate concentration showed a graph typical of Michaelis-Menten kinetics (**Figure 3.15**). This implies that as the substrate concentration increases, the rate of CR release will also increase until the point of saturation by the substrate. This confirms that the process of dye release and the process of substrate recognition are independent of each other. Calculation of kinetic constants from this plot gave k_{cat}/K_m = 3.73 x 10^4 $M^{-1}s^{-1}$, which is comparable to the actual value of 2.72 x 10^2 $M^{-1}s^{-1}$ measured by Ellman's method.

Figure 3.8 shows that it was possible to release more CR after the first addition (0.78 mM in solution) of AtCh by adding more AtCh after the rate of CR had plateaued.

However, the amount of CR release is substantially lower, because free AChE now competes for the AtCh with bound AChE. After the first plateau, an additional aliquot (0.78 mM in solution) of AtCh showed an increase of CR until a second plateau within a similar 20-minute window and a measurable signal within five minutes. Repeating this a third time (0.78 mM in solution) resulted in a similar result. After this point, additional aliquots did not give an increased CR signal. The large amount of free AChE was hydrolyzing the substrate faster than the amount of time it took AtCh to reach the bound AChE.

On the other hand, isolation and resuspension of the particles between the first and second additions of AtCh should eliminate cross-reaction with free AChE. This was indeed the case for the second cycle with a slightly lower maximum release amount (**Figure 3.9**). The smaller amount of CR released was consistent with a smaller amount of AChE on the surface and a smaller amount of CR still remaining in the material. These two different experiments (sequential addition and recycling) showed that the material retained its structural integrity after multiple substrate additions and can be washed and recycled for further use.

Extensive testing of the triggered release system using AtCh showed the stability of the inhibitor-enzyme interaction. To use this triggered-release system as a detection system for organophosphates, the same must hold true. In the presence of an organophosphate, such as paraoxon, a serine residue within the active site of AChE is phosphorylated.[58] The interaction of tacrine with the active site of AChE should therefore be disrupted by the introduction of paraoxon, causing the release of AChE from the surface

of APMS-(s)-Tac-AChE. The release of CR from the interior pore volume could then be tracked in similar fashion as with AtCh.

CR release kinetics could be used to compare the sensitivity of the AChE release in the presence of AtCh versus paraoxon. The initial release rate and maximum release of CR in phosphate buffer with AtCh (**Figure 3.10**; 0.136 mM/min and 1.35 mM) compared to the addition of paraoxon (**Figure 3.11**; 0.455 mM/min and 2.9 mM) was attributed to difference in the mechanism of AChE release. The hydrolysis of AtCh by AChE (1.6×10^4 $M^{-1}min^{-1}$) was lower than the inhibition of AChE with paraoxon (2.9×10^5 $M^{-1}min^{-1}$).[59] This results in a faster rate of release of AChE from the surface and a larger release of CR with the inhibition of AChE. The release of CR using paraoxon confirms the ability of this system to work not only with a substrate but with an organophosphate to allow for direct detection.

3.4.9. Selectivity of Trigger

In phosphate buffer, the triggered release system worked effectively to release CR. Moving away from this controlled environment to a solution containing other molecules and proteins allowed for the selectivity of the trigger to be tested. Cell culture media, 10% FBS, contained a small amount of proteins and other growth factors[60] that could potentially interfere with substrate selectivity or release of AChE.

Simple exposure of APMS-CR-(s)-Tac-AChE to 10% FBS showed no release of CR. This showed that the presence of other molecules did not interfere with the immobilization of AChE with tacrine. The release of CR from APMS-CR-(s)-Tac-AChE did not occur until after the addition of AtCh (**Figure 3.10**) or paraoxon (**Figure 3.11**). The

release of CR using either of the substrates resulted in a slightly decreased initial release rate and maximum release amount than under the ideal conditions using only phosphate buffer. The lower rates were expected due to the interference with other proteins within the reaction mixture that will limit the diffusion rate as well as possible interactions with the substrate. In the case of paraoxon, phosphorylation of other proteins can occur, decreasing the actual amount of paraoxon reaching the particles. To ensure that the release of CR was due to the addition of substrate, in the case of AtCh, addition of Ellman's reagent to the supernatant showed hydrolysis of AtCh. This shows that not only was the system able to release AChE in a complex mixture of other proteins, but specifically releases it when the substrate is present.

Taking the selectivity of this system a step further and increasing the potential for premature triggered release, a similar experiment was performed but using 100 % human serum. The use of 100% serum increases the concentration of proteins to 4.0-9.0 g/dl. With a larger number of proteins in solution, an equilibrium with any binding proteins was allowed to be reached. This ensured that competition between substrate and binding proteins did not occur when forming the corona, a layer of proteins electrostatically bound to the surface of the particle.[61] Despite the large increase in concentration of free proteins and bound proteins, the system still showed CR after the addition of AtCh (**Figure 3.10**) or paraoxon (**Figure 3.11**). The rates of release and overall maximum release amount were slightly higher than FBS but remained less than with the ideal conditions. The lower release of CR in FBS was attributed to the lower amount of CR loaded in the sample (0.65 mM dye/mg particles) compared to testing in human serum and phosphate buffer (0.86 mM/mg

particles). The ability of this system to release CR within a system flooded with other proteins shows the selectivity that is afforded through an enzyme-inhibitor pair and creates an effective detection system.

3.5. Conclusions

The need for an efficient and easily accessible detection system for organophosphorus compounds have expanded this area of research into the need for a system in which no additional external influence is needed other than the neurotoxin itself. The use of mesoporous silica nanoparticles offers a unique scaffold in which the entire detection system can be retained. In this system, the exterior modification using an inhibitor allows an enzyme-inhibitor pairing to act as the trigger and cap of the material. The loading of the interior pore volume with a dye is held intact by the cap and its release was the direct result of the triggered release of the enzyme.

In the detection system described here, the exterior of APMS was functionalized with the competitive inhibitor (tacrine) that was confirmed both free in solution and when immobilized. This was followed by loading the interior pore volume with CR and subsequent inhibition of AChE to tether it to the surface. AChE remained inhibited until the addition of substrate or organophosphorus compound. Addition of either of these substrates prompted the displacement of AChE and allowed for the release of CR. This could be tracked visually and quantified easily by UV-Vis. The specificity of the triggered release system was tested in systems that reflected cell culture media and in full HS. Despite the abundance of proteins contained within these solutions, AChE remained intact

and only the addition of AtCh or paraoxon caused the release of CR.

The design of the detection system is highly advantageous due to the high degree of specificity. Utilizing the enzyme-inhibitor pair for the triggered release system removes the need for an additional influence, chemical or physical, to give a visual response. This shows promise under biological conditions in which the addition of chemical or other external triggers can be detrimental to the system. A self-contained system with direct detection circumvents this problem. Additionally, this system helps eliminate false positives and gives a fast visual indication that can be seen by the naked eye, allowing for use by an untrained individual. The use of the enzyme-inhibitor triggered release system has shown promise within the field of triggered response systems with minimal time to synthesize the scaffold and the ability to tailor the material to the desired enzyme-inhibitor pair.

3.6. References

1. Kim, K.; Tsay, O. G.; Atwood, D. A.; Churchill, D. G. Destruction and detection of chemical warfare agents. *Chem. Rev.* **2011**, *111*, 5345-5403.

2. Yang, Y. C.; Baker, J. A.; Ward, J. R. Decontamination of chemical warfare agents. *Chem. Rev.* **1992**, *92*, 1729-1743.

3. Climent, E.; Marti, A.; Royo, S.; Martinez-Manez, R.; Marcos, M. D.; Sancenon, F.; Soto, J.; Costero, A. M.; Gil, S.; Parra, M. Chromogenic detection of nerve agent mimics by mass transport control at the surface of bifunctionalized silica nanoparticles. *Angew. Chem. Int. Ed. Engl.* **2010**, *49*, 5945-5948.

4. Royo, S.; Martinez-Manez, R.; Sancenon, F.; Costero, A. M.; Parra, M.; Gil, S. Chromogenic and fluorogenic reagents for chemical warfare nerve agents' detection. *Chem. Commun.* **2007**, 4839-4847.

5. Diaz de Grenu, B.; Moreno, D.; Torroba, T.; Berg, A.; Gunnars, J.; Nilsson, T.; Nyman, R.; Persson, M.; Pettersson, J.; Eklind, I.; Wasterby, P. Fluorescent discrimination between traces of chemical warfare agents and their mimics. *J. Am. Chem. Soc.* **2014**, *136*, 4125-4128.

6. El-Boubbou, K.; Schofield, D. A.; Landry, C. C. Enhanced enzymatic activity of oph in ammonium-functionalized mesoporous silica: Surface modification and pore effects. *J. Phys. Chem. C* **2012**, *116*, 17501-17506.

7. Yu, D.; Volponi, J.; Chhabra, S.; Brinker, C. J.; Mulchandani, A.; Singh, A. K. Aqueous sol-gel encapsulation of genetically engineered moraxella spp. Cells for the detection of organophosphates. *Biosens. Bioelectron.* **2005**, *20*, 1433-1437.

8. Colovic, M. B.; Krstic, D. Z.; Lazarevic-Pasti, T. D.; Bondzic, A. M.; Vasic, V. M. Acetylcholinesterase inhibitors: Pharmacology and toxicology. *Curr. Neuropharmacol.* **2013**, *11*, 315-335.

9. Aragay, G.; Pons, J.; Merkoci, A. Recent trends in macro-, micro-, and nanomaterial-based tools and strategies for heavy-metal detection. *Chem. Rev.* **2011**, *111*, 3433-3458.

10. Aragay, G.; Pino, F.; Merkoci, A. Nanomaterials for sensing and destroying pesticides. *Chem. Rev.* **2012**, *112*, 5317-5338.

11. Liu, G.; Lin, Y. Nanomaterial labels in electrochemical immunosensors and immunoassays. *Talanta* **2007**, *74*, 308-317.

12. Pérez-López, B.; Merkoçi, A. Nanoparticles for the development of improved (bio) sensing systems. *Anal. Bioanal. Chem.* **2011**, *399*, 1577-1590.

13. Zhang, X.; Guo, Q.; Cui, D. Recent advances in nanotechnology applied to biosensors. *Sensors* **2009**, *9*, 1033-1053.

14. Massoulié, J.; Pezzementi, L.; Bon, S.; Krejci, E.; Vallette, F. M. Molecular and cellular biology of cholinesterases. *Prog. Neurobiol.* **1993**, *41*, 31-91.

15. Chacko, L. W.; Cerf, J. A. Histochemical localization of cholinesterase in the amphibian spinal cord and alterations following ventral root section. *J. anat.* **1960**, *94*, 74-81.

16. Millard, C. B.; Kryger, G.; Ordentlich, A.; Greenblatt, H. M. Crystal structures of aged phosphonylated acetylcholinesterase: Nerve agent reaction products at the atomic level. *Biochemistry* **1999**.

17. Nieuwenhuizen, M. S.; Harteveld, J. L. N. Studies on a surface acoustic wave (saw) dosimeter sensor for organophosphorous nerve agents. *Sens. Actuators B* **1997**, *40*, 167-173.

18. Ngeh-Ngwainbi, J.; Foley, P. H.; Kaun, S. S.; Guilbault, G. G. Parathion antibodies on piezoelectric crystals. *J. Am. Chem. Soc.* **1986**, *108*, 5444-5447.

19. Yang, Y. M.; Ji, H.-F.; Thundat, T. Nerve agents detection using a cu2+/l-cysteine bilayer-coated microcantilever. *J. Am. Chem. Soc.* **2003**, *125*, 1124-1125.

20. Hartmann-Thompson, C.; Hin, J.; Kaganove, S. N.; Keinath, S. E.; Keeley, D. L.; Dvornic, P. R. Hydrogen-bond acidic hyperbranched polymers for surface acoustic wave (saw) sensors. *Chem. Mater.* **2004**, *16*, 5357-5364.

21. Yuehe, L.; Fang, L.; Joseph, W. Disposable carbon nanotube modified screen-printed biosensor for amperometric detection of organophosphorus pesticides and nerve agents. *Electroanalysis* **2004**, *16*, 145-149.

22. Zhou, Y.; Yu, B.; Shiu, E.; Levon, K. Potentiometric sensing of chemical warfare agents: Surface imprinted polymer integrated with an indium tin oxide electrode. *Anal. Chem.* **2004**, *76*, 2689-2693.

23. Anitha, K.; Mohan, S. V.; Reddy, S. J. Development of acetylcholinesterase silica sol-gel immobilized biosensor - an application towards oxydemeton methyl detection. *Biosens. Bioelectron.* **2004**, *20*, 848-856.

24. Simonian, A. L.; Grimsley, J. K.; Flounders, A. W.; Schoeniger, J. S.; Cheng, T. C.; DeFrank, J. J.; Wild, J. R. Enzyme-based biosensor for the direct detection of fluorine-containing organophosphates. *Anal. Chem. Acta* **2001**, *442*, 15-23.

25. Steiner, W. E.; Klopsch, S. J.; English, W. A.; Clowers, B. H.; Hill, H. H. Detection of a chemical warfare agent simulant in various aerosol matrixes by ion mobility time-of-flight mass spectrometry. *Anal. Chem.* **2005**, *77*, 4792-4799.

26. Wang, J. Microchip devices for detecting terrorist weapons. *Anal. Chem. Acta* **2004**, *507*, 3-10.

27. Ellman, G. L.; Courtney, K. D.; Andres, V., Jr.; Feather-Stone, R. M. A new and rapid colorimetric determination of acetylcholinesterase activity. *Biochem. Pharmacol.* **1961**, *7*, 88-95.

28. Eyer, P.; Worek, F.; Kiderlen, D.; Sinko, G.; Stuglin, A.; Simeon-Rudolf, V.; Reiner, E. Molar absorption coefficients for the reduced ellman reagent: Reassessment. *Anal. Biochem.* **2003**, *312*, 224-227.

29. Oliveira, O. N., Jr.; Iost, R. M.; Siqueira, J. R., Jr.; Crespilho, F. N.; Caseli, L. Nanomaterials for diagnosis: Challenges and applications in smart devices based on molecular recognition. *ACS Appl. Mater. Interfaces* **2014**, *6*, 14745-14766.

30. Rolfe, P. Micro- and nanosensors for medical and biological measurement. *Sensor. Mater.* **2012**, *24*, 275-302.

31. Famulok, M.; Mayer, G. Aptamer modules as sensors and detectors. *Acc. Chem. Res.* **2011**, *44*, 1349-1358.

32. Chen, M.; Huang, C.; He, C.; Zhu, W.; Xu, Y.; Lu, Y. A glucose-responsive controlled release system using glucose oxidase-gated mesoporous silica nanocontainers. *Chem. Commun.* **2012**, *48*, 9522-9524.

33. Sheldon, R. A. Enzyme immobilization: The quest for optimum performance. *Adv. Synth. Catal.* **2007**, *349*, 1289-1307.

34. Cheng, K.; Landry, C. C. Diffusion-based deprotection in mesoporous materials: A strategy for differential functionalization of porous silica particles. *J. Am. Chem. Soc.* **2007**, *129*, 9674-9685.

35. Sing, K. S. W. Reporting physisorption data for gas/solid systems with special reference to the determination of surface area and porosity (recommendations 1984). *Pure Appl. Chem.* **1985**, *57*, 603-619.

36. Bolognesi, M. L.; Cavalli, A.; Valgimigli, L.; Bartolini, M.; Rosini, M.; Andrisano, V.; Recanatini, M.; Melchiorre, C. Multi-target-directed drug design strategy: From a dual binding site acetylcholinesterase inhibitor to a trifunctional compound against alzheimer's disease. *J. Med. Chem.* **2007**, *50*, 6446-6449.

37. Bartolini, M.; Cavrini, V.; Andrisano, V. Characterization of reversible and pseudo-irreversible acetylcholinesterase inhibitors by means of an immobilized enzyme reactor. *J. Chromatogr. A* **2007**, *1144*, 102-110.

38. Ouberai, M.; Brannstrom, K.; Vestling, M.; Olofsson, A.; Dumy, P.; Chierici, S.; Garcia, J. Clicked tacrine conjugates as acetylcholinesterase and beta-amyloid directed compounds. *Org. Biomol. Chem.* **2011**, *9*, 1140-1147.

39. Kozurkova, M.; Hamulakova, S.; Gazova, Z.; Paulikova, H.; Kristian, P. Neuroactive multifunctional tacrine congeners with cholinesterase, anti-amyloid aggregation and neuroprotective properties. *Pharmaceuticals* **2011**, *4*, 382-418.

40. Houghton, P. J.; Ren, Y.; Howes, M. J. Acetylcholinesterase inhibitors from plants and fungi. *Nat Prod Rep* **2006**, *23*, 181-199.

41. Heilbronn, E. Inhibition of cholinesterases by tetrahydroaminacrin. *Acta chem. Scand.* **1961**, *15*, 1386-1390.

42. Dawson, R. M.; Dowling, M. H.; Poretski, M. Assessment of the competition between tacrine and gallamine for binding-sites on acetylcholinesterase. *Neurochem. Int.* **1991**, *19*, 125-133.

43. Landry, C. C.; Nassivera, T. W. *US Patent Appl. 20090220791*.

44. Gallis, K. W.; Landry, C. C. *US Patent* **2002**, 6334988.

45. Chan, L. C.; Cox, B. G. Kinetics of amide formation through carbodiimide/n-hydroxybenzotriazole (hobt) couplings. *J Org Chem* **2007**.

46. Smith, P. K.; Krohn, R. I.; Hermanson, G. T.; Mallia, A. K. Measurement of protein using bicinchoninic acid. *Analytical …* **1985**.

47. Garrett, R. H.; Grisham, C. M., *Biochemistry*. 4th ed.; Brooks/Cole: Boston, 2010.

48. Lane, R. M.; Potkin, S. G.; Enz, A. Targeting acetylcholinesterase and butyrylcholinesterase in dementia. *Int. J. Neuropsychopharmacol.* **2006**, *9*, 101-124.

49. Tro, N. J., *Chemistry: A molecular approach*. 3rd ed.; Pearson Boston, 2014.

50. Steinberg, G. M.; Mednick, M. L.; Maddox, J.; Rice, R. A hydrophobic binding site in acetylcholinesterase. *J. Med. Chem.* **1975**, *18*, 1057-1061.

51. Nielsen, J. A.; Mena, E. E.; Williams, I. H.; Nocerini, M. R.; Liston, D. Correlation of brain levels of 9-amino-1,2,3,4-tetrahydroacridine (tha) with neurochemical and behavioral changes. *Eur. J. Pharmacol.* **1989**, *173*, 53-64.

52. Dawson, R. M. Tacrine slows the rate of ageing of sarin-inhibited acetylcholinesterase. *Neurosci. Lett.* **1989**, *100*, 227-230.

53. El-Boubbou, K.; Schofield, D. A.; Landry, C. C. Enhanced enzymatic thermal stability and activity in functionalized mesoporous silica monitored by (31) p nmr. *Adv. Healthc. Mater.* **2012**, *1*, 183-188.

54. Munoz, B.; Ramila, A.; Perez-Pariente, J.; Diaz, I.; Vallet-Regi, M. Mcm-41 organic modification as drug delivery rate regulator. *Chem. Mat.* **2003**, *15*, 500-503.

55. Chothia, C.; Leuzinger, W. Acetylcholinesterase: The structure of crystals of a globular form from electric eel. *J. Mol. Biol.* **1975**, *97*, 55-60.

56. Krajewska, B.; Zaborska, W. a.; Leszko, M. Inhibition of chitosan-immobilized urease by slow-binding inhibitors: Ni2+, f− and acetohydroxamic acid. *J. Mol. Catal. B-Enzym.* **2001**, *14*, 101-109.

57. Brown, M. A.; Huthwelker, T.; Redondo, A.; Janousch, M.; Faubel, M.; Arrell, C. A.; Scarongella, M.; Chergui, M.; Bokhoven, J. A. Changes in the silanol protonation state measured in situ at the silica–aqueous interface. *The Journal of Physical Chemistry Letters* **2012**, *3*, 231-235.

58. Forsberg, A.; Puu, G. Kinetics for the inhibition of acetylcholinesterase from the electric eel by some organophosphates and carbamates. *Eur. J. Biochem.* **1984**, *140*, 153-156.

59. Villatte, F.; Marcel, V.; Estrada-Mondaca, S.; Fournier, D. Engineering sensitive acetylcholinesterase for detection of organophosphate and carbamate insecticides. *Biosens. Bioelectron.* **1998**, *13*, 157-164.

60. Vetsch, J. R.; Paulsen, S. J.; Muller, R.; Hofmann, S. Effect of fetal bovine serum on mineralization in silk fibroin scaffolds. *Acta Biomater.* **2015**, *13*, 277-285.

61. Clemments, A. M.; Muniesa, C.; Landry, C. C.; Botella, P. Effect of surface properties in protein corona development on mesoporous silica nanoparticles. *RSC Adv.* **2014**, *4*, 29134-29138.

CHAPTER 4: DETERMINATION OF PHOSPHORYLATION RATE BY CONGO RED RELEASE

4.1. Introduction

Nerve agent detection methods have continually evolved to help limit the exposure of military and civilian personnel to these potentially deadly organophosphorus compounds. Optical biosensors, particularly those based on colorimetric[1-3] assays, have several benefits including increased portability and real-time detection.[4-15] Many of these assays are inhibition-based detection systems measuring the change in activity of acetylcholinesterase (AChE).[15-20] The rationale for the use of AChE as the basis for these biosensors lies with its interaction with organophosphates, resulting in the phosphorylation of the AChE active site. The hydrolysis rate of acetylcholine by AChE can then be measured before and after exposure to an organophosphate, and the kinetics determined.

Recently, the development of two direct response systems; one for detection and decontamination using organophosphorus hydrolase (OPH) and the other using AChE for increased sensitivity for detection were developed by our group. The use of a porous silica support allowed a competitive inhibitor of each enzyme to be attached to the nanoparticle surface, temporarily tethering the enzyme to the surface. This allowed the enzyme to block the pores of the silica, acting as a triggered release mechanism when in the presence of a substrate. In the case of AChE, organophosphates can also release the enzyme by permanently modify its active site. If the interior pore volume of the silica is loaded with a dye, the release of the enzyme caused release of the dye, which could be visually tracked

with the naked eye, allowing for use by an untrained individual without complex instrumentation and quantified by UV-Visible spectroscopy. The use of an enzyme-inhibitor trigger allowed for high specificity of the system, in which release of the enzyme occurred only in the presence of the substrate or organophosphate, for the AChE based system (**Figure 4.1**).

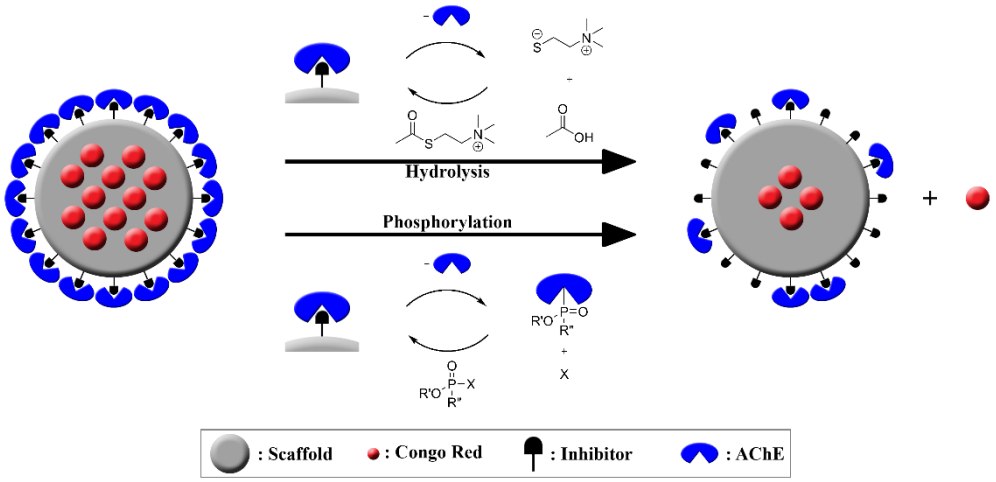

Figure 4.1: Release of CR due to presence of substrate (hydrolysis) or organophosphate (phosphorylation).

The initial purpose in designing these detection systems was to combine fast detection with limited false positives, regardless of the specific organophosphate detected. While the detection system using AChE does show a fast response, further experiments were required to determine and compare the rates of release using different organophosphates. Using the same mesoporous silica scaffold and competitive tacrine inhibitor-AChE pair, described in Chapter 3, several organophosphates were tested and the

kinetics of dye release compared to the rate of AChE phosphorylation.

4.2. Experimental Section

4.2.1. Materials and Instrumentation

See All materials were purchased from Sigma-Aldrich, VWR and Life Technologies. UV/Vis spectra were measured using a Perkin-Elmer Lambda 35 spectrophotometer system. Thermogravimetric analysis (TGA) was performed on a PerkinElmer Pyris 1 DSC-TGA. Scans were performed under a mixed flow of nitrogen (85%) and oxygen (15%) between 25 °C and 800 °C at 20 °C/min with a thermal hold at 100°C for 15 minutes to remove any residual water. N_2 adsorption and desorption isotherms were obtained on a Micromeritics TriStar instrument. Surface areas were measured using the Brunauer-Emmett-Teller (BET) method and pore size distributions were calculated from a modified Kruk, Jaronic and Sayari (KJS) method using the adsorption branch.

4.2.2. Synthesis, Functionalization and Characterization of APMS

4.2.2.1. Synthesis of Acid-Prepared Mesoporous Silica (APMS)

APMS was synthesized as previously described.[21-22]

4.2.2.2. Synthesis of APMS-(s)-NH_2

Pore-blocked APMS (1.8 g) was suspended in hexanes (400 mL) to which 3-aminoproplytriethoxysilane (APTES) (1.8 mL) was added. The solution was refluxed for 3.5 hours under an inert atmosphere (N_2) to form the product APMS-(s)-NH_2. To remove surfactant from the pores, APMS-(s)-NH_2 was extracted by refluxing with acidified ethanol

(0.1 M HCl in ethanol) for 24 hours (3X), filtering and letting dry between each cycle. The degree of modification was characterized by thermogravimetric analysis (2.02 mmol modification/g APMS) and the physical properties characterized by nitrogen physisorption. The resulting APMS was then placed under vacuum to keep dry until further modification.

4.2.2.3. Synthesis of APMS-(s)-NH-COOH

Extracted APMS-(s)-NH_2 (1.5 g) was suspended in acetonitrile (dry) under an inert atmosphere (N_2) to which triethylamine (950 µL) and succinic anhydride (355 mg) was added. The solution was stirred at 60°C for 21.5 hours then collected by vacuum filtration. Several washings with trifluoroacetic acid (0.1% in water) and acetonitrile were followed by drying overnight. The degree of modification was characterized by thermogravimetric analysis (0.61 mmol modification/g APMS) and the physical properties characterized by nitrogen physisorption. The resulting APMS-(s)-NH-COOH was then placed under vacuum to keep dry until further modification.

4.2.2.4. Synthesis of APMS-(s)-Tac

In a typical synthesis, APMS-(s)-NH-COOH (57 mg) was suspended in 8 mL dimethylformamide (DMF) to which, hydroxybenzotriazole (HOBt) (82 mg), N, N'-diisopropylcarbodiimide (90 mg) and 4-dimethylaminopyridine (DMAP) (4 mg) were added and stirred for 1 hour. Tacrine hydrochloride (Tac) (14 mg) was then added and stirred for 19 hours. The particles were collected by vacuum filtration and washed with DMF then MeOH and left to dry overnight. The degree of modification (0.28 mmol modification/g APMS) was determined by thermogravimetric analysis and the physical properties characterized by nitrogen physisorption. The resulting APMS-(s)-Tac was then

placed under vacuum to keep dry until further modification.

4.2.3. Congo Red Loading and Release Using APMS-CR-(s)-Tac-AChE

4.2.3.1. Loading of Congo Red (APMS-CR-(s)-Tac)

In a typical loading procedure, Congo Red (CR) (40 mg) was added to a citrate buffer (5 mL, 0.01 M, pH 3.98) to make a CR stock. APMS-(s)-Tac (4.0 mg) was shaken (24 hr) with the CR stock (3 mL, 11.5 mM). The sample was centrifuged and the supernatant measured by UV-Vis to determine the amount of CR loaded. The material was washed once with citrate buffer and phosphate buffer (100 mM, pH = 7.3) to prepare for loading with AChE.

4.2.3.2. Determination of [AChE]

Free AChE concentrations and AChE immobilized onto APMS-(s)-Tac were calculated using a Pierce™ BCA protein assay kit using a standard bovine serum albumin (BSA) calibration curve.[23] Triplicate samples measured for the standard curve.

4.2.3.3. Loading AChE (APMS-CR-(s)-Tac-AChE)

A typical loading required 4.0 mg APMS-CR-(s)-Tac suspended in a stock AChE solution (508 µg/mL in phosphate buffer (100 mM, pH = 7.3)) and placed on a rotating platform for 24 hours. The sample was centrifuged, supernatant removed and immobilized AChE determined by the BCA assay. The particles were washed with phosphate buffer until all non-encapsulated CR was removed. The particles were then re-suspended in the appropriate amount of phosphate buffer for kinetics testing.

4.2.3.4. Release of Congo Red from APMS-CR-(s)-Tac-AChE

In a typical reaction, APMS-CR-(s)-Tac-AChE (0.11 mg AChE total, 0.608 µM)

was suspended in phosphate buffer (629.18 µL, 100 mM, pH = 7.3). The sample was shaken for 15 minutes, centrifuged and supernatant measure to show no CR releasing. An aliquot of paraoxon was then added to give the desired concentration in solution (5.06, 7.08 or 8.23 mM). The sample was shaken for a set time interval (2.5 - 5 min) and the reaction stopped by centrifugation. The supernatant was then measured by UV-Vis to measure the amount of CR released based on a calibration curve. This procedure was repeated with additional organophosphates (parathion, demeton-s and malathion), adjusting the experimental conditions for the desired concentrations in solution.

4.2.3.5. Inhibition of AChE After Release from APMS-(s)-Tac-AChE

After release of CR from APMS-CR-(s)-Tac-AChE using demeton-s, the sample was centrifuged and the supernatant removed. To the supernatant (200 µL), Ellman's reagent, 5, 5'-dithio-bis-(2-nitrobenzoic acid) (20 µL) and acetylthiocholine (AtCh) (2 µL) from an AtCh stock (7.64 mM) was added. The reaction was allowed to react for 25 min and measured by UV-Vis. This was compared to a background standard sample of the same concentrations but without AChE and measured by UV-Vis.

4.3. Results

4.3.1. Preparation and Characterization of APMS-(s)-Tac

Synthesis and characterization was the same as described in Chapter 3. The material designated APMS-(s)-Tac (med), was used that had 0.28 mmol tacrine per gram of APMS.

4.3.2. Release of CR from APMS-CR-(s)-Tac-AChE

The loading of CR and attachment of AChE was the same as described in Chapter

3. Experiments were then performed to compare the rates of release using different organophosphates. Prior to organophosphate addition, the particles were shaken for 15 minutes in phosphate buffer and the supernatant measured to ensure no CR was releasing. An aliquot of organophosphate (paraoxon, parathion, demeton-s or malathion) was then added, resulting in the desired concentration in solution (5.06, 7.08 and 8.23 mM). The concentration of CR in the supernatant was measured after a set time interval of five minutes to track the release of CR after detachment of AChE from the nanoparticle surface. Varying the concentration of organophosphate and measuring the release of CR within a set time period allowed for the plotting of this data in a Lineweaver-Burk plot to calculate the release kinetics (**Table 4.1**) before the CR release plateau.

Table 4.1: CR release kinetics with different organophosphates.[24-25]

Surrogate	LD^{50} (mg/m^3)	V_{max} (M/min)	K_m (M)	k_{cat} (min^{-1})	k_{cat}/K_m ($M^{-1}\ min^{-1}$)
Paraoxon	1	2.96×10^{-6}	1.21×10^{-6}	4.87	403
Parathion	35	1.88×10^{-6}	1.92×10^{-6}	3.09	160
Demeton-S	55	1.84×10^{-6}	2.28×10^{-6}	3.03	133
Malathion	1330	3.88×10^{-7}	2.55×10^{-6}	0.64	25

4.4. Discussion

4.4.1. Mechanism of Phosphorylation

Previous testing of the detection system with AtCh and paraoxon showed its high specificity for these compounds. At this point, we were interested in exploring the ability of this detection system to detect and decontaminate other, related organophosphates. Differences among the organophosphates were controlled by the rate of phosphorylation within the AChE active site. Increased toxicity results in increasing rates of AChE phosphorylation, inhibiting the activity of AChE.[26-27]

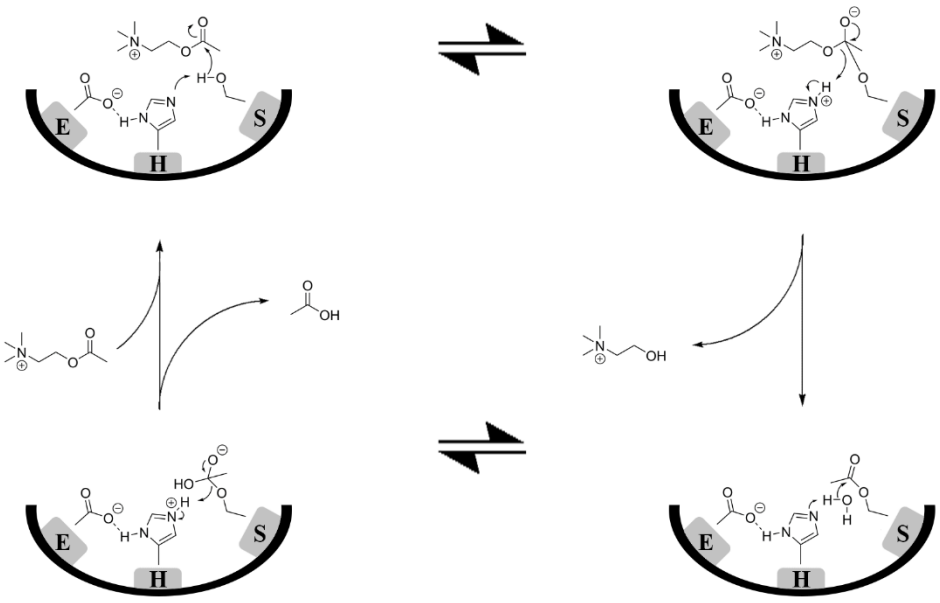

Figure 4.2: Hydrolysis of acetylcholine within the AChE active site.[26]

The AChE active site consists of a catalytic triad of serine (S), glutamic acid (E)

and histidine (H) (**Figure 4.2**).[26] The negatively charged glutamic acid interacts with the positively charged nitrogen on ACh to stabilize ACh within the active site. The serine hydroxyl is acetylated by ACh with the assistance of the nearby histidine, leading to the release of choline. This is followed by a nucleophilic attack by a water molecule, causing deacetylation and regenerating the enzyme. In the poisoning of AChE by organophosphates, a similar process is followed by the rate of deacetylation is exceedingly slow, varying depending on the substituents on the phosphorus atom. Thus, AChE cannot function and a buildup of ACh occurs (**Figure 4.3**).[26]

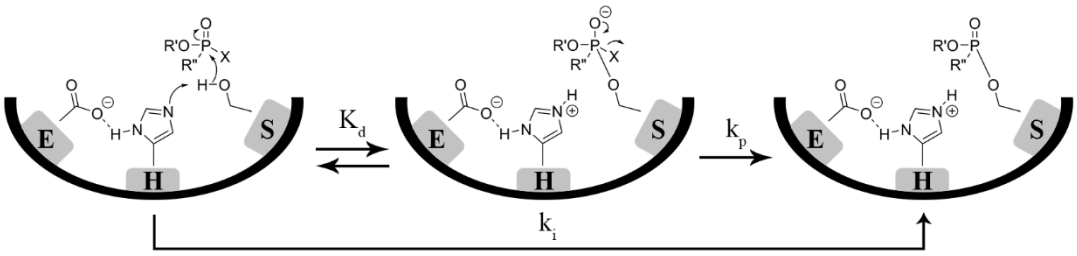

Figure 4.3: Phosphorylation of the AChE active site.[26]

Inhibition of AChE by organophosphorus compounds has been characterized by the inhibition constant, k_i. This constant is comprised of two factors that control the overall rate of inhibition. The first is the dissociation constant (K_d) that is determined by the affinity of the organophosphate for the serine residue. The formation of the organophosphate-enzyme intermediate relies heavily on the reactivity of the phosphorus ester and steric constraints of the organophosphate. The second determining factor is based on the rate of formation of the organophosphorus ester (k_p), which has been shown to be controlled by

the leaving group (X). Overall, these two rates determine the inhibition constant (k_i) for a particular organophosphate which is equal to k_p/K_d.[27-28] This provides a basis to compare the rates at which organophosphates inhibit AChE.

4.4.2. Organophosphate Surrogates

Due to the extreme toxicity of organophosphate nerve agents, chemical surrogates with similar structures are often used in a laboratory setting. These surrogates are usually commercially available pesticides (**Figure 4.4**).[26, 29] (these are not three dimensional at the phosphorus center) Testing of the proposed detection system used surrogate species that contained similar structure characteristics to both G and V-agents. In general, G-agents contain a halide leaving group bound to the phosphorous (P-X) such as with sarin and V-agents contain a sulfur-containing leaving group (P-S) such as with VX.[27]

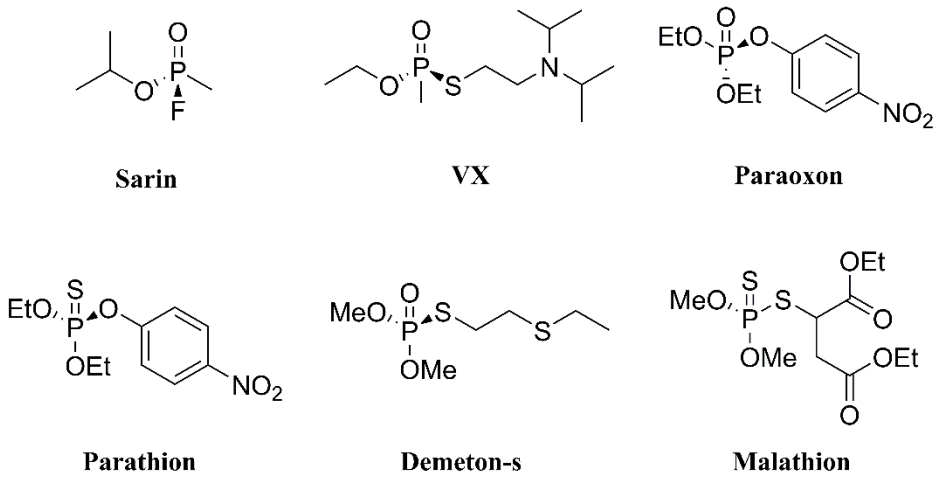

Figure 4.4: Nerve agents and organophosphate surrogates. [26, 29]

Altering the rate of phosphorylation has been a commonly pursued strategy in the development of pesticides, giving a large library of surrogates to select from. The surrogates selected (paraoxon, parathion, demeton-s, and malathion) were chosen to represent a range of organophosphate structures. In particular, paraoxon and parathion were used as G-agent surrogates, and demeton-s and malathion were selected as V-agent surrogates.

One difference among these surrogates is the replacement of the P=O bond for a P=S bond. This has shown to decrease the rate of phosphorylation due to the decreased polarizability of the P=S bond. The electropositive character of the phosphorus atom that is created by the P=O bond facilitates nucleophilic attack by the serine at the active site of AChE. With this in mind, the rates of inhibition (k_i) for free AChE have been previously determined for several organophosphates such as paraoxon (2.9×10^5 M^{-1} min^{-1}) and demeton-s (1.0×10^3 M^{-1} min^{-1}) for specific AChE sources such as an electric eel, used in this work.[28] These values are representative of the inhibition rate of AChE in which half of the concentration of enzyme has been inhibited. This would allow for a comparison of each of the selected surrogates species by the rates of AChE inhibition. With higher k_i values, the faster AChE will be released from the surface due to disruption of the inhibitor in the enzyme active site and the opposite with smaller k_i values. This can be used to track the sensitivity of the system with decreasing rates of inhibition from paraoxon to parathion to demeton-s to malathion.[27] For direct comparison between all surrogates, the use of LD_{50} was used. This value represents the dose at which half of the population does not survive. The LD_{50} for the mouse model (oral) was found to be 1, 35, 55, and 1330 mg/m^3 for

paraoxon, parathion, demeton-s, and malathion, respectively (**Table 4.1**).[24-25]

4.4.3. CR Release Kinetics

Disruption of the interaction between the competitive inhibitor tacrine (Tac) and the active site of AChE can be caused by the substrate or organophosphate through two different mechanisms. Competition between Tac and the substrate for the active site causes the release of AChE from the scaffold, opening the pores and allowing CR to escape. The AChE is now free to hydrolyze AtCh into product. The rate at which this occurs is dependent on the substrate concentration. In the case of organophosphates, the phosphorylation of the serine residue disrupts the interaction between Tac and AChE, resulting in the uncapping of the pores and release of CR. AChE is now free but inactive due to phosphorylation of the active site. The rate at which this response occurs is dependent on the rate at which AChE is phosphorylated, (k_i) determined by the fitment of the organophosphate within the active and the reactivity of the organophosphorus ester.[24]

With the current detection system, the kinetics of CR release are related to the rate at which AChE is released from the surface, which are in turn related to the rate of AChE inhibition. Our expectation was therefore the rate of CR release should be highest for paraoxon and lowest for malathion, based on their LD_{50} values (**Table 4.1**).[24-25] Importantly, the AChE should also continue to be inhibited after release from the surface, allowing successive cycles of CR release to occur upon repeated exposures to organophosphorus compounds. To ensure that inhibition of the released AChE was occurring, post-CR release, the activity of AChE was tested using the Ellman's method[30-31] and confirmed inhibition with the lack of 2-nitro-5-thiobenzoate production. Because of

these connections, the Michaelis-Menten kinetics model[32] can be used to provide an indirect assessment of organophosphorus inhibition of AChE.

Measurement of activity was determined by measuring the amount of CR released within a time period after the addition of an aliquot of surrogate. This was then repeated with several additional concentrations of the surrogate and measuring the amount of CR released. For each surrogate, the rate of CR release compared to surrogate concentration was used to create a Lineweaver-Burk plot to determine the release kinetics. CR release was determined for each of the preselected surrogates and compared (**Table 4.1**). Using the information calculated, several characteristics about the detection system can be determined.

The maximum velocity (V_{max}) for each of surrogates represents the maximum release rate of CR from APMS-CR-(s)-Tac-AChE. This is directly related to the rate at which AChE is released from the surface due to phosphorylation. From paraoxon to malathion, the V_{max} correlates with the decrease in phosphorylation rate of each surrogates with the largest velocity reaching 2.96×10^{-6} M/min for paraoxon (**Table 4.1**). The V_{max} for parathion and demeton-s are similar with parathion having a slightly elevated velocity. The similarity in rates can be attributed to a balance between the decreased polarizability of having a P=S (parathion) versus a slower leaving group (demeton-s) both factors resulting in changes to the rate of phosphorylation.[27] Despite this, differentiation between the surrogates was attainable and this differentiation was held constant throughout the rest of the kinetic factor comparisons.

Typically, the K_m is a measure of how much substrate is needed to reach $V_{max}/2$.

The smaller the K_m, the less substrate that is needed to reach half of the maximum velocity. This is controlled by the affinity the enzyme has for its substrate. The higher the affinity, the faster substrate is converted to product. In the case of the current detection system, the K_m represents the same situation but is the affinity the substrate has for the enzyme. Increased rates of phosphorylation are a direct result of the organophosphate reacting faster with the enzyme, giving smaller K_m values and the K_m increasing with the decrease in phosphorylation rates. This correlates directly with the CR release data (**Table 4.1**) in which the K_m values increase from paraoxon (1.21×10^{-2} M) to the largest for malathion (2.55×10^{-2} M).

The k_{cat} can be defined as the turn over number of an enzyme, representing the number of substrate molecules that are converted to product per enzyme. The higher the k_{cat}, the more active the enzyme in substrate conversion. The measurement of k_{cat} for the triggered release system is based on the rate at which CR is released. This is controlled by the displacement of AChE due to phosphorylation. The faster this process occurs results in a higher k_{cat} and is directly proportional to the rate of phosphorylation. This was seen with an increase in the k_{cat} of CR release from malathion to paraoxon (**Table 4.1**).

While the V_{max}, K_m, and k_{cat} each define different aspects of the kinetics for an enzyme and its substrate, variability in solvents and total enzyme concentration can hinder comparisons between different enzymes. Commonly, the use of catalytic efficiency (k_{cat}/K_m) defines the overall ability of an enzyme to convert substrate to product. While experimental conditions and enzyme concentration remained the same, variability between each of the surrogate species represents a wide range of structural and electronic

differences that all influence the rate of phosphorylation. The use of k_{cat}/K_m for comparison to the surrogates and the ability to discern between them. This results in the catalytic efficiency of the system to be higher for stronger phosphorylating surrogates, i.e. larger k_{cat} and smaller K_m. The k_{cat}/K_m for paraoxon compared to malathion represents the ability for the detection system to differentiate between organophosphates by having a 16-fold difference in catalytic efficiency for CR released between these two surrogates (403 $M^{-1}min^{-1}$ versus 25 $M^{-1}min^{-1}$). Comparison of paraoxon catalytic efficiency to demeton-s (3-fold) and parathion (2.5-fold) represents the sensitivity of the system by allowing for differentiation based on the amount of CR released.

4.5. Conclusion

The ability for organophosphate detection systems to work fast and efficiently decreases the probability for a civilian or military personnel to be exposed. This requires ease of use of the system while limiting false positives. Using a direct response system that is triggered directly by the organophosphate allows for a faster response time to determine the threat of exposure faster and the appropriate next step to be taken. Using a mesoporous silica scaffold, the proposed detection system uses the interior pore volume to hold a dye and its release controlled by an enzyme-inhibitor pair trigger that responded distinctly to different organophosphates.

The exterior modification of the scaffold, APMS, with the competitive inhibitor tacrine was used to tether ACHE to the scaffold after loading the interior pore volume with CR. AChE capped the pore of APMS and remained there until the presence of an

organophosphate surrogate. Phosphorylation of AChE disrupted the enzyme-inhibitor interaction, displacing AChE and releasing CR. This has been previously shown to be tracked visually but more importantly could be quantified by UV-Vis. This allowed for the direct determination of CR release kinetics based on the rate of phosphorylation of AChE by each of the different surrogate organophosphates tested.

The design of the detection system to differentiate between organophosphates by releasing CR consistent with the rate of phosphorylation is highly advantageous. The ability for a detection system to quickly and easily discern the threat level of an exposed area is crucial to limiting exposure. With the current enzyme-inhibitor trigger system using the specific enzyme that becomes inhibited when exposed to a nerve agent, allows for the response of the system to be directly proportional and limits false positives. This has shown promise within triggered-release systems in which the specificity of the trigger can be defined by the enzyme for its substrate.

4.6. References

1. Climent, E.; Marti, A.; Royo, S.; Martinez-Manez, R.; Marcos, M. D.; Sancenon, F.; Soto, J.; Costero, A. M.; Gil, S.; Parra, M. Chromogenic detection of nerve agent mimics by mass transport control at the surface of bifunctionalized silica nanoparticles. *Angew. Chem. Int. Ed. Engl.* **2010**, *49*, 5945-5948.

2. Royo, S.; Martinez-Manez, R.; Sancenon, F.; Costero, A. M.; Parra, M.; Gil, S. Chromogenic and fluorogenic reagents for chemical warfare nerve agents' detection. *Chem. Commun.* **2007**, 4839-4847.

3. Lee, J.; Seo, S.; Kim, J. Colorimetric detection of warfare gases by polydiacetylenes toward equipment-free detection. *Adv. Funct. Mater.* **2012**, *22*, 1632-1638.

4. Nieuwenhuizen, M. S.; Harteveld, J. L. N. Studies on a surface acoustic wave (saw) dosimeter sensor for organophosphorous nerve agents. *Sens. Actuators B* **1997**, *40*, 167-173.

5. Ngeh-Ngwainbi, J.; Foley, P. H.; Kaun, S. S.; Guilbault, G. G. Parathion antibodies on piezoelectric crystals. *J. Am. Chem. Soc.* **1986**, *108*, 5444-5447.

6. Yang, Y. M.; Ji, H.-F.; Thundat, T. Nerve agents detection using a cu2+/l-cysteine bilayer-coated microcantilever. *J. Am. Chem. Soc.* **2003**, *125*, 1124-1125.

7. Hartmann-Thompson, C.; Hin, J.; Kaganove, S. N.; Keinath, S. E.; Keeley, D. L.; Dvornic, P. R. Hydrogen-bond acidic hyperbranched polymers for surface acoustic wave (saw) sensors. *Chem. Mater.* **2004**, *16*, 5357-5364.

8. Yuehe, L.; Fang, L.; Joseph, W. Disposable carbon nanotube modified screen-printed biosensor for amperometric detection of organophosphorus pesticides and nerve agents. *Electroanalysis* **2004**, *16*, 145-149.

9. Zhou, Y.; Yu, B.; Shiu, E.; Levon, K. Potentiometric sensing of chemical warfare agents: Surface imprinted polymer integrated with an indium tin oxide electrode. *Anal. Chem.* **2004**, *76*, 2689-2693.

10. Yu, D.; Volponi, J.; Chhabra, S.; Brinker, C. J.; Mulchandani, A.; Singh, A. K. Aqueous sol-gel encapsulation of genetically engineered moraxella spp. Cells for the detection of organophosphates. *Biosens. Bioelectron.* **2005**, *20*, 1433-1437.

11. Anitha, K.; Mohan, S. V.; Reddy, S. J. Development of acetylcholinesterase silica sol-gel immobilized biosensor - an application towards oxydemeton methyl detection. *Biosens. Bioelectron.* **2004**, *20*, 848-856.

12. Simonian, A. L.; Grimsley, J. K.; Flounders, A. W.; Schoeniger, J. S.; Cheng, T. C.; DeFrank, J. J.; Wild, J. R. Enzyme-based biosensor for the direct detection of fluorine-containing organophosphates. *Anal. Chem. Acta* **2001**, *442*, 15-23.

13. Wang, J. Microchip devices for detecting terrorist weapons. *Anal. Chem. Acta* **2004**, *507*, 3-10.

14. Steiner, W. E.; Klopsch, S. J.; English, W. A.; Clowers, B. H.; Hill, H. H. Detection of a chemical warfare agent simulant in various aerosol matrixes by ion mobility time-of-flight mass spectrometry. *Anal. Chem.* **2005**, *77*, 4792-4799.

15. Miao, Y.; He, N.; Zhu, J. J. History and new developments of assays for cholinesterase activity and inhibition. *Chem. Rev.* **2010**, *110*, 5216-5234.

16. Mulchandani, P.; Chen, W.; Mulchandani, A. Microbial biosensor for direct determination of nitrophenyl-substituted organophosphate nerve agents using genetically engineered moraxella sp. *Anal Chim Acta* **2006**, *568*, 217-221.

17. Wang, M.; Gu, X.; Zhang, G.; Zhang, D.; Zhu, D. Continuous colorimetric assay for acetylcholinesterase and inhibitor screening with gold nanoparticles. *Langmuir* **2009**, *25*, 2504-2507.

18. Van Dyk, J. S.; Pletschke, B. Review on the use of enzymes for the detection of organochlorine, organophosphate and carbamate pesticides in the environment. *Chemosphere* **2011**, *82*, 291-307.

19. Hossain, S. M.; Luckham, R. E.; Smith, A. M.; Lebert, J. M.; Davies, L. M.; Pelton, R. H.; Filipe, C. D.; Brennan, J. D. Development of a bioactive paper sensor for detection of neurotoxins using piezoelectric inkjet printing of sol-gel-derived bioinks. *Anal. Chem.* **2009**, *81*, 5474-5483.

20. Simonian, A. L.; Good, T. A.; Wang, S. S.; Wild, J. R. Nanoparticle-based optical biosensors for the direct detection of organophosphate chemical warfare agents and pesticides. *Anal. Chim. Acta.* **2005**, *534*, 69-77.

21. Landry, C. C.; Nassivera, T. W. *US Patent Appl. 20090220791*.

22. Gallis, K. W.; Landry, C. C. *US Patent* **2002**, 6334988.

23. Smith, P. K.; Krohn, R. I.; Hermanson, G. T.; Mallia, A. K. Measurement of protein using bicinchoninic acid. *Analytical …* **1985**.

24. Pickering, W. R.; Malone, J. C. The acute toxicity of dichloroalkyl aryl phosphates in relation to chemical structure. *Biochemical pharmacology* **1967**.

25. Chemical listing and documentation of revised idlh values http://www.cdc.gov/niosh/idlh/intridl4.html (accessed April 4, 2016).

26. Kim, K.; Tsay, O. G.; Atwood, D. A.; Churchill, D. G. Destruction and detection of chemical warfare agents. *Chem. Rev.* **2011**, *111*, 5345-5403.

27. Fukuto, T. R. Mechanism of action of organophosphorus and carbamate insecticides. *Environ. Health Perspect.* **1990**, *87*, 245-254.

28. Villatte, F.; Marcel, V.; Estrada-Mondaca, S.; Fournier, D. Engineering sensitive acetylcholinesterase for detection of organophosphate and carbamate insecticides. *Biosens. Bioelectron.* **1998**, *13*, 157-164.

29. Lewis, V. E.; Donarski, W. J.; Wild, J. R.; Raushel, F. M. Mechanism and stereochemical course at phosphorus of the reaction catalyzed by a bacterial phosphotriesterase. *Biochemistry* **1988**, *27*, 1591-1597.

30. Ellman, G. L.; Courtney, K. D.; Andres, V., Jr.; Feather-Stone, R. M. A new and rapid colorimetric determination of acetylcholinesterase activity. *Biochem. Pharmacol.* **1961**, *7*, 88-95.

31. Eyer, P.; Worek, F.; Kiderlen, D.; Sinko, G.; Stuglin, A.; Simeon-Rudolf, V.; Reiner, E. Molar absorption coefficients for the reduced ellman reagent: Reassessment. *Anal. Biochem.* **2003**, *312*, 224-227.

32. Garrett, R. H.; Grisham, C. M., *Biochemistry*. 4th ed.; Brooks/Cole: Boston, 2010.

CHAPTER 5: CONCLUSION

The goal of this study was to develop a molecular recognition system for organophosphate detection to eliminate the problem with false positives seen with previous detection systems. To do this, the use of a MSN as the scaffold to contain the optical signal, the dye Congo Red, is capped with an enzyme to block the pores to retain the loaded dye. The mode of attachment of the enzyme (OPH or AChE) was through the use of a competitive inhibitor of the enzyme. Testing of the triggered-release mechanism with either substrate or organophosphates was thoroughly explored to test the stability of the tethering, and relate the dye release kinetics to the rate of AChE inhibition.

In the first molecular recognition system utilized OPH for a dual detection and decontamination system. The enzyme was tethered to the surface of the particle with the competitive inhibitor DEABP. The competitive inhibition of OPH, both free in solution and immobilized DEABP, was confirmed through enzyme kinetics testing using ^{31}P NMR. The competitive inhibition was used as the trigger for the release of OPH, uncapping the pores and releasing of CR. Color change of the particles was used as visual indication, along with quantification by UV-Vis. This system worked with not only the ideal conditions, but within cell culture media containing a variety proteins and growth factors, maintain the activity of OPH and detection of CR. While OPH had a fast rate of hydrolysis, this hindered probing the release system further. As more paraoxon was added, free OPH would hydrolyze the organophosphate faster than the OPH could be displaced from the surface of APMS. The use of a sacrificial enzyme that would become inactive after its

release would allow for further testing to be completed.

The selection of a sacrificial enzyme relied on an enzyme that would become inactive after the addition of an organophosphate. Organophosphorus compounds target AChE and inhibit the hydrolysis of ACh through inhibition of the AChE active site. This would allow the use of AChE as a sacrificial enzyme that would release from the surface of the particle, allowing CR to escape. For this system, the competitive inhibitor tacrine was used to temporarily tether AChE to the surface of APMS. Confirmation of the competitive inhibition was performed using the Ellman's method to confirm the competitive inhibition of tacrine. This would ensure that the enzyme was tethered through its active site and would be displaced by the introduction of an organophosphate. Similar testing to the OPH-based system, the visual color change of the particles was confirmed and quantified by UV-Vis. Testing the system against false positives was conducted with both the AChE substrate, AtCh, and paraoxon. This included phosphate buffer, FBS and human serum, which CR released only after the introduction of AtCh or paraoxon. This showed the benefit of having a molecular recognition system that only released in when exposed to an organophosphate, despite having a large concentration of proteins in solution.

The final exploration of the AChE-based detection system was testing against different organophosphates. The nerve agent surrogates used were paraoxon, parathion, demeton-s, and malathion, ranked from the highest rate of inhibition to the lowest. Changes in the rate of AChE inhibition could be tracked with changes in the rate and amount of CR released. The decrease in inhibition rate resulted in a slower release of AChE from the

surface of APMS due to the disruption of the inhibitor-enzyme tether. The slower AChE was released, the smaller amount of CR released from the material. The sensitivity of the system to different inhibition rates represents the use of this system for the detection of a variety of organophosphates, with an increased signal for faster inhibiting organophosphates.

The use of an enzyme-inhibitor molecular recognition system shows promise in the area of organophosphate detection by eliminating the problem with false positives and giving a visual detection. The visual detection broadens the scope of use among untrained individuals, and limiting the exposure to the population.

COMPREHENSIVE BIBLIOGRAPHY

Ahn, S.-k.; Kasi, R. M.; Kim, S.-C.; Sharma, N.; Zhou, Y., Stimuli-responsive polymer gels. *Soft Matter* **2008**, *4*, 1151-1157.

Andersson, J.; Rosenholm, J.; Areva, S.; Lindén, M., Influences of Material Characteristics on Ibuprofen Drug Loading and Release Profiles from Ordered Micro- and Mesoporous Silica Matrices. *Chem. Mater.* **2004**, *16*, 4160-4167.

Angelos, S.; Yang, Y. W.; Khashab, N. M.; Stoddart, J. F.; Zink, J. I., Dual-controlled nanoparticles exhibiting AND logic. *J. Am. Chem. Soc.* **2009**, *131*, 11344-11346.

Anitha, K.; Mohan, S. V.; Reddy, S. J., Development of acetylcholinesterase silica sol-gel immobilized biosensor - an application towards oxydemeton methyl detection. *Biosens. Bioelectron.* **2004**, *20*, 848-856.

Aragay, G.; Pino, F.; Merkoci, A., Nanomaterials for sensing and destroying pesticides. *Chem. Rev.* **2012**, *112*, 5317-5338.

Aragay, G.; Pons, J.; Merkoci, A., Recent trends in macro-, micro-, and nanomaterial-based tools and strategies for heavy-metal detection. *Chem. Rev.* **2011**, *111*, 3433-3458.

Argyo, C.; Weiss, V.; Bräuchle, C.; Bein, T., Multifunctional Mesoporous Silica Nanoparticles as a Universal Platform for Drug Delivery. *Chem. Mater.* **2014**, *26*, 435-451.

Ariga, K.; Ji, Q.; Mori, T.; Naito, M.; Yamauchi, Y.; Abe, H.; Hill, J. P., Enzyme nanoarchitectonics: organization and device application. *Chem. Soc. Rev.* **2013**, *42*, 6322-6345.

Aubert, S. D.; Li, Y.; Raushel, F. M., Mechanism for the Hydrolysis of Organophosphates by the Bacterial Phosphotriesterase. *Biochemistry* **2004**, *43*, 5707.

Aznar, E.; Marcos, M. D.; Martinez-Manez, R.; Sancenon, F.; Soto, J.; Amoros, P.; Guillem, C., pH- and photo-switched release of guest molecules from mesoporous silica supports. *J. Am. Chem. Soc.* **2009**, *131*, 6833-6843.

Aznar, E.; Mondragón, L.; Ros-Lis, J. V.; Sancenón, F.; Marcos, M. D.; Martínez-Máñez, R.; Soto, J.; Pérez-Payá, E.; Amorós, P., Finely Tuned Temperature-Controlled Cargo Release Using Paraffin-Capped Mesoporous Silica Nanoparticles. *Angew. Chem.* **2011**, *123*, 11368-11371.

Balas, F.; Manzano, M.; Horcajada, P.; Vallet-Regi, M., Confinement and controlled release of bisphosphonates on ordered mesoporous silica-based materials. *J. Am. Chem. Soc.* **2006**, *128*, 8116-8117.

Bartolini, M.; Cavrini, V.; Andrisano, V., Characterization of reversible and pseudo-irreversible acetylcholinesterase inhibitors by means of an immobilized enzyme reactor. *J. Chromatogr. A* **2007**, *1144*, 102-110.

Basabe-Desmonts, L.; Reinhoudt, D. N.; Crego-Calama, M., Design of fluorescent materials for chemical sensing. *Chem. Soc. Rev.* **2007**, *36*, 993-1017.

Beck, J. S.; Vartuli, J. C.; Roth, W. J.; Leonowicz, M. E.; Kresge, C. T.; Schmitt, K. D.; Chu, C. T. W.; Olson, D. H.; Sheppard, E. W., A new family of mesoporous molecular sieves prepared with liquid crystal templates. *J. Am. Chem. Soc.* **1992**, *114*, 10834-10843.

Benning, M. M.; Kuo, J. M.; Raushel, F. M.; Holden, H. M., Three-dimensional structure of phosphotriesterase: an enzyme capable of detoxifying organophosphate nerve agents. *Biochemistry* **1994**, *33*, 15001-15007.

Bernardos, A.; Aznar, E.; Coll, C.; Martinez-Manez, R.; Barat, J. M.; Marcos, M. D.; Sancenon, F.; Benito, A.; Soto, J., Controlled release of vitamin B2 using mesoporous materials functionalized with amine-bearing gate-like scaffoldings. *J. Control. Release* **2008**, *131*, 181-189.

Blum, A. P.; Kammeyer, J. K.; Rush, A. M.; Callmann, C. E.; Hahn, M. E.; Gianneschi, N. C., Stimuli-responsive nanomaterials for biomedical applications. *J. Am. Chem. Soc.* **2015**, *137*, 2140-2154.

Bocharova, V.; Zavalov, O.; MacVittie, K.; Arugula, M. A.; Guz, N. V.; Dokukin, M. E.; Halámek, J.; Sokolov, I.; Privman, V.; Katz, E., A biochemical logic approach to biomarker-activated drug release. *J. Mater. Chem.* **2012**, *22*, 19709-19717.

Bolognesi, M. L.; Cavalli, A.; Valgimigli, L.; Bartolini, M.; Rosini, M.; Andrisano, V.; Recanatini, M.; Melchiorre, C., Multi-target-directed drug design strategy: from a dual binding site acetylcholinesterase inhibitor to a trifunctional compound against Alzheimer's disease. *J. Med. Chem.* **2007**, *50*, 6446-6449.

Bonini, M.; Berti, D.; Baglioni, P., Nanostructures for magnetically triggered release of drugs and biomolecules. *Curr. Opin. Colloid In.* **2013**, *18*, 459-467.

Casasus, R.; Climent, E.; Marcos, M. D.; Martinez-Manez, R.; Sancenon, F.; Soto, J.; Amoros, P.; Cano, J.; Ruiz, E., Dual aperture control on pH- and anion-driven supramolecular nanoscopic hybrid gate-like ensembles. *J. Am. Chem. Soc.* **2008**, *130*, 1903-1917.

Chacko, L. W.; Cerf, J. A., Histochemical localization of cholinesterase in the amphibian spinal cord and alterations following ventral root section. *J. anat.* **1960**, *94*, 74-81.

Chang, B.; Sha, X.; Guo, J.; Jiao, Y.; Wang, C.; Yang, W., Thermo and pH dual responsive, polymer shell coated, magnetic mesoporous silica nanoparticles for controlled drug release. *J. Mater. Chem.* **2011**, *21*, 9239-9247.

Chauhan, S.; Chauhan, S.; D'Cruz, R.; Faruqi, S.; Singh, K. K.; Varma, S.; Singh, M.; Karthik, V., Chemical warfare agents. *Environ. Toxicol. Pharmacol.* **2008**, *26*, 113-122.

Chen, B.; Lei, C.; Shin, Y.; Liu, J., Probing mechanisms for enzymatic activity enhancement of organophosphorus hydrolase in functionalized mesoporous silica. *Biochem. Biophys. Res. Commun.* **2009**, *390*, 1177-1181.

Chen, C.; Geng, J.; Pu, F.; Yang, X.; Ren, J.; Qu, X., Polyvalent nucleic acid/mesoporous silica nanoparticle conjugates: dual stimuli-responsive vehicles for intracellular drug delivery. *Angew. Chem. Int. Ed. Engl.* **2011**, *50*, 882-886.

Chen, M.; Huang, C.; He, C.; Zhu, W.; Xu, Y.; Lu, Y., A glucose-responsive controlled release system using glucose oxidase-gated mesoporous silica nanocontainers. *Chem. Commun.* **2012**, *48*, 9522-9524.

Chen, P.-J.; Hu, S.-H.; Hsiao, C.-S.; Chen, Y.-Y.; Liu, D.-M.; Chen, S.-Y., Multifunctional magnetically removable nanogated lids of Fe3O4–capped mesoporous silica nanoparticles for intracellular controlled release and MR imaging. *J. Mater. Chem.* **2011**, *21*, 2535.

Cheng, K.; Landry, C. C., Diffusion-based deprotection in mesoporous materials: a strategy for differential functionalization of porous silica particles. *J. Am. Chem. Soc.* **2007**, *129*, 9674-9685.

Cho, D. G.; Sessler, J. L., Modern reaction-based indicator systems. *Chem. Soc. Rev.* **2009**, *38*, 1647-1662.

Chothia, C.; Leuzinger, W., Acetylcholinesterase: the structure of crystals of a globular form from electric eel. *J. Mol. Biol.* **1975**, *97*, 55-60.

Chung, P.-W.; Kumar, R.; Pruski, M.; Lin, V. S. Y., Temperature Responsive Solution Partition of Organic-Inorganic Hybrid Poly(N-isopropylacrylamide)-Coated Mesoporous Silica Nanospheres. *Adv. Funct. Mater.* **2008**, *18*, 1390-1398.

Clemments, A. M.; Muniesa, C.; Landry, C. C.; Botella, P., Effect of surface properties in protein corona development on mesoporous silica nanoparticles. *RSC Adv.* **2014**, *4*, 29134-29138.

Climent, E.; Bernardos, A.; Martinez-Manez, R.; Maquieira, A.; Marcos, M. D.; Pastor-Navarro, N.; Puchades, R.; Sancenon, F.; Soto, J.; Amoros, P., Controlled delivery systems using antibody-capped mesoporous nanocontainers. *J. Am. Chem. Soc.* **2009**, *131*, 14075-14080.

Climent, E.; Marti, A.; Royo, S.; Martinez-Manez, R.; Marcos, M. D.; Sancenon, F.; Soto, J.; Costero, A. M.; Gil, S.; Parra, M., Chromogenic detection of nerve agent mimics by mass transport control at the surface of bifunctionalized silica nanoparticles. *Angew. Chem. Int. Ed. Engl.* **2010**, *49*, 5945-5948.

Climent, E.; Martinez-Manez, R.; Sancenon, F.; Marcos, M. D.; Soto, J.; Maquieira, A.; Amoros, P., Controlled delivery using oligonucleotide-capped mesoporous silica nanoparticles. *Angew. Chem. Int. Ed. Engl.* **2010**, *49*, 7281-7283.

Coll, C.; Bernardos, A.; Martinez-Manez, R.; Sancenon, F., Gated silica mesoporous supports for controlled release and signaling applications. *Acc. Chem. Res.* **2013**, *46*, 339-349.

Colovic, M. B.; Krstic, D. Z.; Lazarevic-Pasti, T. D.; Bondzic, A. M.; Vasic, V. M., Acetylcholinesterase inhibitors: Pharmacology and toxicology. *Curr. Neuropharmacol.* **2013**, *11*, 315-335.

Dawson, R. M., Tacrine slows the rate of ageing of sarin-inhibited acetylcholinesterase. *Neurosci. Lett.* **1989**, *100*, 227-230.

Dawson, R. M.; Dowling, M. H.; Poretski, M., Assessment of the Competition between Tacrine and Gallamine for Binding-Sites on Acetylcholinesterase. *Neurochem. Int.* **1991**, *19*, 125-133.

de Silva, A. P.; Uchiyama, S.; Vance, T. P.; Wannalerse, B., A supramolecular chemistry basis for molecular logic and computation. *Coordin. Chem. Rev.* **2007**, *251*, 1623-1632.

Diaz de Grenu, B.; Moreno, D.; Torroba, T.; Berg, A.; Gunnars, J.; Nilsson, T.; Nyman, R.; Persson, M.; Pettersson, J.; Eklind, I.; Wasterby, P., Fluorescent discrimination between traces of chemical warfare agents and their mimics. *J. Am. Chem. Soc.* **2014**, *136*, 4125-4128.

Du, L.; Liao, S.; Khatib, H. A.; Stoddart, J. F.; Zink, J. I., Controlled-access hollow mechanized silica nanocontainers. *J. Am. Chem. Soc.* **2009**, *131*, 15136-15142.

Dumas, D. P.; Caldwell, S. R.; Wild, J. R.; Raushel, F. M., Purification and properties of the phosphotriesterase from Pseudomonas diminuta. *J. Biol. Chem.* **1989**, *264*, 19659-19665.

Efremenko, E. N.; Sergeeva, V. S., Organophosphate hydrolase an enzyme catalyzing degradation of phosphorus-containing toxins and pesticides. *Russ. Chem. B+* **2001**, *50*, 1826-1832.

El-Boubbou, K.; Schofield, D. A.; Landry, C. C., Enhanced Enzymatic Activity of OPH in Ammonium-Functionalized Mesoporous Silica: Surface Modification and Pore Effects. *J. Phys. Chem. C* **2012**, *116*, 17501-17506.

El-Boubbou, K.; Schofield, D. A.; Landry, C. C., Enhanced enzymatic thermal stability and activity in functionalized mesoporous silica monitored by (31) p NMR. *Adv. Healthc. Mater.* **2012**, *1*, 183-188.

Ellman, G. L.; Courtney, K. D.; Andres, V., Jr.; Feather-Stone, R. M., A new and rapid colorimetric determination of acetylcholinesterase activity. *Biochem. Pharmacol.* **1961**, *7*, 88-95.

Esser-Kahn, A. P.; Odom, S. A.; Sottos, N. R.; White, S. R.; Moore, J. S., Triggered Release from Polymer Capsules. *Macromolecules* **2011**, *44*, 5539-5553.

Eyer, P.; Worek, F.; Kiderlen, D.; Sinko, G.; Stuglin, A.; Simeon-Rudolf, V.; Reiner, E., Molar absorption coefficients for the reduced Ellman reagent: reassessment. *Anal. Biochem.* **2003**, *312*, 224-227.

Famulok, M.; Mayer, G., Aptamer modules as sensors and detectors. *Acc. Chem. Res.* **2011**, *44*, 1349-1358.

Fang, W.; Yang, J.; Gong, J.; Zheng, N., Photo- and pH-Triggered Release of Anticancer Drugs from Mesoporous Silica-Coated Pd@Ag Nanoparticles. *Adv. Funct. Mater.* **2012**, *22*, 842-848.

Ferris, D. P.; Zhao, Y. L.; Khashab, N. M.; Khatib, H. A.; Stoddart, J. F.; Zink, J. I., Light-operated mechanized nanoparticles. *J. Am. Chem. Soc.* **2009**, *131*, 1686-1688.

Fleige, E.; Quadir, M. A.; Haag, R., Stimuli-responsive polymeric nanocarriers for the controlled transport of active compounds: concepts and applications. *Adv. Drug Deliv. Rev.* **2012**, *64*, 866-884.

Forsberg, A.; Puu, G., Kinetics for the inhibition of acetylcholinesterase from the electric eel by some organophosphates and carbamates. *Eur. J. Biochem.* **1984**, *140*, 153-156.

Fukuto, T. R., Mechanism of action of organophosphorus and carbamate insecticides. *Environ. Health Perspect.* **1990**, *87*, 245-254.

Gallis, K. W.; Landry, C. C., *US Patent* **2002**, 6334988.

Gan, Q.; Lu, X.; Yuan, Y.; Qian, J.; Zhou, H.; Lu, X.; Shi, J.; Liu, C., A magnetic, reversible pH-responsive nanogated ensemble based on Fe3O4 nanoparticles-capped mesoporous silica. *Biomaterials* **2011**, *32*, 1932-1942.

Ganta, S.; Devalapally, H.; Shahiwala, A.; Amiji, M., A review of stimuli-responsive nanocarriers for drug and gene delivery. *J. Control. Release* **2008**, *126*, 187-204.

Gao, W.; Chan, J. M.; Farokhzad, O. C., pH-Responsive nanoparticles for drug delivery. *Mol. Pharm.* **2010**, *7*, 1913-1920.

Garrett, R. H.; Grisham, C. M., *Biochemistry*. 4th ed.; Brooks/Cole: Boston, 2010.

Germain, M. E.; Knapp, M. J., Optical explosives detection: from color changes to fluorescence turn-on. *Chem. Soc. Rev.* **2009**, *38*, 2543-2555.

Giacobini, E., Invited review: Cholinesterase inhibitors for Alzheimer's disease therapy: from tacrine to future applications. *Neurochem. Int.* **1998**, *32*, 413-419.

Giri, S.; Trewyn, B. G.; Stellmaker, M. P.; Lin, V. S., Stimuli-responsive controlled-release delivery system based on mesoporous silica nanorods capped with magnetic nanoparticles. *Angew. Chem. Int. Ed. Engl.* **2005**, *44*, 5038-5044.

Grimsley, J. K.; Calamini, B.; Wild, J. R.; Mesecar, A. D., Structural and mutational studies of organophosphorus hydrolase reveal a cryptic and functional allosteric-binding site. *Arch. Biochem. Biophys.* **2005**, *442*, 169-179.

Grimsley, J. K.; Scholtz, J. M.; Pace, C. N.; Wild, J. R., Organophosphorus Hydrolase Is a Remarkably Stable Enzyme That Unfolds through a Homodimeric Intermediate. *Biochemistry* **1997**, *36*, 14366.

Guo, W.; Wang, J.; Lee, S. J.; Dong, F.; Park, S. S.; Ha, C. S., A general pH-responsive supramolecular nanovalve based on mesoporous organosilica hollow nanospheres. *Chem. Eur. J.* **2010**, *16*, 8641-8646.

Hartmann-Thompson, C.; Hin, J.; Kaganove, S. N.; Keinath, S. E.; Keeley, D. L.; Dvornic, P. R., Hydrogen-Bond Acidic Hyperbranched Polymers for Surface Acoustic Wave (SAW) Sensors. *Chem. Mater.* **2004**, *16*, 5357-5364.

Heilbronn, E., Inhibition of cholinesterases by tetrahydroaminacrin. *Acta chem. Scand.* **1961**, *15*, 1386-1390.

Hoffmann, F.; Cornelius, M.; Morell, J.; Froba, M., Silica-based mesoporous organic-inorganic hybrid materials. *Angew. Chem. Int. Ed. Engl.* **2006**, *45*, 3216-3251.

Hong, C.-Y.; Li, X.; Pan, C.-Y., Smart Core−Shell Nanostructure with a Mesoporous Core and a Stimuli-Responsive Nanoshell Synthesized via Surface Reversible Addition−Fragmentation Chain Transfer Polymerization. *J. Phys. Chem. C* **2008**, *112*, 15320-15324.

Horcajada, P.; Rámila, A.; Pérez-Pariente, J.; Vallet-Regí, M., Influence of pore size of MCM-41 matrices on drug delivery rate. *Micropor. Mesopor. Mat.* **2004**, *68*, 105-109.

Hossain, S. M.; Luckham, R. E.; Smith, A. M.; Lebert, J. M.; Davies, L. M.; Pelton, R. H.; Filipe, C. D.; Brennan, J. D., Development of a bioactive paper sensor for detection of neurotoxins using piezoelectric inkjet printing of sol-gel-derived bioinks. *Anal. Chem.* **2009**, *81*, 5474-5483.

Houghton, P. J.; Ren, Y.; Howes, M. J., Acetylcholinesterase inhibitors from plants and fungi. *Nat. Prod. Rep.* **2006**, *23*, 181-199.

Hu, J.; Liu, S., Responsive polymers for detection and sensing applications: current status and future developments. *Macromolecules* **2010**, *43*, 8315-8330.

Hu, X.; Hao, X.; Wu, Y.; Zhang, J.; Zhang, X.; Wang, P. C.; Zou, G.; Liang, X. J., Multifunctional hybrid silica nanoparticles for controlled doxorubicin loading and release with thermal and pH dually response. *J. Mater. Chem. B* **2013**, *1*, 1109-1118.

Huo, Q.; Margolese, D. I.; Ciesla, U.; Demuth, D. G.; Feng, P.; Gier, T. E.; Sieger, P.; Firouzi, A.; Chmelka, B. F., Organization of Organic Molecules with Inorganic Molecular Species into Nanocomposite Biphase Arrays. *Chem. Mater.* **1994**, *6*, 1176-1191.

Huo, Q.; Margolese, D. I.; Ciesla, U.; Feng, P.; Gier, T. E.; Sieger, P.; Leon, R.; Petroff, P. M.; Schüth, F.; Stucky, G. D., Generalized synthesis of periodic surfactant/inorganic composite materials. *Nature* **1994**, *368*, 317-321.

Izquierdo-Barba, I.; Sousa, E.; Doadrio, J. C.; Doadrio, A. L.; Pariente, J. P.; Martínez, A.; Babonneau, F.; Vallet-Regí, M., Influence of mesoporous structure type on the controlled delivery of drugs: release of ibuprofen from MCM-48, SBA-15 and functionalized SBA-15. *J. Sol-Gel Sci. Techn.* **2009**, *50*, 421-429.

Jeong, B.; Gutowska, A., Lessons from nature: stimuli-responsive polymers and their biomedical applications. *Trends Biotechnol.* **2002**, *20*, 305-311.

Jiao, Y.; Sun, Y.; Chang, B.; Lu, D.; Yang, W., Redox- and temperature-controlled drug release from hollow mesoporous silica nanoparticles. *Chem. Eur. J.* **2013**, *19*, 15410-15420.

Johnson, B. F. G., Nanoparticles in Catalysis. *Top. Catal.* **2003**, *24*, 147-159.

Katz, E.; Pingarron, J. M.; Mailloux, S.; Guz, N.; Gamella, M.; Melman, G.; Melman, A., Substance Release Triggered by Biomolecular Signals in Bioelectronic Systems. *J. Phys. Chem. Lett.* **2015**, *6*, 1340-1347.

Kim, K.; Tsay, O. G.; Atwood, D. A.; Churchill, D. G., Destruction and detection of chemical warfare agents. *Chem. Rev.* **2011**, *111*, 5345-5403.

Knezevic, N. Z.; Trewyn, B. G.; Lin, V. S., Functionalized mesoporous silica nanoparticle-based visible light responsive controlled release delivery system. *Chem. Commun.* **2011**, *47*, 2817-2819.

Kost, J.; Langer, R., Responsive polymeric delivery systems. *Adv. Drug Deliv. Rev.* **2001**, *46*, 125-148.

Kozurkova, M.; Hamulakova, S.; Gazova, Z.; Paulikova, H.; Kristian, P., Neuroactive Multifunctional Tacrine Congeners with Cholinesterase, Anti-Amyloid Aggregation and Neuroprotective Properties. *Pharmaceuticals* **2011**, *4*, 382-418.

Krajewska, B.; Zaborska, W. a.; Leszko, M., Inhibition of chitosan-immobilized urease by slow-binding inhibitors: Ni2+, F− and acetohydroxamic acid. *J. Mol. Catal. B-Enzym.* **2001**, *14*, 101-109.

Kresge, C. T.; Leonowicz, M. E.; Roth, W. J.; Vartuli, J. C.; Beck, J. S., Ordered mesoporous molecular sieves synthesized by a liquid-crystal template mechanism. *Nature* **1992**, *359*, 710-712.

Lai, C. Y.; Trewyn, B. G.; Jeftinija, D. M.; Jeftinija, K.; Xu, S.; Jeftinija, S.; Lin, V. S., A mesoporous silica nanosphere-based carrier system with chemically removable CdS nanoparticle caps for stimuli-responsive controlled release of neurotransmitters and drug molecules. *J. Am. Chem. Soc.* **2003**, *125*, 4451-4459.

Landry, C. C.; Nassivera, T. W., *US Patent Appl. 20090220791*.

Lane, R. M.; Potkin, S. G.; Enz, A., Targeting acetylcholinesterase and butyrylcholinesterase in dementia. *Int. J. Neuropsychopharmacol.* **2006**, *9*, 101-124.

Lavey, B. J.; Janda, K. D., Catalytic Antibody Mediated Hydrolysis of Paraoxon. *J. Org. Chem.* **1996**, *61*, 7633-7636.

Lee, C. H.; Cheng, S. H.; Huang, I. P.; Souris, J. S.; Yang, C. S.; Mou, C. Y.; Lo, L. W., Intracellular pH-responsive mesoporous silica nanoparticles for the controlled release of anticancer chemotherapeutics. *Angew. Chem. Int. Ed. Engl.* **2010**, *49*, 8214-8219.

Lee, J. E.; Lee, N.; Kim, T.; Kim, J.; Hyeon, T., Multifunctional mesoporous silica nanocomposite nanoparticles for theranostic applications. *Acc. Chem. Res.* **2011**, *44*, 893-902.

Lee, J.; Seo, S.; Kim, J., Colorimetric Detection of Warfare Gases by Polydiacetylenes Toward Equipment-Free Detection. *Adv. Funct. Mater.* **2012**, *22*, 1632-1638.

Lee, S.-M.; Nguyen, S. T., Smart Nanoscale Drug Delivery Platforms from Stimuli-Responsive Polymers and Liposomes. *Macromolecules* **2013**, *46*, 9169-9180.

Lei, C.; Shin, Y.; Magnuson, J. K.; Fryxell, G.; Lasure, L. L.; Elliott, D. C.; Liu, J.; Ackerman, E. J., Characterization of functionalized nanoporous supports for protein confinement. *Nanotechnology* **2006**, *17*, 5531-5538.

Lei, C.; Soares, T. A.; Shin, Y.; Liu, J.; Ackerman, E. J., Enzyme specific activity in functionalized nanoporous supports. *Nanotechnology* **2008**, *19*, 125102.

Lewis, V. E.; Donarski, W. J.; Wild, J. R.; Raushel, F. M., Mechanism and stereochemical course at phosphorus of the reaction catalyzed by a bacterial phosphotriesterase. *Biochemistry* **1988**, *27*, 1591-1597.

Li, Z.; Barnes, J. C.; Bosoy, A.; Stoddart, J. F.; Zink, J. I., Mesoporous silica nanoparticles in biomedical applications. *Chem. Soc. Rev.* **2012**, *41*, 2590-2605.

Lin, Y. S.; Hurley, K. R.; Haynes, C. L., Critical Considerations in the Biomedical Use of Mesoporous Silica Nanoparticles. *J. Phys. Chem. Lett.* **2012**, *3*, 364-374.

Lin, Y.; Lu, F.; Wang, J., Disposable Carbon Nanotube Modified Screen-Printed Biosensor for Amperometric Detection of Organophosphorus Pesticides and Nerve Agents. *Electroanalysis* **2004**, *16*, 145-149.

Liong, M.; Lu, J.; Kovochich, M.; Xia, T.; Ruehm, S. G.; Nel, A. E.; Tamanoi, F.; Zink, J. I., Multifunctional inorganic nanoparticles for imaging, targeting, and drug delivery. *Nano* **2008**, *2*, 889-896.

Liu, C.; Guo, J.; Yang, W.; Hu, J.; Wang, C.; Fu, S., Magnetic mesoporous silica microspheres with thermo-sensitive polymer shell for controlled drug release. *J. Mater. Chem.* **2009**, *19*, 4764-4770.

Liu, G.; Lin, Y., Nanomaterial labels in electrochemical immunosensors and immunoassays. *Talanta* **2007**, *74*, 308-317.

Liu, J.; Li, C.; Li, F., Fluorescence turn-on chemodosimeter-functionalized mesoporous silica nanoparticles and their application in cell imaging. *J. Mater. Chem.* **2011**, *21*, 7175-7181.

Loy, D. A.; Shea, K. J., Bridged Polysilsesquioxanes. Highly Porous Hybrid Organic-Inorganic Materials. *Chem. Rev.* **1995**, *95*, 1431-1442.

Lu, J.; Choi, E.; Tamanoi, F.; Zink, J. I., Light-activated nanoimpeller-controlled drug release in cancer cells. *Small* **2008**, *4*, 421-426.

Lu, Y.; Sun, W.; Gu, Z., Stimuli-responsive nanomaterials for therapeutic protein delivery. *J. Control. Release* **2014**, *194*, 1-19.

Mailloux, S.; Zavalov, O.; Guz, N.; Katz, E.; Bocharova, V., Enzymatic filter for improved separation of output signals in enzyme logic systems towards 'sense and treat' medicine. *Biomater. Sci.* **2014**, *2*, 184-191.

Mancin, F.; Rampazzo, E.; Tecilla, P.; Tonellato, U., Self-assembled fluorescent chemosensors. *Chem. Eur. J.* **2006**, *12*, 1844-1854.

Manzano, M.; Aina, V.; Areán, C. O.; Balas, F.; Cauda, V.; Colilla, M.; Delgado, M. R.; Vallet-Regí, M., Studies on MCM-41 mesoporous silica for drug delivery: Effect of particle morphology and amine functionalization. *Chem. Eng. J.* **2008**, *137*, 30-37.

Massoulié, J.; Pezzementi, L.; Bon, S.; Krejci, E.; Vallette, F. M., Molecular and cellular biology of cholinesterases. *Prog. Neurobiol.* **1993**, *41*, 31-91.

Mendez, J.; Monteagudo, A.; Griebenow, K., Stimulus-responsive controlled release system by covalent immobilization of an enzyme into mesoporous silica nanoparticles. *Bioconjug. Chem.* **2012**, *23*, 698-704.

Meng, H.; Xue, M.; Xia, T.; Zhao, Y. L.; Tamanoi, F.; Stoddart, J. F.; Zink, J. I.; Nel, A. E., Autonomous in vitro anticancer drug release from mesoporous silica nanoparticles by pH-sensitive nanovalves. *J. Am. Chem. Soc.* **2010**, *132*, 12690-12697.

Miao, Y.; He, N.; Zhu, J. J., History and new developments of assays for cholinesterase activity and inhibition. *Chem. Rev.* **2010**, *110*, 5216-5234.

Michalak, M.; Marek, A. A.; Zawadiak, J.; Kawalec, M.; Kurcok, P., Synthesis of PHB-based carrier for drug delivery systems with pH-controlled release. *Euro. Polym. J.* **2013**, *49*, 4149-4156.

Mortera, R.; Vivero-Escoto, J.; Slowing, II; Garrone, E.; Onida, B.; Lin, V. S., Cell-induced intracellular controlled release of membrane impermeable cysteine from a mesoporous silica nanoparticle-based drug delivery system. *Chem. Commun.* **2009**, 3219-3221.

Muhammad, F.; Guo, M.; Qi, W.; Sun, F.; Wang, A.; Guo, Y.; Zhu, G., pH-Triggered controlled drug release from mesoporous silica nanoparticles via intracelluar dissolution of ZnO nanolids. *J. Am. Chem. Soc.* **2011**, *133*, 8778-8781.

Mulchandani, A.; Rajesh, Microbial biosensors for organophosphate pesticides. *Appl. Biochem. Biotechnol.* **2011**, *165*, 687-699.

Munkhjargal, M.; Matsuura, Y.; Hatayama, K.; Miyajima, K.; Arakawa, T.; Kudo, H.; Mitsubayashi, K., Glucose-sensing and glucose-driven "organic engine" with co-immobilized enzyme membrane toward autonomous drug release systems for diabetes. *Sensor. Actuat. B-Chem.* **2013**, *188*, 831-836.

Munoz, B.; Ramila, A.; Perez-Pariente, J.; Diaz, I.; Vallet-Regi, M., MCM-41 organic modification as drug delivery rate regulator. *Chem. Mat.* **2003**, *15*, 500-503.

Mura, S.; Nicolas, J.; Couvreur, P., Stimuli-responsive nanocarriers for drug delivery. *Nat. Mater.* **2013**, *12*, 991-1003.

Myrick, J. M.; Vendra, V. K.; Krishnan, S., Self-assembled polysaccharide nanostructures for controlled-release applications. *Nanotechnol. Rev.* **2014**, *3*, 319-346.

Ngeh-Ngwainbi, J.; Foley, P. H.; Kaun, S. S.; Guilbault, G. G., Parathion antibodies on piezoelectric crystals. *J. Am. Chem. Soc.* **1986**, *108*, 5444-5447.

Nielsen, J. A.; Mena, E. E.; Williams, I. H.; Nocerini, M. R.; Liston, D., Correlation of brain levels of 9-amino-1,2,3,4-tetrahydroacridine (THA) with neurochemical and behavioral changes. *Eur. J. Pharmacol.* **1989**, *173*, 53-64.

Nieuwenhuizen, M. S.; Harteveld, J. L. N., Studies on a surface acoustic wave (SAW) dosimeter sensor for organophosphorous nerve agents. *Sens. Actuators B* **1997**, *40*, 167-173.

Nolan, E. M.; Lippard, S. J., Tools and tactics for the optical detection of mercuric ion. *Chem. Rev.* **2008**, *108*, 3443-3480.

Oliveira, O. N., Jr.; Iost, R. M.; Siqueira, J. R., Jr.; Crespilho, F. N.; Caseli, L., Nanomaterials for diagnosis: challenges and applications in smart devices based on molecular recognition. *ACS Appl. Mater. Interfaces* **2014**, *6*, 14745-14766.

Ouberai, M.; Brannstrom, K.; Vestling, M.; Olofsson, A.; Dumy, P.; Chierici, S.; Garcia, J., Clicked tacrine conjugates as acetylcholinesterase and beta-amyloid directed compounds. *Org. Biomol. Chem.* **2011**, *9*, 1140-1147.

Park, C.; Kim, H.; Kim, S.; Kim, C., Enzyme responsive nanocontainers with cyclodextrin gatekeepers and synergistic effects in release of guests. *J. Am. Chem. Soc.* **2009**, *131*, 16614-16615.

Park, C.; Lee, K.; Kim, C., Photoresponsive cyclodextrin-covered nanocontainers and their sol-gel transition induced by molecular recognition. *Angew. Chem. Int. Ed. Engl.* **2009**, *48*, 1275-1278.

Park, C.; Oh, K.; Lee, S. C.; Kim, C., Controlled release of guest molecules from mesoporous silica particles based on a pH-responsive polypseudorotaxane motif. *Angew. Chem. Int. Ed. Engl.* **2007**, *46*, 1455-1457.

Patel, K.; Angelos, S.; Dichtel, W. R.; Coskun, A.; Yang, Y. W.; Zink, J. I.; Stoddart, J. F., Enzyme-responsive snap-top covered silica nanocontainers. *J. Am. Chem. Soc.* **2008**, *130*, 2382-2383.

Pearson, G. S.; Magee, R. S., Critical evaluation of proven chemical weapon destruction technologies (IUPAC Technical Report). *Pure Appl. Chem.* **2002**, *74*, 187-316.

Pérez-López, B.; Merkoçi, A., Nanoparticles for the development of improved (bio) sensing systems. *Anal. Bioanal. Chem.* **2011**, *399*, 1577-1590.

Peterson, G. I.; Larsen, M. B.; Boydston, A. J., Controlled Depolymerization: Stimuli-Responsive Self-Immolative Polymers. *Macromolecules* **2012**, *45*, 7317-7328.

Popat, A.; Hartono, S. B.; Stahr, F.; Liu, J.; Qiao, S. Z.; Qing Max Lu, G., Mesoporous silica nanoparticles for bioadsorption, enzyme immobilisation, and delivery carriers. *Nanoscale* **2011**, *3*, 2801-2818.

Randolph, L. M.; Chien, M. P.; Gianneschi, N. C., Biological stimuli and biomolecules in the assembly and manipulation of nanoscale polymeric particles. *Chem. Sci.* **2012**, *3*, 1363-1380.

Rapoport, N., Physical stimuli-responsive polymeric micelles for anti-cancer drug delivery. *Prog. Polym. Sci.* **2007**, *32*, 962-990.

Reeves, T. E.; Wales, M. E.; Grimsley, J. K.; Li, P.; Cerasoli, D. M.; Wild, J. R., Balancing the stability and the catalytic specificities of OP hydrolases with enhanced V-agent activities. *Protein Eng. Des. Sel.* **2008**, *21*, 405-412.

Rolfe, P., Micro- and Nanosensors for Medical and Biological Measurement. *Sensor. Mater.* **2012**, *24*, 275-302.

Rosenholm, J. M.; Linden, M., Towards establishing structure-activity relationships for mesoporous silica in drug delivery applications. *J. Control. Release* **2008**, *128*, 157-164.

Royo, S.; Martinez-Manez, R.; Sancenon, F.; Costero, A. M.; Parra, M.; Gil, S., Chromogenic and fluorogenic reagents for chemical warfare nerve agents' detection. *Chem. Commun.* **2007**, 4839-4847.

Russell, A. J.; Berberich, J. A.; Drevon, G. F.; Koepsel, R. R., Biomaterials for Mediation of Chemical and Biological Warfare Agents. *Annu. Rev. Biomed. Eng.* **2003**, *5*, 1.

Sakamoto, Y.; Kim, T. W.; Ryoo, R.; Terasaki, O., Three-dimensional structure of large-pore mesoporous cubic Ia3d silica with complementary pores and its carbon replica by electron crystallography. *Angew. Chem. Int. Ed. Engl.* **2004**, *43*, 5231-5234.

Sauer, A. M.; Schlossbauer, A.; Ruthardt, N.; Cauda, V.; Bein, T.; Brauchle, C., Role of endosomal escape for disulfide-based drug delivery from colloidal mesoporous silica evaluated by live-cell imaging. *Nano Lett.* **2010**, *10*, 3684-3691.

Schmidt-Winkel, P.; Lukens, W. W.; Zhao, D.; Yang, P.; Chmelka, B. F.; Stucky, G. D., Mesocellular Siliceous Foams with Uniformly Sized Cells and Windows. *J. Am. Chem. Soc.* **1999**, *121*, 254-255.

Schneider, H. J.; Strongin, R. M., Supramolecular interactions in chemomechanical polymers. *Acc. Chem. Res.* **2009**, *42*, 1489-1500.

Shea, K. J.; Loy, D. A., Bridged Polysilsesquioxanes. Molecular-Engineered Hybrid Organic−Inorganic Materials. *Chem. Mater.* **2001**, *13*, 3306-3319.

Sheldon, R. A., Enzyme Immobilization: The Quest for Optimum Performance. *Adv. Synth. Catal.* **2007**, *349*, 1289-1307.

Simonian, A. L.; Good, T. A.; Wang, S. S.; Wild, J. R., Nanoparticle-based optical biosensors for the direct detection of organophosphate chemical warfare agents and pesticides. *Anal. Chim. Acta.* **2005**, *534*, 69-77.

Simonian, A. L.; Grimsley, J. K.; Flounders, A. W.; Schoeniger, J. S.; Cheng, T. C.; DeFrank, J. J.; Wild, J. R., Enzyme-based biosensor for the direct detection of fluorine-containing organophosphates. *Anal. Chem. Acta* **2001**, *442*, 15-23.

Simonian, A. L.; Grimsley, J. K.; Flounders, A. W.; Schoeniger, J. S.; Cheng, T. C.; DeFrank, J. J.; Wild, J. R., Enzyme-based biosensor for the direct detection of fluorine-containing organophosphates. *Anal. Chem. Acta* **2001**, *442*, 15-23.

Sing, K. S. W., Reporting physisorption data for gas/solid systems with special reference to the determination of surface area and porosity (Recommendations 1984). *Pure Appl. Chem.* **1985**, *57*, 603-619.

Sing, K. S. W.; Everett, D. H.; Haul, R. A. W.; Moscou, L.; Pierotti, R. A.; Rouquerol, J.; Siemieniewska, T., *Pure Appl. Chem.* **1985**, *57*, 603.

Skirtach, A. G.; Yashchenok, A. M.; Mohwald, H., Encapsulation, release and applications of LbL polyelectrolyte multilayer capsules. *Chem. Commun.* **2011**, *47*, 12736-12746.

Slowing, I. I.; Vivero-Escoto, J. L.; Trewyn, B. G.; Lin, V. S. Y., Mesoporous silica nanoparticles: structural design and applications. *J. Mater. Chem.* **2010**, *20*, 7924-7937.

Spruell, J. M.; Hawker, C. J., Triggered structural and property changes in polymeric nanomaterials. *Chem. Sci.* **2011**, *2*, 18-26.

Steinberg, G. M.; Mednick, M. L.; Maddox, J.; Rice, R., A hydrophobic binding site in acetylcholinesterase. *J. Med. Chem.* **1975**, *18*, 1057-1061.

Steiner, W. E.; Klopsch, S. J.; English, W. A.; Clowers, B. H.; Hill, H. H., Detection of a chemical warfare agent simulant in various aerosol matrixes by ion mobility time-of-flight mass spectrometry. *Anal. Chem.* **2005**, *77*, 4792-4799.

Syria and the Organisation for the Prohibition of Chemical Weapons. http://www.opcw.org/special-sections/syria-and-the-opcw/ (accessed April 18, 2014).

Theato, P.; Sumerlin, B. S.; O'Reilly, R. K.; Epps, T. H., 3rd, Stimuli responsive materials. *Chem. Soc. Rev.* **2013**, *42*, 7055-7056.

Thevenot, J.; Oliveira, H.; Sandre, O.; Lecommandoux, S., Magnetic responsive polymer composite materials. *Chem. Soc. Rev.* **2013**, *42*, 7099-7116.

Tian, B.-S.; Yang, C., Temperature-Responsive Nanocomposites Based on Mesoporous SBA-15 Silica and PNIPAAm: Synthesis and Characterization. *J. Phys. Chem. C* **2009**, *113*, 4925-4931.

Tro, N. J., *Chemistry: A Molecular Approach*. 3rd ed.; Pearson Boston, 2014.

Tsai, P.-C.; Bigley, A.; Li, Y.; Ghanem, E.; Cadieux, C. L.; Kasten, S. A.; Reeves, T. E.; Cerasoli, D. M.; Raushel, F. M., Stereoselective hydrolysis of organophosphate nerve agents by the bacterial phosphotriesterase. *Biochemistry* **2010**, *49*, 7978.

Vallet-Regí, M.; Balas, F.; Colilla, M.; Manzano, M., Bone-regenerative bioceramic implants with drug and protein controlled delivery capability. *Prog. Solid State Ch.* **2008**, *36*, 163-191.

Van Dyk, J. S.; Pletschke, B., Review on the use of enzymes for the detection of organochlorine, organophosphate and carbamate pesticides in the environment. *Chemosphere* **2011**, *82*, 291-307.

Vetsch, J. R.; Paulsen, S. J.; Muller, R.; Hofmann, S., Effect of fetal bovine serum on mineralization in silk fibroin scaffolds. *Acta Biomater.* **2015**, *13*, 277-285.

Villatte, F.; Marcel, V.; Estrada-Mondaca, S.; Fournier, D., Engineering sensitive acetylcholinesterase for detection of organophosphate and carbamate insecticides. *Biosens. Bioelectron.* **1998**, *13*, 157-164.

Vivero-Escoto, J. L.; Slowing, II; Wu, C. W.; Lin, V. S., Photoinduced intracellular controlled release drug delivery in human cells by gold-capped mesoporous silica nanosphere. *J. Am. Chem. Soc.* **2009**, *131*, 3462-3463.

Wang, H. C.; Zhang, Y.; Possanza, C. M.; Zimmerman, S. C.; Cheng, J.; Moore, J. S.; Harris, K.; Katz, J. S., Trigger chemistries for better industrial formulations. *Appl. Mater. Interfaces* **2015**, *7*, 6369-6382.

Wang, J., Microchip devices for detecting terrorist weapons. *Anal. Chem. Acta* **2004**, *507*, 3-10.

Wang, M.; Gu, X.; Zhang, G.; Zhang, D.; Zhu, D., Continuous colorimetric assay for acetylcholinesterase and inhibitor screening with gold nanoparticles. *Langmuir* **2009**, *25*, 2504-2507.

Xu, J.; Liu, S., Polymeric nanocarriers possessing thermoresponsive coronas. *Soft Matter* **2008**, *4*, 1745-1749.

Yang, P.; Gai, S.; Lin, J., Functionalized mesoporous silica materials for controlled drug delivery. *Chem. Soc. Rev.* **2012**, *41*, 3679-3698.

Yang, Q.; Wang, S.; Fan, P.; Wang, L.; Di, Y.; Lin, K.; Xiao, F.-S., pH-Responsive Carrier System Based on Carboxylic Acid Modified Mesoporous Silica and Polyelectrolyte for Drug Delivery. *Chem. Mater.* **2005**, *17*, 5999-6003.

Yang, Y. C.; Baker, J. A.; Ward, J. R., Decontamination of Chemical Warfare Agents. *Chem. Rev.* **1992**, *92*, 1729-1743.

Yang, Y. M.; Ji, H.-F.; Thundat, T., Nerve agents detection using a Cu2+/L-cysteine bilayer-coated microcantilever. *J. Am. Chem. Soc.* **2003**, *125*, 1124-1125.

Yildiz, I.; Deniz, E.; Raymo, F. M., Fluorescence modulation with photochromic switches in nanostructured constructs. *Chem. Soc. Rev.* **2009**, *38*, 1859-1867.

Yu, D.; Volponi, J.; Chhabra, S.; Brinker, C. J.; Mulchandani, A.; Singh, A. K., Aqueous sol-gel encapsulation of genetically engineered Moraxella spp. cells for the detection of organophosphates. *Biosens. Bioelectron.* **2005**, *20*, 1433-1437.

Yuehe, L.; Fang, L.; Joseph, W., Disposable Carbon Nanotube Modified Screen-Printed Biosensor for Amperometric Detection of Organophosphorus Pesticides and Nerve Agents. *Electroanalysis* **2004**, *16*, 145-149.

Zhang, X.; Guo, Q.; Cui, D., Recent advances in nanotechnology applied to biosensors. *Sensors* **2009**, *9*, 1033-1053.

Zhao, W.; Zhang, H.; He, Q.; Li, Y.; Gu, J.; Li, L.; Li, H.; Shi, J., A glucose-responsive controlled release of insulin system based on enzyme multilayers-coated mesoporous silica particles. *Chem. Commun.* **2011**, *47*, 9459-9461.

Zhao, Y. L.; Li, Z.; Kabehie, S.; Botros, Y. Y.; Stoddart, J. F.; Zink, J. I., pH-operated nanopistons on the surfaces of mesoporous silica nanoparticles. *J. Am. Chem. Soc.* **2010**, *132*, 13016-13025.

Zhou, K.; Wang, Y.; Huang, X.; Luby-Phelps, K.; Sumer, B. D.; Gao, J., Tunable, ultrasensitive pH-responsive nanoparticles targeting specific endocytic organelles in living cells. *Angew. Chem. Int. Ed. Engl.* **2011**, *50*, 6109-6114.

Zhou, Y.; Yu, B.; Shiu, E.; Levon, K., Potentiometric sensing of chemical warfare agents: surface imprinted polymer integrated with an indium tin oxide electrode. *Anal. Chem.* **2004**, *76*, 2689-2693.

Zhu, S.; Zhou, Z.; Zhang, D., Control of drug release through the in situ assembly of stimuli-responsive ordered mesoporous silica with magnetic particles. *ChemPhysChem* **2007**, *8*, 2478-2483.

Zhu, Y.; Meng, W.; Gao, H.; Hanagata, N., Hollow Mesoporous Silica/Poly(l-lysine) Particles for Codelivery of Drug and Gene with Enzyme-Triggered Release Property. *J. Phys. Chem. C* **2011**, *115*, 13630-13636.

Zhu, Y.; Shi, J., A mesoporous core-shell structure for pH-controlled storage and release of water-soluble drug. *Micropor. Mesopor. Mat.* **2007**, *103*, 243-249.

Zhu, Y.; Shi, J.; Shen, W.; Dong, X.; Feng, J.; Ruan, M.; Li, Y., Stimuli-responsive controlled drug release from a hollow mesoporous silica sphere/polyelectrolyte multilayer core-shell structure. *Angew. Chem. Int. Ed. Engl.* **2005**, *44*, 5083-5087.